# FEMTOSECOND FIBER LASERS AND AMPLIFIERS BASED ON THE PULSE PROPAGATION AT NORMAL DISPERSION

A Dissertation

Presented to the Faculty of the Graduate School

of Cornell University

in Partial Fulfillment of the Requirements for the Degree of

Doctor of Philosophy

by

Chin Yu Chong

August 2008

# FEMTOSECOND FIBER LASERS AND AMPLIFIERS BASED ON THE PULSE PROPAGATION AT NORMAL DISPERSION

Chin Yu Chong, Ph.D.

Cornell University 2008

The applications of ultrafast optical pulses exploded in last two decade since the discovery of a mode-locked Ti:sapphire laser. Ti:Sapphire lasers are great ultrafast optical pulse sources but they are not suitable for some applications since they are are bulky, expensive, and unreliable. So far, solid-state lasers including Ti:sapphire lasers are dominant as ultrafast pulse sources. However, compact, inexpensive and stable fiber lasers recently started to replace solid-state lasers. Even though fiber lasers have many practical advantages, the performance of fiber lasers is still below that of the solid-state fiber lasers. Among many kinds of fiber lasers, a mode-locked ytterbium (Yb)-doped fiber lasers has been received a broad attention for medical applications such as the biomedical imaging. This thesis summarizes the effort of the Yb-doped fiber laser performance enhancement utilizing the pulse propagation at high normal dispersion.

In this thesis, femtosecond Yb-doped fiber lasers without anomalous dispersion element, so called all-normal-dispersion (ANDi) fiber lasers, are demonstrated based on unique pulse shaping mechanism of the chirped pulse spectral filtering. ANDi fiber lasers represent a new paradigm for femtosecond pulse generation. This new type of a laser is very practical because it avoids the technical challenges of providing anomalous dispersion without loss at 1 $\mu$m. Useful features of the ANDi fiber lasers have been demonstrated experimentally in terms of the pulse energy, the pulse duration, the environmentally stability, and controllable multipulsing states. Pulse energies > 20 nJ with >100 kW peak power and pulse durations <100 fs are experimentally demonstrated.

Theoretical studies indicate that further performance improvement is quite possible. The ANDi fiber lasers are not only practical femtosecond lasers, but also great research tools for ultrashort pulse propagation phenomena. Dissipative solitons of complex cubic quintic Ginzburg-Landau equation are demonstrated experimentally from an all-normal dispersion fiber laser.

This thesis is not limited to the demonstration of ANDi lasers. It also covers interesting pulse propagation phenomena in fiber lasers and amplifiers. The formation of a second-order dispersion managed soliton, which is referred as an antisymmetric dispersion managed soliton, in a fiber laser with a strong dispersion map is demonstrated. Finally, the thesis describes the chirped-pulse-amplification system performance enhancement with proper nonlinear phase shift and third-order dispersion.

# BIOGRAPHICAL SKETCH

Chin Yu Chong (Andy Chong) was born in Deajon, Korea 1970. He was an ordinary student who never thought himself as a physicist to be. The year 1988 was a big year for him. He and his family immigrated to a small town in Indiana, U.S. in that year. Within several years of his immigration, he took several physics classes in a high school. Those several high school physics classes were the starting point of his long and somewhat wild journey to be a physicist.

Realizing his undeniable interest in physics, he decided to study physics as a major in a college. In 1995~96, He received B.S. degrees in Mechanical engineering and physics at University of Texas at Austin. After receiving B.S. degrees, he widely deviated from the course of pursuing higher education in physics. The initial idea was to get ‘some’ experience before pursuing further education. However, he worked for several industrial companies for much longer than his initial anticipation. During his career in industry, he always thought of pursuing Ph.D. but his courage was not enough to overcome the momentum of a routine but a stable life-style of an industrial worker. It is certainly true that shifting a strong momentum requires a quite a bit of an impact. A disastrous telecom crash at late 90’s made him look into what he really wanted to do seriously. After many years of service in the industry, he finally decided to pursue his Ph.D. at Cornell University.

He joined Frank Wise group as a Ph.D. candidate in 2004. Since then, he has been researching nonlinear optics and ultrafast pulse propagation phenomena, especially in fiber lasers and amplifiers. During the course of the Ph.D. program, he enjoyed every single day of learning fascinating science. Now, his journey finally has reached the Ph.D. degree and it will continue.

Chin Yu Chong published all the journal publications under the pen name of ‘Andy Chong’ which will be his official name after he obtains a U.S. citizenship. Currently, the citizenship process is delayed but eventually he will be a U.S. citizen with Andy as his first name.

To my family, Rachel, Henry and Michelle.

# ACKNOWLEDGEMENTS

First of all, I thank to my advisor, Professor Frank Wise who has been a such a superb advisor. The depth of his insight in science has been always amazing. At the same time, his patience and encouragement have been invaluable in my research. I also like to thank my committee members, Professor Chris Xu and Professor Michal Lipson for their guidance.

It was such a pleasure to work with Wise group members. Among many group members, I sincerely thank members of the fiber team including, Joel Buckley, Hyungsik Lim, Lyuba Kuznetsova, Shian Zhou, Will Renninger, Khanh Kieu, and Hui Liu. I am very proud what we have accomplished as a team.

Finally, I am indebted forever to my wife Michelle for her love and patient support for all these years.

# TABLE OF CONTENTS

# LIST OF TABLES

# LIST OF FIGURES

# CHAPTER 1

# INTRODUCTION

Ultrafast science is a rapidly growing field. This unique scientific field is not limited to studying interesting ultrafast optical phenomena but it expands its impacts on various other scientific fields and even industrial applications. These days, applying ultrafast science in applications such as ultrafast event measurement, micromachining, medical imaging, telecommunication, etc. is not a breaking science news anymore. Interest in ultrafast science has grown significantly in the last decade and it is expected to grow further. It is strongly believed that the public will face more and more commercial devices based on ultrafast science and technologies.

Ultrafast science has been led by high intensity femtosecond pulse sources. Solid state lasers are great devices to generate intense femtosecond pulses. Among them, most notable is the mode-locked Ti:sapphire laser which was a major discovery to provide intense femtosecond pulse sources to overall ultrafast science to date. Ti:sapphire lasers with highest peak-power and the shortest pulse duration have been such great devices for scientific researches. However, solid-state lasers are not user-friendly in general. The usage of those lasers outside the research laboratories was discouraged because most of solid-state lasers are bulky, expensive, and unreliable. For example, even with a tremendous effort in last two decades to make Ti:sapphire lasers user-friendly devices, the Ti:sapphire lasers are still very bulky, excessively complicated, expensive and requiring continuous maintenance. These cumbersome features of solid-state lasers are very unattractive for numerous important applications requiring short pulses. Compact, inexpensive and robust femtosecond lasers will promote the usage of ultrafast technologies not only in the industries but also in many other scientific researches.

Fiber lasers are strong candidates to relieve the obstacles to proliferate femtosecond mode-locked lasers beyond research laboratories. Femtosecond fiber lasers have major practical advantages over solid state lasers. Most notable practical advantages of fiber lasers are as follows. Fiber lasers are impervious to the bulk optics misalignment with light confined within the optical fiber. The stability against the misalignment makes the fiber lasers low maintenance devices. The lasers can be made very compact since the flexible fiber can be packed to occupy a negligibly small volume comparing to bulky solid state lasers. Since the laser beam is the mode of the fiber, the spatial quality of the beam is outstanding. A large fiber surface to volume ratio makes complicated cooling devices unnecessary for fiber lasers. Many parts for the fiber lasers are already developed and commercially available targeting telecommunication industries. Therefore, fiber lasers can be manufactured with low cost since many parts are mass produced for telecommunication industries.

Even though fibers lasers are attractive solutions for the wide-spread usage of femtosecond mode-locked lasers, they certainly have their own problems. The performance of fiber lasers, such as peak-power, pulse energy and pulse durations, is still below that of the solid state laser. At some lasing wavelength, fiber lasers still contained appreciable bulk optical components which is against the practical advantage of the waveguide medium. Recognizing practical advantages of fiber lasers, scientists and researchers devoted tremendous efforts to improve the performance of the fiber lasers. As the result of active researches, not only the significant performance improvement was achieved but also the scientific knowledge of the fiber lasers dramatically increased recently.

However, the best performance was achieved still from fiber lasers with appreciable intracavity bulk optical components. The necessity of intracavity bulk optical components is mostly due to the anomalous dispersive segment. It was commonly believed that a fiber laser should have a dispersion, which is composed of a normally dispersive segment and an anomalously dispersive segment, to produce femtosecond pulses. Many fiber lasers were built based on that common knowledge but for certain lasing wavelengths (*i.e.* 1 $\mu$m of Ytterbium (Yb)-doped fiber), providing intracavity anomalous dispersion is quite challenging. Except the cases of specially designed fibers such as photonic crystal fibers (PCF) and hollow photonic bandgap fibers (PBF), regular single-mode fibers (SMF) at 1 $\mu$m are normally dispersive. As the result, high performance Yb-doped fiber lasers usually contained bulk anomalous dispersion components such as a grating pair, a prism pair, etc. Of course, Yb-doped fiber lasers with PCF or PBF were demonstrated successfully but the performance did not reach that of fiber lasers with bulk components.

The difficulty was relieved recently. Femtosecond fiber lasers without anomalous dispersion elements was demonstrated based on unique pulse shaping mechanism of chirped pulse spectral filtering. The new pulse shaping mechanism is quite different from conventional fiber laser pulse shaping mechanisms. The demonstration of femtosecond fiber lasers with only normal dispersion, which was referred as all-normal dispersion (ANDi) fiber laser, has shattered the dispersion map requirement. The discovery of ANDi fiber laser provides an immediate practical benefit of femtosecond fiber lasers without bulk anomalous dispersive segments or complex specially designed fibers. Due to its simplicity, several different research groups already devoted efforts to produce all-fiber integrated version of ANDi fiber lasers. The simplicity is not the only strength of ANDi fiber lasers. Experimental observations and theoretical studies show that the potential of the ANDi laser is remarkable. Pulse energies > 20 nJ with >100 kW peak power and pulse durations <100 fs are already demonstrated. Theoretical studies indicate that further performance improvement is quite possible. The ANDi fiber lasers are not only practical femtosecond lasers, but also great research tools for ultrashort pulse propagation phenomena. Dissipative solitons of complex cubic quintic Ginzburg-

Landau Eq. were demonstrated from a laser cavity for the first time using an ANDi fiber laser.

In this thesis, the features of the ANDi fiber laser along with a theoretical study is proudly presented. The performance of ANDi fiber lasers is described in terms of the pulse energy, the pulse duration, and the environmental stability. The systematic behavior study of the ANDi fiber lasers and the observation of dissipative solitons of a famous complex cubic quintic Ginzburg-Landau Eq. are also presented. We believe that simple, high-performing ANDi fiber lasers will find many applications not only in industries but also as research tools in various fields of science.

## 1.1 Organization of the thesis

The rest of the thesis is organized as follows. Chapter 1 provides the background mode-locked laser theories including nonlinear Schrödinger equation, Ginzburg-Landau equation and their solitary analytic solutions. The pulse shaping mechanisms of the mode-locked fiber lasers are discussed based on the soliton, the dispersion managed (DM) soliton, and the self-similar pulse evolution in the laser cavity. The important laser components such as a saturable absorber and a spectral filter which determine the characteristic of fiber lasers are covered briefly.

Chapter 2 describes the ANDi fiber laser pulse shaping mechanism and a design rationale based on the numerical simulations. Experimental results based on various spectral filters and gain fibers including Erbium-doped fibers.

In Chapter 3, a systematic study of ANDi fiber lasers with numerical simulations and experiments is presented. The systematic study shows the laser characteristic depends mainly on three laser design parameters of the group velocity dispersion (GVD), the nonlinear-phase shift ($\Phi^{NL}$) and the spectral filter bandwidth (BW). The chapter describes the effect of each parameters. Along with the theoretical study based on numerical simulations, the connection between the ANDi fiber lasers and the analytic solutions of complex cubic quintic Ginzburg-Landau equation is discussed. The similarities between the ANDi fiber laser operations and the dissipative solitons of complex cubic quintic Ginzburg-Landau equations are presented.

Chapter 4 presents the investigation of high pulse energy generation in ANDi fiber lasers. By selecting appropriate GVD, spectral filter and proper pump power, $\sim$25 nJ pulse energy with $\sim$150 fs pulse duration is achieved.

Chapter 5 presents the investigation of short pulse generation in ANDi fiber lasers. Pulse durations of 70~80 fs are obtained experimentally. The chapter also presents the numerical simulation result showing the possibility of $\sim$10 cycle pulse generation in ANDi fiber lasers.

Chapter 6 describes the experimental demonstration of environmentally stable version of ANDi fiber lasers utilizing polarization maintaining fibers. The self-starting is initiated by the semiconductor saturable absorber. The unique pulse shaping mechanism of chirped pulse spectral filtering gives femtosecond pulses at very high normal GVD.

Chapter 7 describes the observation of high-harmonic mode-locked operations of ANDi fiber lasers. Interestingly, the operation is tunable from a soliton bunch state to a high-harmonic mode-locked state by adjusting the spectral filtering. The theoretical understanding of the phenomena is discussed.

In Chapter 8, the subject is changed from ANDi fiber lasers to an interesting second-order DM soliton mode of a fiber laser with a dispersion map. The second-order DM soliton is referred as the antisymmetric DM (ASDM) soliton. The observation of the

ASDM soliton in an fiber laser oscillator is reported.

In Chapter 9, theoretical study of the chirped-pulse amplification (CPA) system with high nonlinearity and third-order dispersion (TOD) is described. Interestingly, with a substantial $\Phi^{NL}$ and proper TOD, the final amplified pulse duration and quality are improved. This chapter provides the theory to optimize the CPA system performance by manipulating the $\Phi^{NL}$ and TOD.

In Chapter 10, future research directions for fiber lasers and amplifiers are suggested.

## 1.2 Passive pulse propagation in a fiber

The optical pulse propagation in a non-resonant third-order nonlinear medium such as an optical fiber can be well described by the nonlinear Schrödinger equation (NLSE). By solving the NLSE, one can predict the pulse evolution in various fiber systems. In this section, three important passive solitary-wave solutions of the fiber system described by the NLSE are discussed. Those solutions are directly related to the mode-locked fiber laser pulse shaping mechanisms.

### 1.2.1 Nonlinear Schrödinger equation and solitons

The derivation of the NLSE equation from the well-known Maxwell's equation is well covered in numbers of textbooks such as Ref [1, 2]. The final equation obtained through a somewhat lengthy derivation is

$$\frac{\partial A}{\partial z} + \frac{\alpha}{2}A + i\frac{\beta_2}{2}\frac{\partial^2 A}{\partial t^2} - \frac{\beta_3}{6}\frac{\partial^3 A}{\partial t^3} = i\gamma[|A|^2 A + \frac{i}{\omega_o}\frac{\partial}{\partial t}(|A|^2 A) - T_R A\frac{\partial |A|^2}{\partial t}]. \tag{1.1}$$

The Equation 1.1 describes how the slowly-varying envelope function $A = A(t,z)$ evolves in a third-order nonlinear medium (*i.e.* $\chi_2$ =0, $\chi_3$ ≠0 ) where $t$ is the local time and $z$ is the propagation distance. $\alpha$ represents the gain / loss coefficient. $\beta_2$ and $\beta_3$ are coefficients of the Taylor expanded propagation constant $\beta(\omega)$ around the carrier frequency $\omega_o$ given by the following equation.

$$\beta(\omega) = \beta_o + \beta_1(\omega - \omega_o) + \frac{1}{2}\beta_2(\omega - \omega_o)^2 + \frac{1}{6}\beta_3(\omega - \omega_o)^3 + ... \tag{1.2}$$

$\beta_2$ and $\beta_3$ are referred as the GVD and TOD coefficient respectively. Fourth and higher-order dispersion coefficients are neglected in Equation 1.1 since their effects on the pulse propagation are negligible in most cases especially for fibers. $\gamma$ is referred as the nonlinear coefficient which is defined as $\gamma = \omega_o n_2/(cA_{eff})$ where $n_2$ is the nonlinear index coefficient and $A_{eff}$ is the effective mode area. $\frac{i}{\omega_o}\frac{\partial}{\partial t}(|A|^2 A)$ and $T_R A\frac{\partial |A|^2}{\partial t}$ terms are higher-order nonlinear terms related to the self-steepening and the raman self-frequency shift respectively. For a relatively long pulse duration >100 fs with a low peak power, which is valid for most of fiber lasers, the TOD and higher-order nonlinear terms are negligible. Moreover, the gain / loss ($\alpha$) of the pulse while it propagates within the fiber is negligible. By eliminating the gain / loss, the TOD and higher-order nonlinear terms from Equation 1.1, the famous NLSE is obtained.

$$\frac{\partial A}{\partial z} + i\frac{\beta_2}{2}\frac{\partial^2 A}{\partial t^2} = i\gamma|A|^2 A. \tag{1.3}$$

The NLSE contains only two phase modulation terms due to the GVD and the nonlinearity. This equation is integrable using the inverse scattering method. The soliton solution of the NLSE is report by Zakharov and Shabat in 1971 [3]. In fact, the NLSE has many solutions for each integer value of $N = \gamma P_o(t_o)^2/|\beta_2|$. When $N$=1, the phase modulation due to the GVD and the self-phase modulation (SPM) can cancel each other perfectly if $\beta_2$ and $\gamma$ have different signs. In case of a silica fiber, $\gamma$ is always positive and therefore, Equation 1.3 requires negative $\beta_2$ (anomalous dispersion) to have a perfect phase cancelation. In this case, Equation 1.3 has a soliton solution which propagates the nonlinear medium without changing its shape. This solution is referred as a fundamental soliton. When $N$ >1, Equation 1.3 has complicated breathing solutions which are referred as higher-order solitons. The fundamental ($N$=1) soliton has a characteristic hyper-secant functional form as shown in Equation 1.4.

$$A(t,z) = A_o Sech(t/t_o)e^{iz/2}. \tag{1.4}$$

For $N$=1 case, one more analytic solution exists with a characteristic hyper-tangent functional form for positive $\beta_2$. This solution is referred as a dark soliton while the ordinary soliton with a hyper-secant pulse shape is referred as a bright soliton. Since solitons in fiber lasers are most likely to be bright solitons, a soliton in this thesis always means a bright soliton. The amplitude $A_o$ of the fundamental soliton is a function of $\beta_2$ and $\gamma$.

$$A_o = (\frac{|\beta_2|}{\gamma t_o})^{1/2} \tag{1.5}$$

Equation 1.5 can be reduced to a simple relationship of $A_o t_o = const$ which is known as the soliton area theorem. It means that for a given pulse duration, the soliton energy is fundamentally limited. The existence of solitons in an anomalously dispersive optical fiber was first demonstrated in 1980 [4]. Since the fundamental soliton does not change its shape while it propagates in an anomalously dispersive fiber, a soliton is a good candidate for pulses in mode-locked fiber lasers. The boundary condition of the cavity can be automatically satisfied by a soliton. Famous soliton fiber lasers are based on the soliton pulse shaping in a passive propagation. The soliton pulse shaping mechanisms will be discussed in a later section along with other conventional pulse shaping mechanisms.

When two or more waves co-propagate inside a nonlinear material, they can interact each other nonlinearly to modulate the phase of the adjacent wave. This phenomenon is referred as cross-phase modulation (XPM). The NLSE is valid when there is no birefringence in a fiber. However, in a case of a fiber with nonzero linear birefringence, which is true in general, two different modes (polarization modes) have to be counted separately to describe the pulse propagation appropriately. For a fiber with large linear birefringence, the pulse propagation can be presented by a set of two coupled equations with proper XPM terms [2].

$$\frac{\partial A_x}{\partial z} + i\frac{\beta_2}{2}\frac{\partial^2 A_x}{\partial t^2} = i\gamma(|A_x|^2 + \frac{2}{3}|A_y|^2)A_x. \tag{1.6}$$

$$\frac{\partial A_y}{\partial z} + i\frac{\beta_2}{2}\frac{\partial^2 A_y}{\partial t^2} = i\gamma(|A_y|^2 + \frac{2}{3}|A_x|^2)A_y. \tag{1.7}$$

$x$ and $y$ represent birefringence principle axes of a fiber. $\frac{2}{3}i\gamma|A_y|^2$ and $\frac{2}{3}i\gamma|A_x|^2$ are XPM terms. Without XPM, the coupled equations reduced into two separate NLSEs.

### 1.2.2 Dispersion-managed solitons

The first discovery of an interesting soliton solution in a fiber transmission line with a dispersion map of periodically alternating signs ( + for normal and - for anomalous

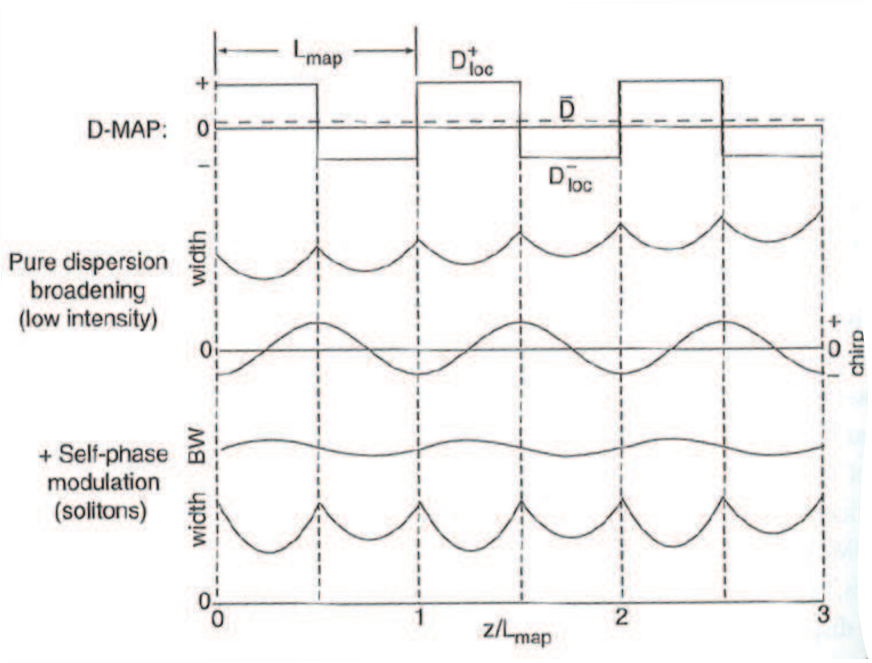

Figure 1.1: DM solitons in a nutshell. Top: Scheme of a prototypical dispersion map. Middle: Pulse behavior (pulse width above and chirp below) in the linear limit. Bottom: Pulse behavior at the power level for solitons. Note that the plots of pulse BW (above) and the pulse width (below) refer to the same zero. From [6].

GVD fibers) of the GVD was by Suzuki *et al.* in 1985 [5]. The soliton solutions of the dispersion map were called dispersion managed (DM) solitons and the technique of utilizing dispersion maps to obtain desired pulse propagation is referred as a dispersion management. The DM soliton received tremendous attention owing to its energy scalability to have less timing jitter in the optical telecommunications. As a DM soliton propagates in a dispersion map, the pulse duration is strongly varied periodically. However, at the end of each dispersion map period, a DM soliton returns to its original pulse profile. Therefore, it effectively acts like a soliton in average. The DM soliton propagation in a dispersion map can be visualized by plotting pulse parameters *vs.* the propagation distance (Figure 1.1).

The top of Figure 1.1 shows a fiber passive transmission line with numbers of dispersion maps. The net GVD of the dispersion map is not zero but slightly anomalous (dotted line in Figure 1.1 top). It is useful to investigate how a pulse with negligible intensity (*i.e.* $\Phi^{NL} \approx 0$) propagates in a DM transmission line. Since the nonlinear effect is negligible, the pulse only experiences periodically alternating GVD. As the consequence, the pulse duration breathes heavily nd the average pulse duration slowly increases since the pulse experiences non-compensable net GVD (Figure 1.1 middle). Once the pulse intensity is at the level of a DM soliton to counterpart the dispersion broadening effect, the pulse becomes a soliton solution of a dispersion map. The pulse still breathes heavily but it comes back to its original pulse duration and spectral BW at the end of each dispersion map (Figure 1.1 bottom). The typical DM soliton evolution shows local pulse duration maxima at the end of each dispersive segment while minima are located around the mid-point of the each dispersive segment.

Theoretically, DM soliton evolution is still governed by Equation 1.3 but with $\beta_2$ and $\gamma$ which are functions of the propagation distance $z$.

$$\frac{\partial A}{\partial z} + i\frac{\beta_2(z)}{2}\frac{\partial^2 A}{\partial t^2} = i\gamma(z)|A|^2 A \tag{1.8}$$

Unfortunately, Equation 1.8 is not integrable even for the simplest dispersion map. Equation 1.8 can be solved numerically or approximated solutions can be obtained by the variational or the perturbational method. Various approaches indicate that the DM soliton is quite close to a breathing Gaussian ansatz such as $A(z,\tau) = A_o exp(-(1 + iC)t^2/2t_o^2 + i\phi)$. Again, since DM solitons return to their original shapes periodically, they are also good candidates for pulses in mode-locked fiber lasers since they can satisfy the cavity boundary condition. The pulse energy of the DM soliton is much higher than that of the regular soliton. Therefore, larger pulse energy is expected from a DM soliton fiber laser than that from a soliton fiber laser.

### 1.2.3 Self-similar pulse propagation and similariton

Anderson *et al.* showed that the a sufficient condition to avoid pulse-breaking in a normally dispersive nonlinear medium is to have a pulse acquiring monotonic chirp as it propagates [7]. In a sequential work, they suggested a unique wave-breaking free solutions of the NLSE in a purely normally dispersive medium with a form of

$$\begin{cases} A(t,z) = A_o\sqrt{1-(t/t_o(z))^2}exp(ib(z)t^2) \qquad |t| < t_o(z) \\ A(t,z) = 0 \qquad |t| > t_o(z). \end{cases} \tag{1.9}$$

The pulse is a highly chirped solution with a parabolic temporal and spectral profile. This type of pulse propagates self-similarly in a normally dispersive nonlinear medium meaning that the pulse shape is maintained and it is always a scaled up version of itself. The $\Phi^{NL}$ acquired by this type of a pulse is parabolic which converts to a linear chirp in the frequency domain. Hence, even for a very large $\Phi^{NL}$, the parabolic pulse propagates without wave-breaking which is a qualitatively different feature from a soliton or a DM soliton. The discovery of self-similar propagation immediately opens the possibility of generating wave-breaking free pulses with very large pulse energies in a normal GVD fiber. Consequently, the pulse behavior in an amplifier to generate large pulse energies quickly became a subject of interest.

$$\frac{\partial A}{\partial z} + \frac{\alpha}{2}A + i\frac{\beta_2}{2}\frac{\partial^2 A}{\partial t^2} = i\gamma|A|^2A. \tag{1.10}$$

A slightly modified NLSE (Equation 1.10) with a gain term was theoretical investigated to see the pulse propagation in an amplifier. It was indeed proved that the parabolic pulses surely propagates self-similarly [8] followed by the experimentally verification in a fiber amplifier [9]. This type of a parabolic pulse is called a ‘similariton’ to emphasize a solitary-wave feature of the pulse. The analytic solution of the similariton under an amplification is given by

$$\begin{cases} A(t,z) = A_o(z)\sqrt{1-(t/t_o(z))^2}exp(ib(z,t)t^2) & |t| < t_o(z) \\ b(z,t) = b_o + 3\gamma(2\alpha)^{-1}A_o^2(z) - \alpha(6\beta_2)^{-1}t^2 \\ A_o(z) = 0.5(\alpha E_{in})^{1/3}(\gamma\beta_2)^{-1/6}exp(\alpha z/3) \\ t_o(z) = 3\alpha^{-2/3}(\gamma\beta_2)^{1/3}E_{in}^{1/3}exp(\alpha z/3). \end{cases} \tag{1.11}$$

$E_{in}$ in Equation 1.11 is the amplifier input pulse energy. The self-similar propagations of the parabolic pulse in an optical fiber and a fiber amplifier are illustrated in Figure 1.2.

Even though the similariton does not return to its original pulse profile as it propagates in the normally dispersive fiber, it is still a good candidate for pulses in mode-locked fiber lasers since the pulse does not experience wave-breaking with a self-similarly evolving pulse shape. Furthermore, since the similariton does not break up even at a very large $\Phi^{NL}$, a similariton fiber laser is expected to have much higher pulse energies. The generation of solitons, DM solitons and similaritons in fiber lasers will be covered in the next section.

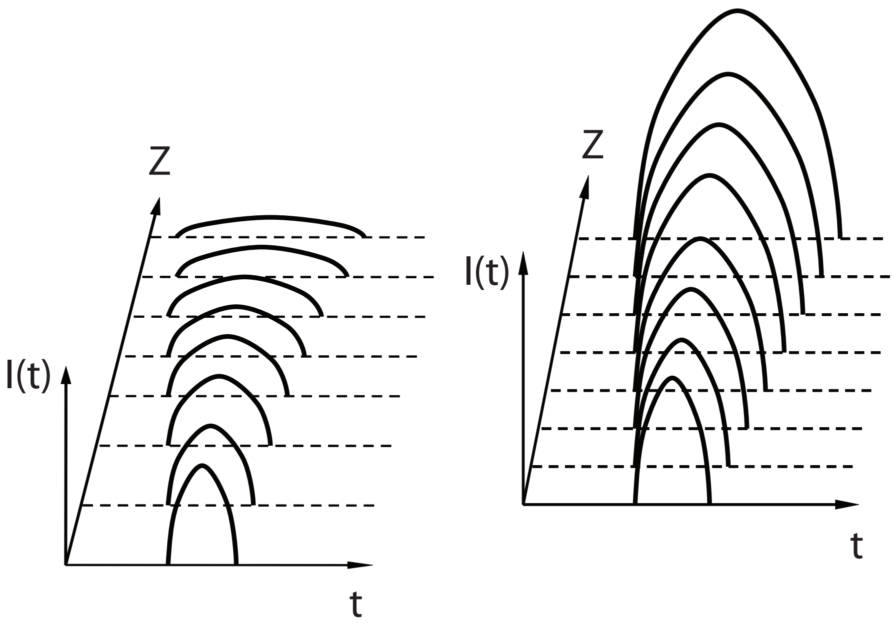

Figure 1.2: Illustration of self-similar evolution in ordinary fiber (left) or amplifier fiber (right).

## 1.3 Pulse shaping in fiber lasers

A laser is referred as mode-locked when the laser has a short pulse solution due to the phase-locking of multi-longitudinal modes of the laser cavity. The mode-locking techniques are categorized as a passive mode-locking and a active mode-locking. Passive mode-locking means that the pulse formation is due to the dynamics of pulse propagation in a resonant cavity without external (active) components to induce mode-locking. Passive mode-locking is known for shorter pulses than those of the active mode-locking. The passive mode-locking is easily achieved by a saturable absorber (SA). A SA is an element with a nonlinear loss which increases as the incident light intensity decreases (Figure 1.3). As shown in Figure 1.3, when a given noisy field profile travels through a SA repeatedly in a cavity, a pulse with a high peak intensity and a short pulse duration can be promoted by the nonlinear loss from a SA.

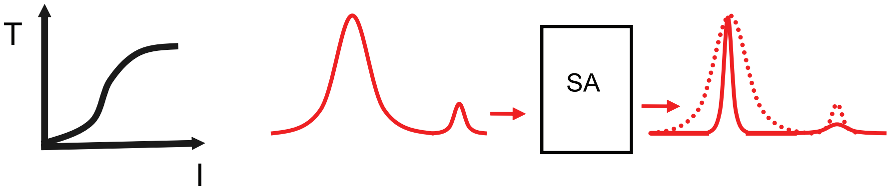

Figure 1.3: Transmittance *vs.* intensity for a saturable absorber (SA), and illustration of its effect on pulses.

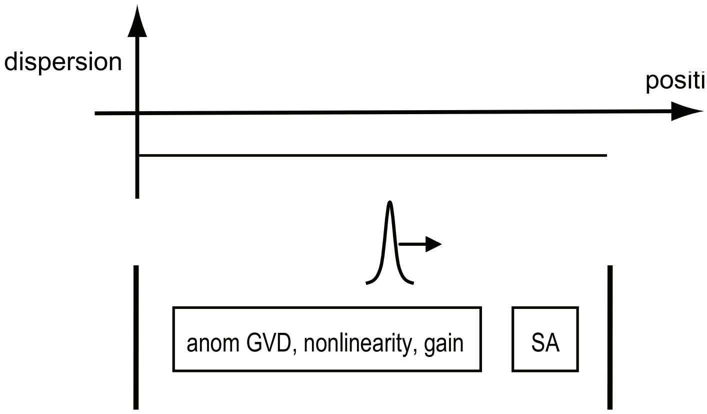

Figure 1.4: Schematic of a soliton fiber laser. The pulse is nominally constant throughout the laser.

By using an intracavity SA with an appropriate dispersion map, soliton, DM soliton and similariton pulses in a fiber laser can be realized. A soliton fiber laser [10, 11, 12] is schematically presented in Figure 1.3.

The soliton fiber laser cavity consists of an anomalously dispersive fiber, an anomalously dispersive gain fiber and a SA. A soliton, which is a natural solution of an anomalously dispersive fiber according to the NLSE, preserves its shape while it propagates in an anomalously dispersive fiber. As the soliton is amplified in a gain fiber, the pulse is not an exact soliton anymore due to the excessive energy and some possible small distortions. However, the excessive energy is coupled out of the cavity as a laser output and the SA compensate the small distortion due to the gain fiber. The SA actions is

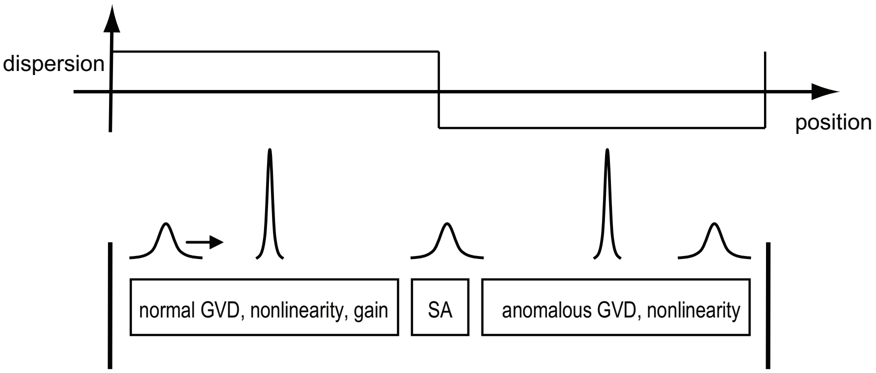

Figure 1.5: Schematic of a DM soliton fiber laser, with the corresponding dispersion map above. The pulse has maximum duration at the end of each segment of the dispersion map, and compresses to minimum duration in the center of the segment.

crucial to start the pulse in a laser but after the soliton is established in a laser, the effect of the SA becomes a small perturbation. After the SA and the laser output coupling out, the remaining pulse, which goes back into the fiber cavity, evolves into an exact soliton again. Therefore, the pulse in a soliton fiber laser is nominally constant throughout the laser except some perturbing distortions introduced by the gain and the SA. The soliton fiber lasers are stable and good for generating femtosecond pulses. However, the pulse energy in a soliton fiber laser is limited fundamentally. For a given dispersion and the pulse duration, the pulse energy is already determined by the soliton area theorem (Equation 1.5). Consequently, the typical pulse energies from fiber lasers are limited to ~0.1 nJ.

Another important pulse in a fiber laser is the DM soliton. A fiber cavity with a proper SA and a dispersion map, which consists of a normally dispersive fiber segment and an anomalously dispersive fiber segment, with close to zero net GVD can generate DM solitons. The schematic of a DM soliton fiber laser with a characteristic pulse propagation is shown in Figure 1.5.

As observed in the passive propagation of a DM soliton, the intracavity pulse evolution has local minima around mid-points of the each dispersive segment. Again, the pulse is distorted by the gain and the laser output coupling but compensated by the SA. However, their effects are not significant enough to disturb the characteristic pulse evolution of the DM soliton. The SA action is again important for the starting but again it becomes a small perturbation when the DM solitons are established in the fiber laser. The first DM soliton laser was demonstrated by Tamura *et al.* in 1993 [13]. Tamura and coworkers referred this type of a laser as a "stretched-pulse" laser emphasizing the characteristic stretched (chirped) pulse evolution. The soliton and DM soliton fiber laser are based on so-called "soliton-like" pulse shaping relying on the phase compensation due to the anomalous GVD and the positive nonlinearity. As expected from the passive propagation analysis, the pulse energy from the stretched pulse fiber laser was roughly an order of magnitude higher than that of the soliton fiber laser.

When the net cavity GVD is large normal, the soliton-like pulse shaping is not possible anymore. However, the fiber laser still can be mode-locked for various interesting modes with unique evolutions. One of those modes is the realization of the similariton in a fiber laser. The first similariton fiber laser was by Ilday et al. [14]. The pulse evolution in a similariton fiber laser is presented in Figure 1.6.

The pulse evolution in the similariton laser is qualitatively different from that in lasers with a soliton-like pulse shaping. Ilday and coworker's approach was to generate a 'Anderson' similariton in a normally dispersive fiber. Once a similariton is established in a normally dispersive fiber, the pulse propagates self-similarly with a monotonically increasing pulse duration and a linear chirp. The self-similarly evolving pulse is amplified by the gain fiber again with a linear chirp but amplified to have a higher intensity level (Figure 1.2). The SA not only shortens the pulse duration in time domain but also

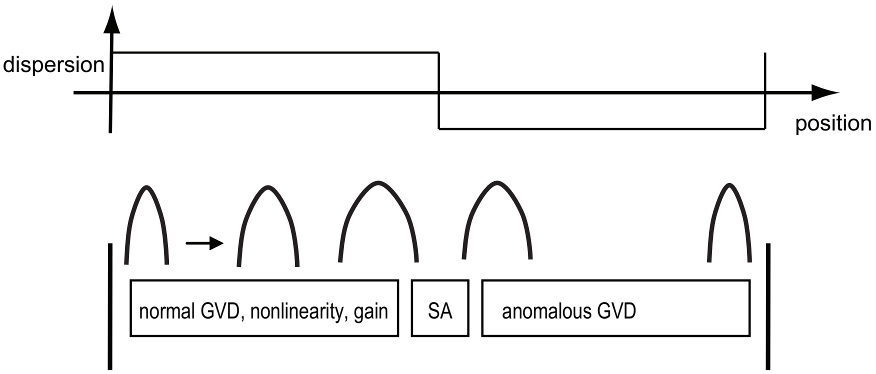

Figure 1.6: Schematic of a similariton fiber laser, with the corresponding dispersion map above. The pulse evolves self-similarly in the normal dispersion segment, and compresses in the anomalous dispersion segment. Note that the anomalous dispersion segment has no nonlinearity.

reduces the spectral BW since the pulse is highly chirped. After the SA, an anomalous dispersive delay line with negligible nonlinearity reduces the pulse duration further to go back to the original input pulse shape. Unlike the soliton-like pulse shaping, the SA still contributes heavily to stabilize the pulse evolution even after the similariton is established in the cavity . As predicted from the passive propagation analysis, the pulse energy from this kind of a laser was remarkable. The pulse energy was even compatible to that of the Ti:Sapphire at ~1 $\mu$m wavelength [15].

## 1.4 Ginzburg-Landau equation and dissipative solitons

The passive pulse propagation in a fiber can be modeled well by the NLSE. However, fiber lasers have components which cannot be modeled by several phase modulation terms in the NLSE. For example, a fiber laser has a gain with a limited gain BW and a SA. They don't induce the phase modulation but they surely cause the amplitude modulation in the frequency and the time domain. To count the amplitude modulation effects in a laser cavity properly, more terms are to be added to the NLSE. The resulting differential equation is called a cubic-Ginzburg-Landau equation (CGLE) (Equation 1.12).

$$\frac{\partial A}{\partial z} = gA + (\frac{1}{\Omega} - i\frac{D}{2})\frac{\partial^2 A}{\partial t^2} + (\alpha + i\gamma)|A|^2 A. \tag{1.12}$$

In Equation 1.12, all coefficients are averaged parameters that the pulse experiences in a round trip of the cavity. $g$ is the net gain which is the combination of the gain from the gain fiber and the loss due to the laser output coupling. $\Omega$ is related to the spectral amplitude modulation such as the gain BW or the intracavity spectral filter. $\alpha$ is the cubic intensity dependent amplitude modulation term which is related to the SA. Obviously, since all the parameters are equally distributed with respect to the propagation distance, the equation cannot model the pulse evolution in a cavity. However, the CGLE is successful to model mode-locked lasers with weak pulse-shaping [16]. The general solution of the CGLE is a chirped hyper-secant profile which is given in Equation 1.13.

$$U[t, z] = A_o \mathrm{sech}(\frac{t}{\tau}) exp(i\beta \ln(\mathrm{sech}(\frac{t}{\tau})) + i\theta z) \tag{1.13}$$

The Equation 1.12 is also called a “master equation”. Even though the solution of the master equation does not provide any information about the intracavity pulse evolution, it was successful at least to predict the qualitative trend of the lasers with a strong evolution. For example, the master equation prediction of the pulse energy *vs.* the net GVD and the pulse duration *vs.* the net GVD, which guided fiber laser researchers for many years, were moderately successful to predict the laser performance qualitatively. A typical example is achieving higher pulse energy in a higher the normal net cavity dispersion according to the master equation prediction. Motivated by the master equation prediction, researchers devoted tremendous efforts to generate higher pulse energies with large net normal cavity dispersion successfully. Detailed description of such trends can be found in Ref [16].

The solution of the CGLE can be categorized as a dissipative soliton. A dissipative soliton is a localized structures which exists for an extended period of time, even though parts of the structure experience gain and loss of energy and /or mass [17]. Dissipative solitons were found variety of physical chemical and biological systems. Since the dissipative processes (spectral filtering and saturable absorption) in Equation 1.12 are essential to form stable pulses in the fiber cavity, the solution of fiber laser system can be categorized as dissipative solitons. In contrast, when the dissipative processes are not so important for the laser pulse shaping (*i.e.* soliton and DM soliton fiber lasers ), the solutions of the lasers are closer to the solitons in conservative (Hamiltonian) systems. Due to its strong dissipative nature of the ANDi fiber laser, the pulse generated in the ANDi fiber laser definitely shows the features of dissipative solitons. In fact, the pulse generated in the ANDi fiber laser resemble the solution of a cubic-quintic Ginzburg-Landau equation (CQGLE) which is a modified version of Equation 1.12. Detailed description of the dissipative solitons in the ANDi fiber laser is presented in chapter 3.

## 1.5 Fiber laser components for amplitude modulation

A fiber laser consists of a gain fiber, a SA, a wavelength division multiplexer (WDM), a pump laser, etc. They are all important components to build a fiber laser and each of them well deserves a separate attention. However, in this thesis, the main focus will be on the components inducing dissipative processes. Owing to those components, a conservative NLSE fails to model the fiber laser appropriately while the model with a proper dissipative terms such as a CGLE becomes a better model. There are two important dissipative components to be discussed. The first component is the SA which induces a temporal amplitude modulation and the second one is the spectral filter which induces a spectral amplitude modulation. Of course, a gain fiber, which is a critical component to build a fiber laser, also induces some spectral amplitude modulation *via* gain narrowing. However, since the most of spectral filtering is due to physical spectral filters in ANDi fiber lasers, the role of the gain fiber with limited gain BW is not covered in this thesis.

### 1.5.1 Saturable absorber

As pointed out previously, a SA is an element with increasing nonlinear loss as the incident light intensity decreases. This element contributes to start and shape pulses in passively mode-locked fiber lasers. In this subsection, two SAs used in ANDi fiber lasers are briefly discussed. The first one is an artificial SA utilizing a nonlinear polarization evolution (NPE) phenomenon. The second one is a semiconductor saturable absorbing mirror (SESAM).

#### Nonlinear polarization evolution

Utilizing the nonlinear polarization evolution (NPE) conjunction with a polarizer, which was once referred as an ‘artificial’ SA, is a widespread SA scheme in fiber lasers. The NPE occurs due to the self-phase modulation (SPM) and the cross-phase modulation (XPM) of two orthogonally polarized light components. The NPE can be understood by considering how the circular polarization modes $E_{\pm} = E_x \pm iE_y$ evolve nonlinearly. By performing a lengthy Jones matrix algebra, it can be shown that the polarization is rotated in a Kerr ($\chi_3$) medium by angle $\Delta\phi$ without changing the shape. The rotation

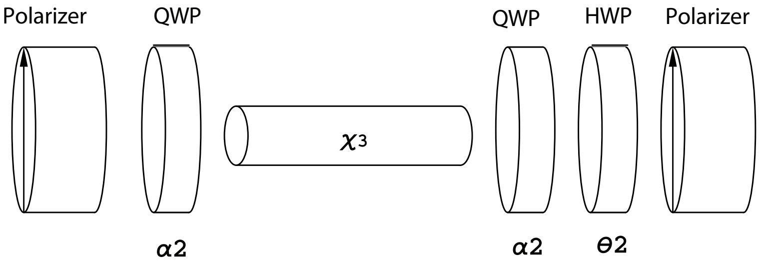

Figure 1.7: Schematic of a NPE conjunction with a polarizer; QWP: quarter-waveplate, HWP: half-waveplate, $\alpha_1$, $\alpha_2$ and $\theta_2$ are angles between the principle axis of the waveplates with respect to the polarizer axis respectively.

angle $\Delta\phi$ is governed by Equation 1.14.

$$\Delta\phi = \frac{\gamma L}{3}(|E_+|^2 - |E_-|^2). \tag{1.14}$$

Note that for linearly polarized cases ($|E_+|^2 = |E_-|^2$), the polarization rotation does not occur. Figure 1.7 shows a typical NPE port used in fiber lasers. After the polarizer, quarter waveplate evolves the linear polarization into the elliptical polarization. The elliptically polarized light experiences NPE to rotate its polarization orientation in a Kerr medium. A half and a quarter waveplate at the end of the Kerr medium adjust the polarization to match the axis of the second polarizer.

By performing some matrix algebra, one can show that the outgoing normalized intensity of the second polarizer becomes as follows.

$$I = \frac{1}{2}[1 - sin(2\alpha_1)sin(2\alpha_2) + cos(2\alpha_1)cos(2\alpha_2)cos(2(\alpha_1 + \alpha_2 - 2\theta_2 + \Delta\phi))]. \tag{1.15}$$

The output intensity is an intrinsic function of the filed intensity since $\Delta\phi$ is a function of the field intensity. The output intensity is not a monotonically increasing function with respect to the input filed intensity but it has some complicated sinusoidal feature due to $cos(2(\alpha_1 + \alpha_2 - 2\theta_2 + \Delta\phi)$ term. By putting waveplates at proper angles, the NPE port can selectively transmit higher intensity to act just like a SA. The NPE port as a saturable absorber was proposed by Hofer *et al.* [18]. The given NPE port configuration (Figure 1.7), which is the standard configuration for the experiments presented in this theses, is not the only possible NPE port configuration. Other configurations are discussed thoroughly in Ref [19].

### Semiconductor saturable absorbing mirror

Another important SA used in experiments is a SESAM. A SESAM consists of a Bragg-mirror on a semiconductor wafer with a saturable absorbing semiconductor material. Important parameters of the SESAM for the fiber laser design are the recovery time, the modulation depth, the spectral BW, and the saturation intensity. For a fast saturable absorber with a response time much shorter than the pulse duration, the reflection of the SESAM can be modeled by Equation 1.16.

$$R = 1 - T_o/(1 + \frac{|A(t)|^2}{P_{sat}}). \tag{1.16}$$

Where $T_o$ is the transmission at low intensity ($|A(t)|^2$=0) and $P_{sat}$ is the saturation energy. Commercially available SESAMs with high modulation depth and fast response time [20] motivated researchers to build a variety of fibers lasers with SESAMs recently. For a broader overview of SESAMs see [20].

### 1.5.2 Spectral filter

The spectral filter, which induces spectral amplitude modulation, is again an important component to generate dissipative solitons in fiber lasers. Important spectral filters used in experiments are interference, birefringence, and birefringence fiber loop filter.

#### Interference filter

An interference filter is a device that reflects spectral bands and transmits others. There are various kind of interference filters such as high-pass, low-pass, and band-pass filters. In this thesis, a band-pass interference filter, which is used in ANDi fiber lasers, is discussed. The band-pass (narrow-band) interference filters selectively transmit spectral components owing to the interference effects between the incident and reflected waves in a the Fabry-Perot interferometer. The simplest structure of the band-pass interference filter is shown in Figure 1.8.

The incident wave is resonantly reflected back and forth between two partially reflective dielectric walls. For a given optical distance between the dielectric walls, selective component of the wavelength pass through the filter without much loss due to the constructive interference of the incident and reflective waves. Other components will be attenuated due to the destructive interference. Consequently, the Fabry-Perot interferometer in Figure 1.8 works as a spectral filter which selectively passes desired spectral components.

When the incident angle is increased, the center wavelength of the spectral filter transmission curve is tuned according to following Equation 1.17.

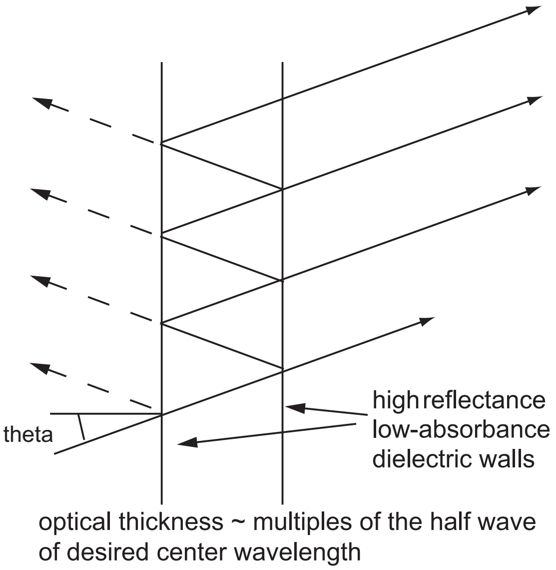

Figure 1.8: Schematic of a Fabry-Perot band-pass (narrow-band) interference filter

$$\lambda_c = \lambda_o \sqrt{(1 - \frac{sin^2\theta}{n^2})}. \tag{1.17}$$

$\theta$ is the incident angle, $\lambda_c$ is the center wavelength of the filter transmission curve, $\lambda_o$ is the filter center wavelength at $\theta$=0 (normal incidence), and $n$ is the refractive index of the material between dielectric walls. The tuned center wavelength is always shorter than $\lambda_o$.

In general, it is tough for interference filters to generate filtering curves matching mathematically well-known functions such as a Gaussian, a parabolic, etc. Figure 1.9 shows a measured transmission curve of a typical interference filter ($\lambda_o$=1030nm, BW=10 nm). With such a structured transmission curve, it is hard to predict how the intracavity interference filter affects the laser performance. The filter also introduces an appreciable loss which also degrades the laser performance. For example, the measured filter peak transmission is ~ 60%.

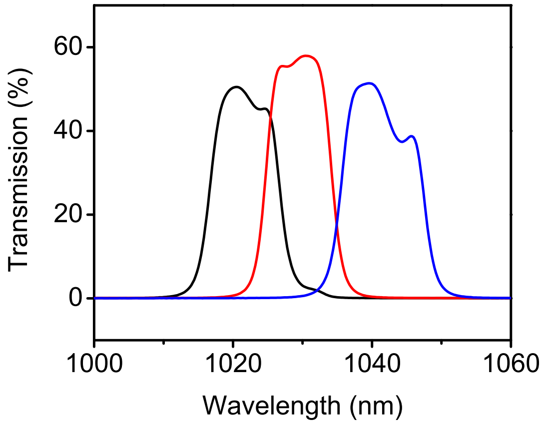

Figure 1.9: Measured transmission of interference filters (the center wavelength of 1020, 1030, and 1040 nm with ~10 nm BW)

### Birefringence filter

The polarization of the wave is evolved in a strong birefringence material due to the phase shift between the ordinary wave (o-wave) and the extraordinary wave (e-wave). This polarization evolution is a strong function of the wavelength. By putting a polarizer, a combination of a birefringence material and a polarizer will act as a spectral filter by transmitting certain wavelength selectively. This type of a spectral filter is referred as a birefringence filter. The spectral filtering mechanism works as follows. In a birefringence medium, the phase shift ($\Delta\phi$) can be expressed as a function of the wavelength and the index difference between the o-wave and the e-wave as follows.

$$\Delta\phi = \frac{2\pi}{\lambda}(n_e - n_o)d. \tag{1.18}$$

If a linearly polarized light has a 45 degrees of incidence angle with respect to the principle axes of the birefringence medium, intensity will be contributed equally in the

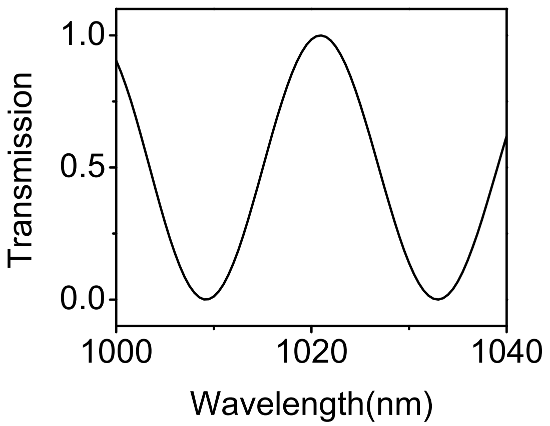

Figure 1.10: Calculated spectral transmission curve for a birefringence filter with d=5 mm

o-axis and the e-axis. By putting a linear polarizer, transmission through the polarizer becomes a function of $\Delta\phi$ such as

$$T = cos^2(\Delta\phi/2). \tag{1.19}$$

The resulted transmission curve is a sinusoidal curve of a cosine squared function. For a real case of a quartz birefringence plate ($n_o$=1.53514,$n_e$=1.54392 at ~1 $\mu$m), which is the material used to build a birefringence filter in experiments, one can theoretically calculate the transmission curve of the spectral filter (Figure 1.10) which matches the experimentally measured transmission curve. For example, for a quartz plate with a 5 mm thickness, calculated spectral filtering BW is ~12 nm (Figure 1.10) while the measurement shows an almost exact match (Figure 1.11). A birefringence filter has a smooth transmission curve which can be modeled as a cosine squared function very accurately.

Theoretically, the spectral filter BW decreases inversely proportional to the bire-

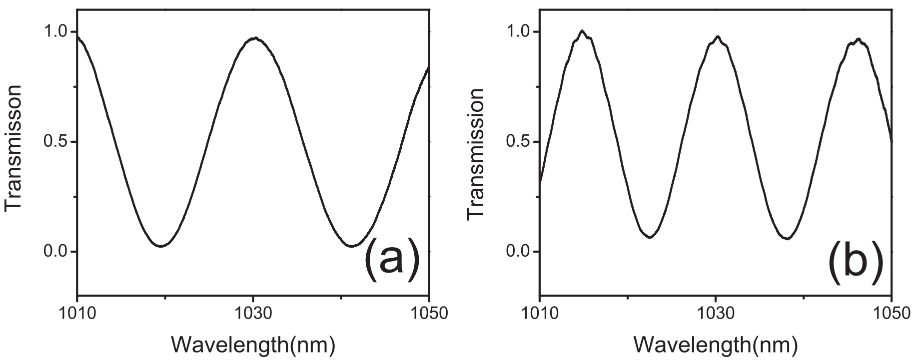

Figure 1.11: Measured birefringence filter transmission with a) d=5 mm and b) 7.5 mm

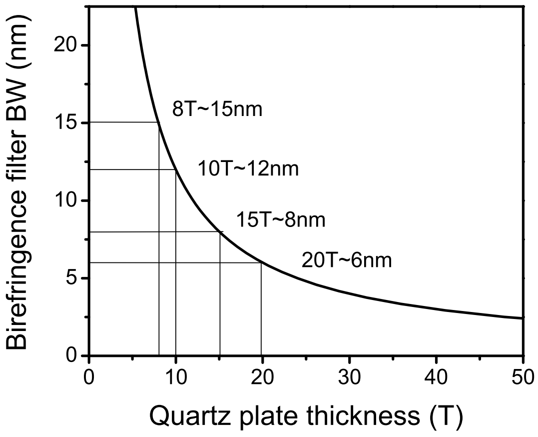

Figure 1.12: Measured birefringence filter BW *vs.* the thickness of the quartz plate. The $\sim 1/\lambda$ line is the best fitting to the measured data. (1T~0.5 mm)

fringence plate thickness. Measured BW with varying birefringence plate thickness confirms the inverse proportionality.

Clever combinations of birefringence plates and polarizers such as a Lyot filter and a Solc filter can generate various combinations of the BW and the free spectral range (FSR). For detailed analysis of the birefringence filter including a Lyot filter, please see Ref [21]. For Solc filters, Ref [22] covers the subject thoroughly. The center wavelength

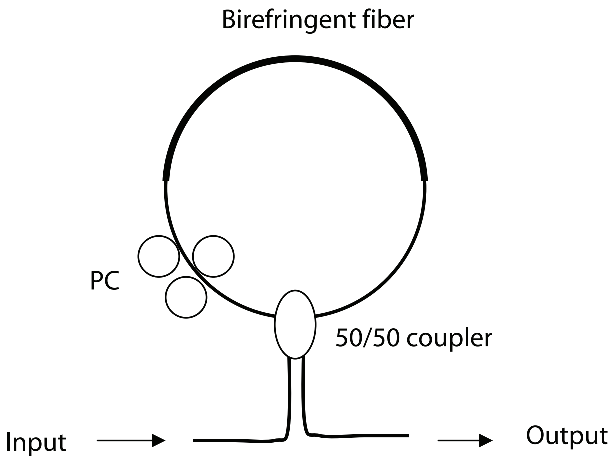

Figure 1.13: Schematic of a birefringence fiber loop filter; PC: polarization controller

of the filter can be tuned easily by adjusting the birefringence plate orientation [23].

### Birefringence fiber loop filter

A fiber-format birefringence filter provides a unique possibility of building an all-fiber integrated ANDi fiber laser. By combining a Sagnac interferometer and a piece of a strongly birefringent fiber, an interesting spectral filter which is referred as a birefringence fiber loop filter can be composed. Figure 1.13. shows the schematic of a birefringence fiber loop filter. This type of a filter can be built easily with a commercially available 50/50 fiber coupler, a polarization controller (PC) and a piece of a highly birefringent fiber such as a polarization maintaining (PM) fiber.

By performing a lengthy Jones matrix algebra conjunction with solving a mode-coupling equation in the 50/50 fiber coupler, it can be shown that the output intensity is wavelength dependent. The output intensity satisfy the relationship in Equation 1.20 [24].

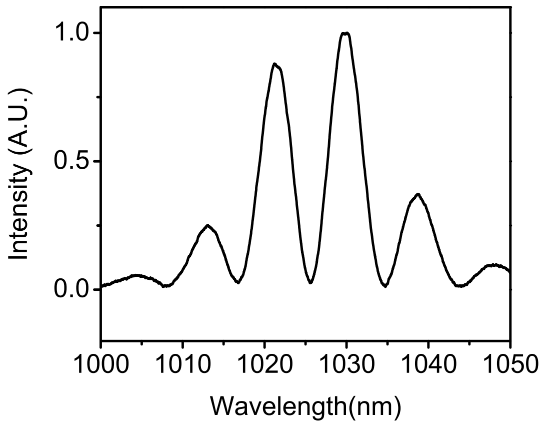

Figure 1.14: Amplified spontaneous emission filtered by a birefringence fiber loop filter

$$I = I_o sin^2(\delta/2). \tag{1.20}$$

$\delta$ is the linear birefringence of the birefringent fiber. Because the linear birefringence is inversely proportional to the wavelength, the filter BW ($\Delta\lambda$) is

$$\Delta\lambda = (2\pi\lambda)/\delta. \tag{1.21}$$

The spectral filter BW is inversely proportional to the linear birefringence. The center wavelength can be easily tuned by adjusting the PC. Since the device is in a fiber format, loss will be much less than that of the bulk type birefringence filter.

Figure 1.14 shows a spectrally filtered amplified spontaneous emission of a Yb-doped fiber. ~25 cm of Corning's PM 980 was used in a birefringence fiber loop filter. The measured BW is ~4.4 nm. Based on measured values, calculated beat length of the PM fiber is ~1.06 mm which roughly matches the manufacturer specification [25].

# BIBLIOGRAPHY

[1] R. W. Boyd, *Nonlinear Optics, 2nd Ed.* (Academic, New York, 2003).

[2] G. P. Agrawal, *Nonlinear Fiber Optics, 2nd Ed.* (Academic, New York, 1995).

[3] W. P. Zakharov, and A. B. Shabat, Sov. Phys. JETP **34**, 62 (1972).

[4] L. F. Mollenauer, R. H. Stolen, and J. P. Gordon, Phys. Rev. Lett. **45**, 1095 (1980).

[5] M. Suzuki, I. Morita, N. Edagawa, S. Yamamoto, H. Taga, and S. Akiba, Electron. Lett. **31**, 2027 (1995).

[6] L. F. Mollenauer, and J. P. Gordon, *Solitons in optical fibers fundamentals and applications* (Academic press, San Diego, CA, 2006).

[7] D. Anderson, M. Desaix, M. Karlsson, M. Lisak, and M. L. Quiroga-Teixeiro, J. Opt. Soc. Am. B **10**, 1185 (1993).

[8] V. I. Kruglov, A. C. Peacock, J. M. Dudley, and J. D. Harvey, Opt. Lett. **25**, 1753 (2000).

[9] M. E. Fermann, V. I. Kruglov, B. C. Thomsen, J. M. Dudley, and J. D. Harvey, Phys. Rev. Lett. **84**, 6010 (2000).

[10] K. Suzuki, M. Nakazawa, and H. A. Haus, Japanese J. of Appl. Phys., Part 2: Letters, **28**, 256 (1989).

[11] D. J. Richardson, R. I. Laming, D. N. Payne, M. W. Phillips, and V. J. Matsas, Electron. Lett., **27**, 730 (1991).

[12] I. N. Duling III, Opt. Lett. **16**, 539 (1991).

[13] K. Tamura, J. Jacobson, H. A. Haus, E. P. Ippen, and J. G. Fujimoto, Opt. Lett. **18**, 1080 (1993).

[14] F. Ö. Ilday, J. R. Buckley, W. G. Clark, and F. W. Wise, Phys. Rev. Lett. **92**, 213902 (2004).

[15] J. R. Buckley, F. O. Ilday, T. Sosnowski, and F. W. Wise, Opt. Lett. **30**, 1888 (2005).

[16] H. A. Haus, J. G. Fujimoto, and E. P. Ippen, J. Opt. Soc. Am. B **8**, 2068 (1991).

[17] *Dissipative Solitons*, edited by N. Akhmediev and A. Ankiewics (Springer, Berlin, 2005).

[18] M. Hofer, M. H. Ober, F. Haberl, and M. Fermann, IEEE J. Quantum Electron., **28**, 720, (1992).

[19] K. Tamura, "Additive pulse mode-locked Erbium-doped fiber lasers," Ph.D. dissertation (MIT, 1996).

[20] www.batop.com.

[21] J. W. Evans, J. Opt. Soc. Am. **39**, 229 (1949).

[22] J. W. Evans, J. Opt. Soc. Am. **48**, 142 (1958).

[23] J. Mentel, E. Schmidt, and T. Mavrudis, Appl. Opt. **31**, 5022 (1992).

[24] X. Fang and R. O. Claus, Opt. Lett. **20**, 2146 (1995).

[25] www.corning.com.

CHAPTER 2

# ALL-NORMAL-DISPERSION (ANDi) FIBER LASERS[1]

This chapter describes a fiber laser with only normally dispersive elements, which referred as an all-normal dispersion (ANDi) fiber laser, with a unique pulse shaping mechanism. The pulse shaping mechanism of a chirped pulse spectral filtering is clearly different from the conventional pulse shaping mechanisms of soliton, DM soliton and similariton fiber lasers. Various ANDi fiber lasers with a variety of spectral filters and gain fibers are presented.

## 2.1 Introduction

The need to compensate group-velocity dispersion (GVD) is ubiquitous in femtosecond pulse generation and propagation. Prisms [2], diffraction gratings [3], and chirped mirrors [4] have all been used to compensate or control GVD. Reliable femtosecond lasers had to await the development of a low-loss means of introducing controllable GVD [2]. Pulse formation in modern femtosecond lasers is dominated by the interplay between nonlinearity and dispersion [5, 6]. In all cases of practical interest, a positive (self-focusing) nonlinearity is balanced by anomalous GVD. The need to compensate normal GVD in the laser, along with the balance of nonlinearity in soliton-like pulse shaping, underlies the presence of anomalous GVD in femtosecond lasers.

Most femtosecond lasers have segments of normal and anomalous GVD, so the cavity consists of a dispersion map, and the net or path-averaged cavity dispersion can be normal or anomalous. With large anomalous GVD, soliton-like pulse shaping produces short pulses with little chirp. Some amplitude modulation is required to stabilize the

---

[1] Most of the results presented in this chapter have been published in Ref [1]

pulse against the periodic perturbations of the laser resonator. Pulse formation and pulse evolution become more complex as the cavity GVD approaches zero, and then becomes normal. The master-equation treatment of solid-state lasers, based on the assumption of small changes of the pulse as it traverses cavity elements, shows that stable pulses can be formed with net normal GVD [6]. Nonlinear phase accumulation, coupled with normal GVD, chirps the pulse. The resulting spectral broadening is balanced by gain-narrowing. By cutting off the wings of the spectrum, gain dispersion shapes the temporal profile of the chirped pulse. Proctor *et al.* showed that the resulting pulses are long and highly-chirped [7], as predicted by the analytic theory [6]. Stable pulse trains can even be produced without dispersion compensation, but the output pulses are picoseconds in duration and deviate substantially from the Fourier-transform limited duration, even after dechirping with anomalous GVD external to the cavity.

Fiber lasers can be constructed entirely of fiber with anomalous GVD, to generate solitons as short as ~200 fs in duration. However, the pulse energy is restricted by the soliton area theorem and spectral sidebands [8] to ~0.1 nJ. Much higher energies are obtained when the laser has segments of normal and anomalous GVD. In general, the pulse breathes (*i.e.*, the pulse duration varies periodically) as it traverses the cavity. Dispersion-managed solitons are observed as the net GVD varies from small and anomalous to small and normal [9], and self-similar [10] and wave-breaking-free [11] pulses are observed with larger normal GVD. The large changes in the pulse as it traverses the laser preclude an accurate analytical treatment, so numerical simulations are employed to study these modes. Among fiber lasers, Yb-based lasers have produced the highest femtosecond-pulse energies, recently reaching 15-20 nJ [12]. The normal GVD of single-mode fiber (SMF) around 1 $\mu$m wavelength has been compensated by diffraction gratings, which detract from the benefits of the waveguide medium.

With the goal of building integrated fiber lasers, microstructure fibers [13, 14] and fiber Bragg gratings [15] have been implemented to compensate dispersion at 1 $\mu$m. However, performance is sacrificed compared to lasers that employ diffraction gratings. From a practical point of view, it would be highly desirable to design femtosecond-pulse fiber lasers without compensation of the GVD of several meters of fiber. However, to our knowledge there is no prior report of any laser that generates ~100-fs pulses without elements that provide anomalous GVD in the cavity.

Recently, Buckley *et al.* showed that the introduction of a frequency filter stabilizes mode-locked operation of a Yb-doped fiber laser with normal cavity GVD (~0.015 $ps^2$), which allows the routine generation of 15-nJ pulses as short as 55 fs [16]. The frequency filter produces self-amplitude modulation, which allows nonlinear polarization evolution (NPE) to be biased for higher pulse energies. By altering the laser cavity to operate at large normal GVD (0.04 - 0.10 $ps^2$), the frequency filter was found to stabilize mode-locked operation characterized by highly chirped, nearly static pulses as predicted by the theory of self-similar lasers [10]. Although Buckley *et al.* succeeded in enhancing the stability of mode-locking at large normal GVD, the laser still required some dispersion compensation with a grating pair.

Here we describe a femtosecond fiber laser with a cavity consisting only of elements with normal GVD. By increasing the nonlinear phase shift accumulated by the pulse and inserting a spectral filter in the cavity, self-amplitude modulation *via* spectral filtering is enhanced. The laser generates chirped picosecond pulses, which are dechirped to 150-300 fs outside the laser. These results are remarkable considering that the cavity consists of ~10 characteristic dispersion lengths of fiber with respect to the dechirped pulse, yet no dispersion control is provided. The pulse energy is 1-3 nJ, and the laser is stable and self-starting. The laser is thus a first step in a new approach to mode-locking.

## 2.2 Design rationale and numerical simulations

The design of a femtosecond fiber laser without dispersion control in the cavity exploits the understanding gained by the recent work of Buckley *et al.* [16]. The master-equation analysis does not apply quantitatively to fiber lasers, but we are guided qualitatively and intuitively by its predictions. The key elements of such a laser (Figure 2.1(a)) are a fairly long segment of SMF, a short segment of gain fiber, a segment of SMF after the gain fiber, and components that produce self-amplitude modulation. A significant nonlinear phase shift is impressed on the pulse in the SMF that follows the gain, and NPE converts the differential phase shift to amplitude modulation. Numerical simulations show that stable solutions do exist in such a laser, for a reasonable range of parameters. The gain bandwidth has a major influence on the pulse evolution. With large gain bandwidth (BW) (>~30 nm), approximately parabolic pulses evolve as in a self-similar laser [10]. As the BW is reduced to ~10 nm, the spectrum develops sharp peaks on its edges, and for narrower bandwidths the solutions do not converge.

Results of simulations with 10-nm gain bandwidth and 2-nJ pulse energy are shown in Figure 2.1. The pulse duration increases monotonically in the SMF, and then decreases abruptly in the gain fiber. In the second segment of SMF the pulse duration increases slightly, before dropping again owing to the NPE. The spectrum (Figure 2.1(b)) exhibits a characteristic shape, with sharp peaks near its steep edges. The pulse is highly-chirped throughout the cavity, with the duration varying from ~10 to ~20 times the transform limit (Figure 2.1(c)).

The simulations show that spectral filtering of a strongly phase-modulated pulse can produce substantial amplitude modulation under realistic conditions. With additional amplitude modulation from NPE, stable solutions exist. The pulse is highly-chirped

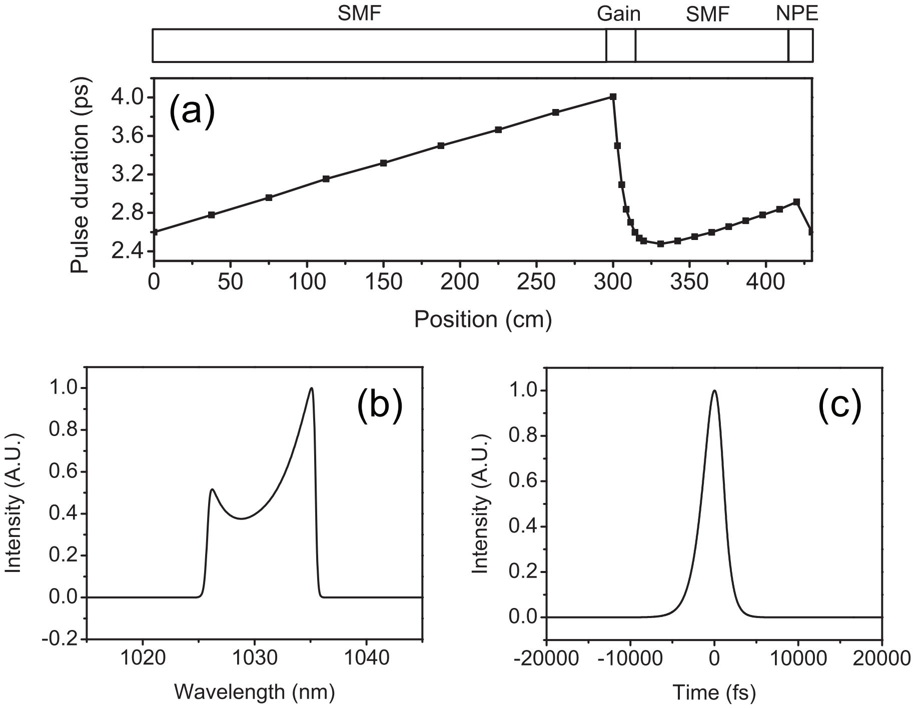

Figure 2.1: Numerical simulation result: a) Numerically simulated pulse evolution of the laser. A ring cavity is assumed, so the pulse enters the first SMF after the NPE. Results of numerical simulations are shown on the bottom. Power spectrum (b) and temporal intensity profile (c) after the second SMF.

inside the cavity, but the phase is roughly parabolic near the peak of the pulse, so the pulse can be dechirped outside the laser. The pulse shaping mechanism of this type of a laser is based on the chirped pulse spectral filtering (CPSF). For a highly chirped pulse, the spectrum is mapped to the time domain. When a highly chirped pulse is spectrally filtered, the time pulse is also shortened. The process is illustrated in Figure 2.2.

In the previous simulation, the spectral filtering relies on a strong gain narrowing effect which is not realistic. The realistic gain narrowing effect is not be strong enough to have a stable mode-locked operation in this particular case. By inserting a spectral filter in the cavity, one can adjust the spectral filtering strength to obtain stable mode-locked operations. By inserting an appropriate spectral filter with realistic gain BW

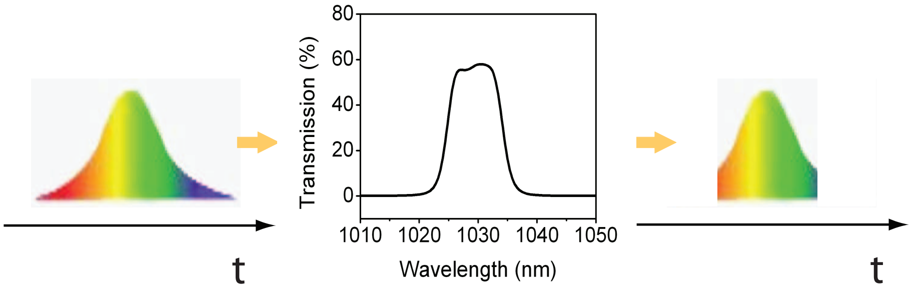

Figure 2.2: Pulse-shaping by spectral filtering of a highly-chirped pulse, in which frequency is mapped to time.

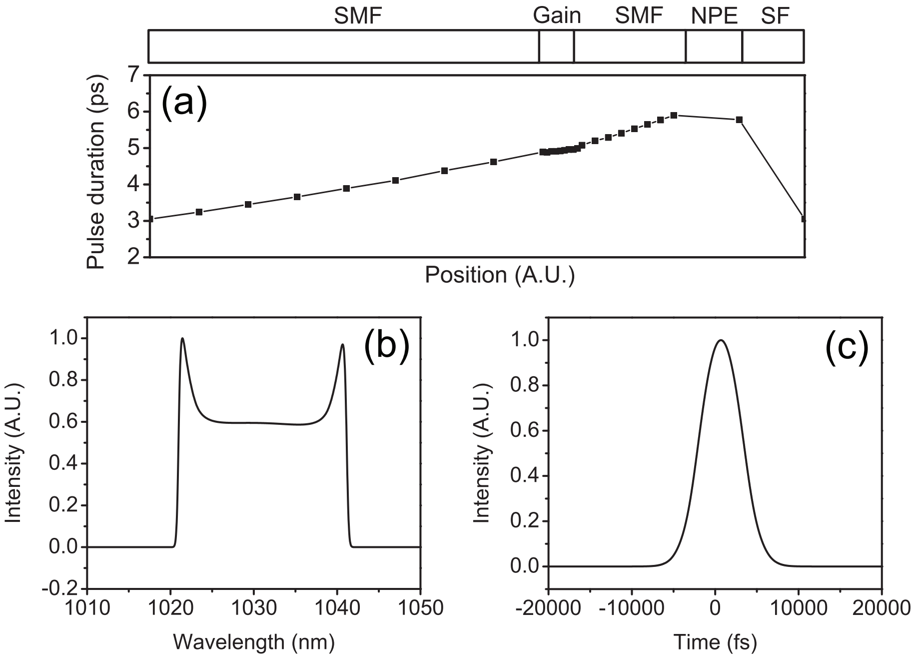

Figure 2.3: Numerical simulation result: a) Numerically simulated pulse evolution of the laser. Results of numerical simulations are shown on the bottom. Power spectrum (b) and temporal intensity profile (c) after the second SMF; SF: spectral filter.

of the gain, the numerical simulation again shows stable mode-locked laser operations. The pulse evolution with an intracavity spectral filter is shown in Figure 2.3. The gain BW is set at ~40 nm which is close to the realistic gain BW of Yb-doped fibers. A Gaussian spectrum filter (~12 nm BW) is inserted at the end of the second SMF.

The laser produces results similar to Figure 2.1 with some noticeable differences in the pulse evolution ( Figure 2.1(a) and Figure 2.3(a)). The output spectrum shows similar characteristic shape with sharp peaks near its edges. It is clear that the pulse amplitude modulation is not mainly due to the gain narrowing. The pulse duration drops abruptly not in the gain fiber but in the spectral filter. The spectral filter BW in this laser can be adjusted conveniently to observe different operating modes.

## 2.3 Experimental results

### 2.3.1 Interference filter

The numerical simulations offer a guide to the construction of a laser without anomalous dispersion. The laser (shown schematically in Figure 2.4) is similar to the Yb fiber laser of Lim *et al.* [17], but without the grating pair that provides anomalous GVD in earlier designs. The fiber section consists of ~3 m of SMF and 20 cm of highly-doped Yb gain fiber, followed by another ~1 m of SMF. Gain fiber with a 4-$\mu m$ core diameter (which is smaller than the 6-$\mu m$ core of SMF) was chosen to increase self-phase modulation (SPM) in the gain fiber. A 980-nm laser diode delivers ~350 mW into the core of the gain fiber. NPE is implemented with quarter-waveplates, a half-waveplate, and a polarizing beamsplitter. The output of laser is taken directly from the NPE ejection port.

An interference filter centered at 1030 nm, with 10 nm bandwidth, is employed. The optimum location for the filter is not clear. Placing it after the gain or second SMF segment would maximize the amplitude modulation from spectral filtering and correspond most closely to the simulations described above. However, we also want to output the broadest spectrum and the largest pulse energy, to achieve the shortest and

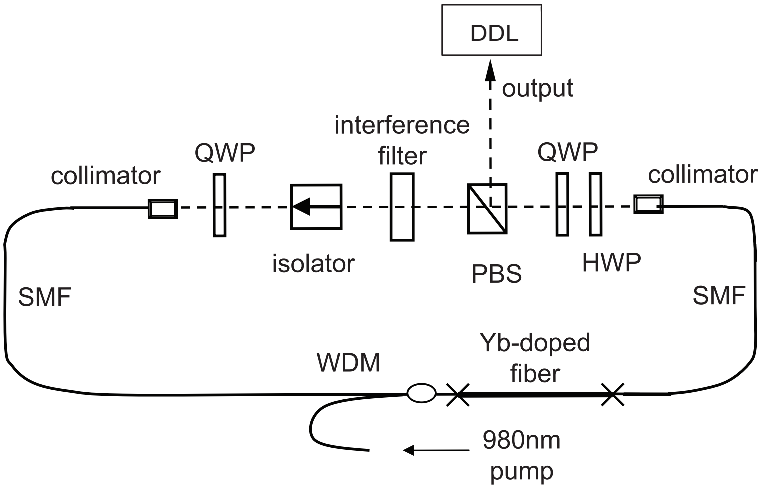

Figure 2.4: Schematic of ANDi fiber laser with a interference filter: QWP: quarter-waveplate; HWP: half-waveplate; PBS: polarizing beam splitter; WDM: wavelength-division multiplexer; DDL: dispersion delay line.

most intense pulse. Considering these factors, we placed the filter after the beam splitter. This location also allows as much of the laser to be spliced together as possible. The total cavity dispersion is ~0.1 $ps^2$.

The threshold pump power for mode-locking is ~300 mW. Self-starting mode-locked operation is achieved by adjustment of the waveplates. The laser produces a stable pulse train with 45 MHz repetition rate. Although the continuous-wave output power can be as high as ~200 mW, in mode-locked operation the power is limited to 120 mW, which corresponds to a pulse energy of ~3 nJ. Stable single-pulsing is verified with a fast detector down to 500 ps, and by monitoring the interferometric autocorrelation out to delays of ~100 ps. Also, the spectrum is carefully monitored for any modulation that would be consistent with multiple pulses in the cavity. Remarkably, there is no evidence of multi-pulsing at any available pump power. However, with a single pump diode the pump power only exceeds the mode-locking threshold by ~20%.

Typical results for the output of the laser are shown in Figure 2.5. The spectrum

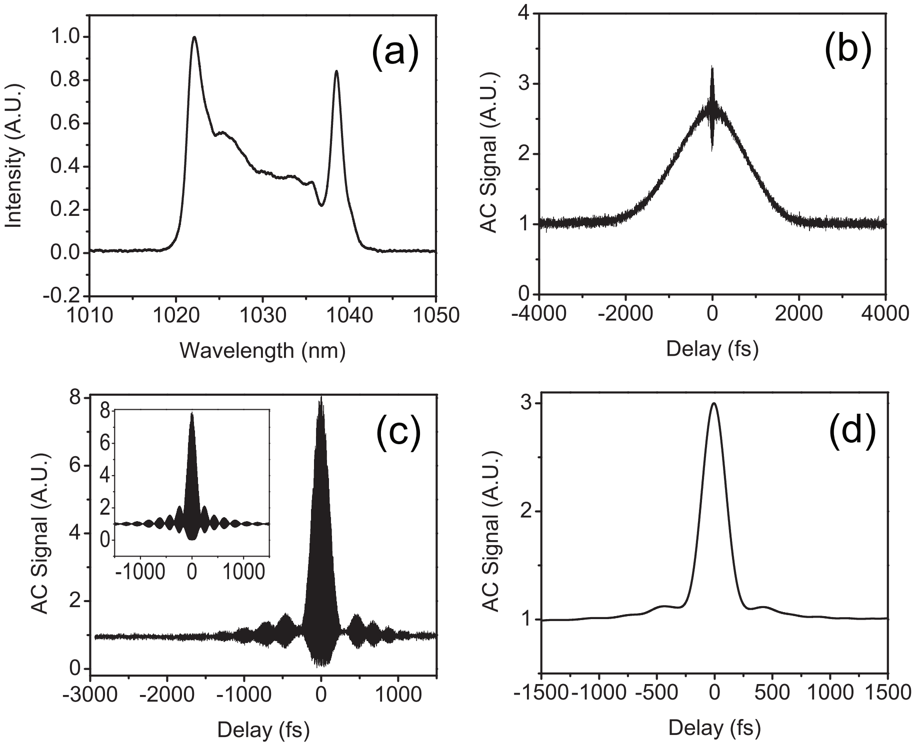

Figure 2.5: Output of the laser: a) spectrum, b) interferometric autocorrelation of the output, c) interferometric autocorrelation of dechirped pulse and the interferometric autocorrelation of zero-phase Fourier-transform of the spectrum (inset), d) intensity autocorrelation of the dechirped pulse.

(Figure 2.5(a)) is qualitatively similar to the simulated spectrum (Figure 2.1(b)) and is consistent with significant SPM within the cavity. The laser generates ~1.4-ps chirped pulses (Figure 2.5(b)), which are dechirped to 170 fs (Figure 2.5(c and d)) with a pair of diffraction gratings outside the laser. The dechirped pulse duration is within ~16% of the Fourier-transform limit (Figure 2.5(c) inset). The interferometric autocorrelation shows noticeable side-lobes, which arise from the steep sides and structure of the spectrum. Nevertheless, these amount to only ~10% of the pulse energy. The output pulse energy is ~2.7 nJ, and after dechirping with lossy gratings the pulse energy is ~1 nJ. Pulse energies of 2 nJ could be obtained by dechirping with high-efficiency gratings or photonic-bandgap fiber. The laser is stable and self-starting. In addition to verifying as carefully as possible that the laser is not multi-pulsing, we compared the pulse peak power to that of a fully-characterized femtosecond laser available in our lab. Within the experimental uncertainties, the two-photon photocurrent induced by the all-normal-dispersion laser scales correctly with the nominal peak power, which is ~5 kW.

The behavior of the laser depends critically on the spectral filter: without it, stable pulse trains are not generated. By rotating the spectral filter to vary the center wavelength, either of the sharp spectral features can be suppressed, which may slightly improve the pulse quality. When the spectrum changes, the magnitude of the chirp on the output pulse can change substantially: the pulse duration varies from approximately 1 to 2 ps. With standard femtosecond Yb-doped fiber lasers, mechanical perturbation of the fiber extinguishes mode-locking. In the laser described here, we find that it is possible to touch and move the fiber without disrupting mode-locking, which indicates that NPE plays a reduced role in pulse-shaping. The simulations (*e.g.*, Figure 2.1) show that the role of NPE is reduced compared to a laser with a dispersion map, but it is still crucial to the generation of stable pulses.

### 2.3.2 Birefringence filter

With a same experimental setup, inserting a birefringent (quartz) plate between polarization sensitive components such as the PBS and the isolator consist a birefringence filter. The birefringent plate is inserted at ~Brewster's angle to minimize the reflection. The birefringence filter used in this particular experiment has ~12 nm BW with a quartz plate with ~6 mm thickness. Figure 2.6 shows the schematics of the experimental setup.

By adjusting waveplates, stable, self-starting mode-locked operations are obtained. Unlike the laser with the interference filter which shows limited numbers of modes, this

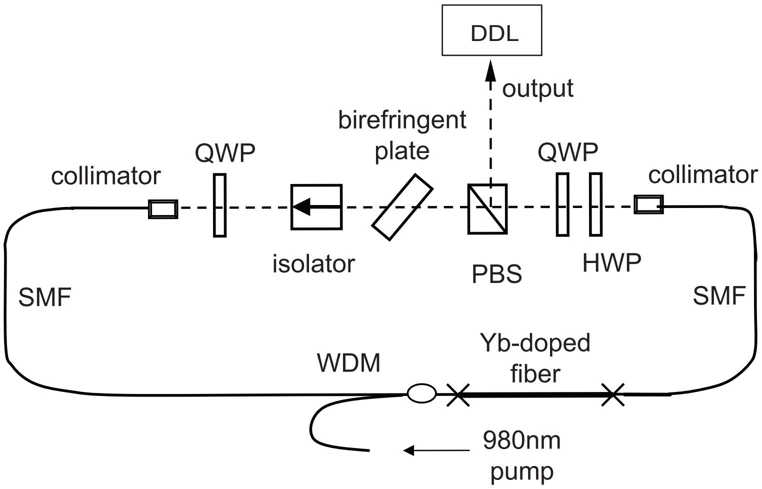

Figure 2.6: Schematic of ANDi fiber laser with a birefringence filter: QWP: quarter-waveplate; HWP: half-waveplate; PBS: polarizing beam splitter; WDM: wavelength-division multiplexer; DDL: dispersion delay line.

laser can generate many different modes even continuously. Figure 2.7 shows continuously evolving modes by adjusting one of the waveplates. The middle column of the Figure 2.7 shows the corresponding dechirped interferometric ACs while the right column shows the theoretically calculated interferometric ACs os the zero-phase Fourier-transform of the spectrum.

The experimental result shows that the pulses can be dechirped quite close to the Fourier-transform limited pulse (within ~10 %). The pulse energy is ranged 2~3 nJ with the pulse duration varies from 150 to 270 fs. As the pulse evolves continuously due to the waveplate tuning, the pulse energy, the dechirped pulse duration, and the chirping follow certain recognizable trends. The details of the trends will be covered in the next chapter.

It was found that modes from the laser with a birefringence filter has the best matching to numerical simulations owing to its clean predictable spectral filtering curve. For example, modes presented in Figure 2.7 were quite predictable from numerical simula-

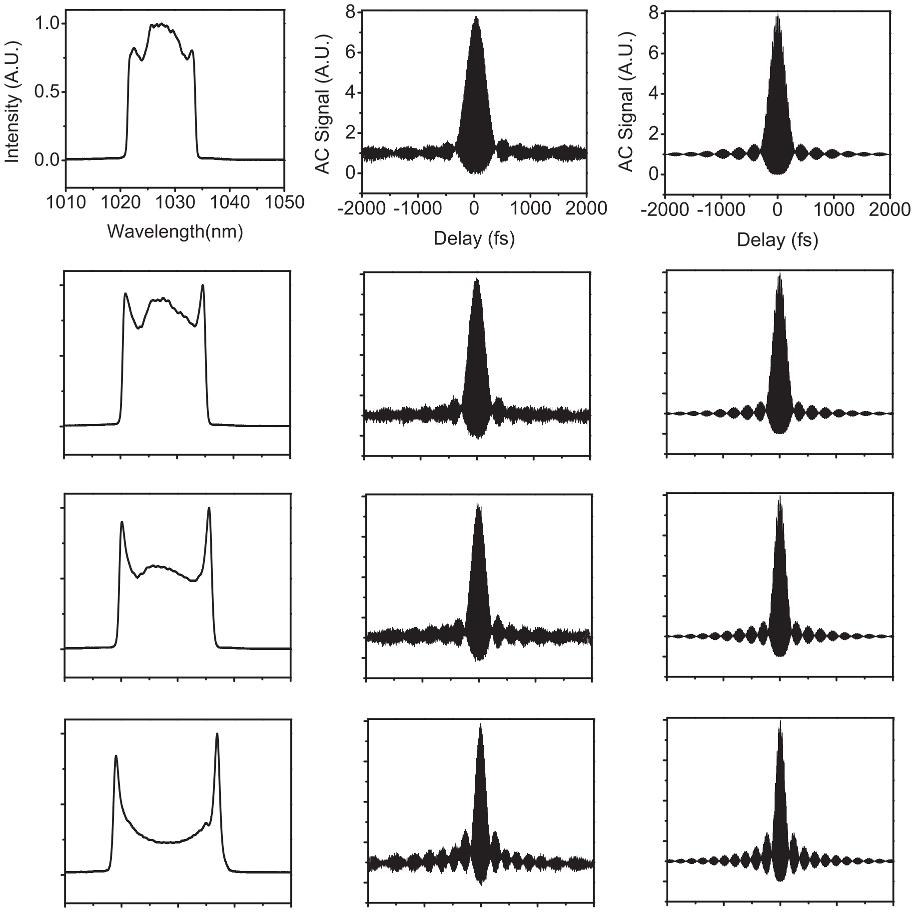

Figure 2.7: Output of the laser: Left column: spectrum evolution with adjusting waveplates, Center column: corresponding dechirped interferometric autocorrelations, Right column: corresponding interferometric autocorrelation of zero-phase Fourier-transform of the spectrum.

tions even with quantitative agreements in the energy, the dechirped pulse duration, etc. Furthermore, the flexibility of the birefringence filter is quite attractive for experiments. The spectral filter BW can be easily adjusted by putting a quartz plate with a different thickness. By combining quartz plates and polarizers, one can created various combinations of the filter BW and the FSR such as a Lyot or a Solc filter. Because of many convenient features of the ANDi fiber laser with a birefringence filter, most of the ANDi laser experiments are with various birefringence filters.

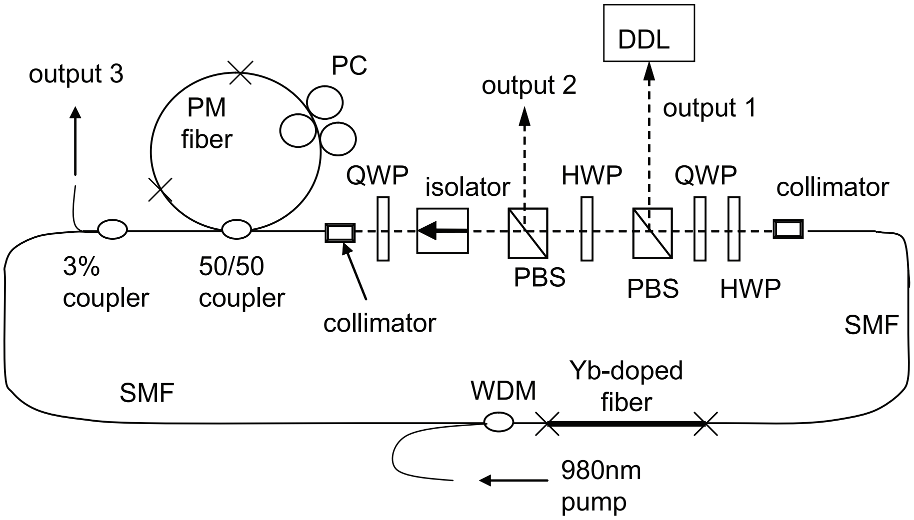

Figure 2.8: Schematic of ANDi fiber laser with a birefringence fiber loop filter: QWP: quarter-waveplate; HWP: half-waveplate; PBS: polarizing beam splitter; WDM: wavelength-division multiplexer; PM: polarization maintaining; DDL: dispersion delay line; PC: polarization controller.

### 2.3.3 Birefringence fiber loop filter

A birefringence fiber loop filter is a fiber-formatted birefringence filter. The unique feature of the fiber integrability is quite attractive for building all-fiber ANDi fiber lasers. The schematic of the ANDi fiber laser with a birefringence fiber loop filter is shown in Figure 2.8. Even though the laser cavity still has some bulk optics in the cavity, replacing bulk optics filters by fiber-formatted filters is a appreciable progress toward the all-fiber ANDi fiber laser. Other bulk optical components such as a PBS, a isolator, and waveplates can be conveniently replaced by commercially available fiber-formatted components.

The cavity consists of ~40 cm of SMF, a birefringence fiber loop filter, another 2.35 m of SMF, ~60 cm Yb-doped gain fiber, and ~1 m of SMF following the gain fiber. Again, the gain fiber was pumped through a WDM with a ~350 mW pump power. A

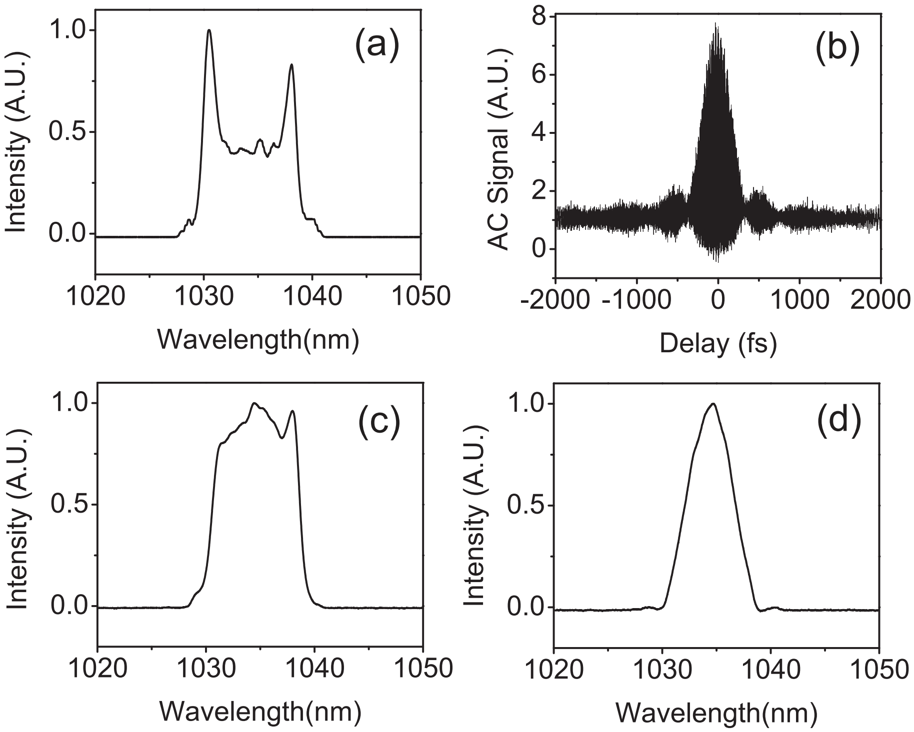

Figure 2.9: Output of the laser: a) output 1 spectrum, b) dechirped interferometric autocorrelation of the output, c) output2 spectrum, d) output spectrum of the 3% coupler

birefringence loop filter consist of a 50/50 fiber coupler with ~25 cm of Corning PM 980 in the loop. The measured spectral filter BW is ~ 4.4 nm. By adjusting the PC, the lasing center wavelength can be tuned. The total loop length including the PM fiber segment is ~1.65 m. Since the pulse travels through the fiber loop, total length of the fiber that the pulse travel is ~6 m. The total length of the fiber that the pulse travels in a round trip gives ~0.14 $ps^2$ total GVD with ~33 MHz repetition rate. A little bit deviated from the previous experimental setups, several more outputs are setup to monitor the intracavity pulse evolution. The output 2 is setup to monitor the spectrum after the NPE port. A 3% coupler is attached after the filter to monitor the spectrum after the spectrum filtering.

Figure 2.9 shows the experimental result of the fiber laser. Output 1 shows a characteristic spectrum shape of sharp peaks around its edges. The output 1 is dechirped by an external grating pair to have ~290 fs pulse duration (Figure 2.9(b)). 44 mW of the output average power corresponds to ~1.3 nJ of pulse energy. It is well known that the mode-locked cavity circulating pulse quality is substantially better than the NPE port ejected pulse [18]. The output 2 (Figure 2.9(c)), which is the thruput pulse of the NPE port, exhibits a much cleaner spectrum as predicted. The spectrum after the birefringence fiber loop filter (Figure 2.9(d)) is the consequence of the narrow spectral filtering of the output 2 spectrum (Figure 2.9(c))

### 2.3.4 Er-doped ANDi fiber laser

Meanwhile, an Erbium (Er)-doped fiber laser with only normal dispersion elements has been reported [19]. This so-called gain-guided soliton fiber laser relies on the limited bandwidth (BW) of the gain medium for the pulse-shaping. It was an important to step to increase the pulse energy since the pulse energy is expected to be larger with increasing net normal cavity dispersion. However, unlike the Yb-doped ANDi fiber lasers, the gain-guided soliton laser only created picosecond pulses. To create shorter pulses, a gain-guided soliton Er fiber laser with a dispersion map and large net normal dispersion (~0.07 $ps^2$) was created [20]. However, the dechirped pulse duration (~1 ps) was still in the picosecond range.

The major difference between the gain-guided soliton fiber lasers and the ANDi fiber lasers is that there is a strong spectral filtering in ANDi fiber lasers. This motivates investigation of the role of the spectral filter in Er fiber lasers. By inserting an appropriate spectral filter within the Er fiber laser, femtosecond dechirped pulses with high pulse energies are expected. Here we present the result of the femtosecond Er fiber laser with

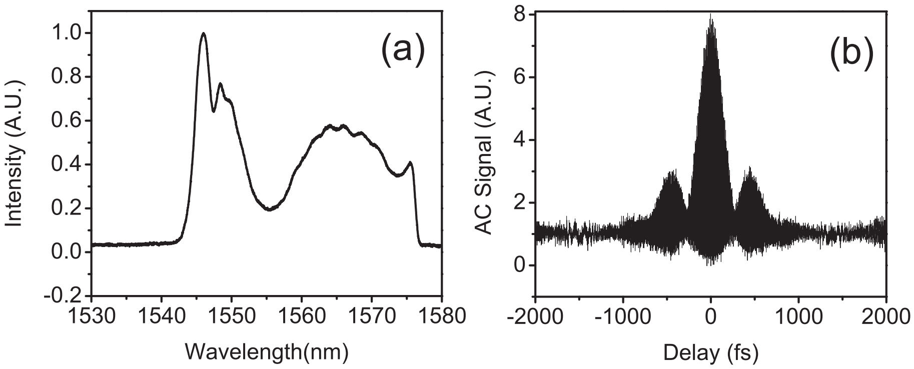

Figure 2.10: Output of the laser: a) spectrum, b) interferometric autocorrelation of the output

a spectral filter at large net normal cavity dispersion (~0.1 $ps^2$). The laser produces 220-fs pulses after dechirping. These results demonstrate the successful translation of the CPSF mechanism to Er fiber lasers. The pulse energy is ~1 nJ, but is expected to improve significantly with an optimal design.

The experimental schematics is same as Figure 2.6. The fiber lasers consists of ~12 m of single-mode fiber (SMF) with normal dispersion at 1550 nm, 3m of Er-doped gain fiber (also with normal dispersion), and another ~3 m of SMF. Because commercially-available WDM and collimators are anomalously dispersive at 1550 nm, some short anomalous dispersion segments are unavoidable. However, the laser has a very weak dispersion map; the anomalous dispersion segments compensate only ~10% of the normal dispersion. The pulse evolution will be essentially that of an ANDi laser. The net cavity dispersion is ~0.1 $ps^2$. NPE provides some self-amplitude modulation. A birefringent filter with 15 nm BW is used to implement CPSF, and provides the dominant self-amplitude modulation. The repetition rate of the laser is 9.9 MHz. By adjusting the waveplates, stable, self-starting mode-locked operation is obtained.

Figure 2.10 shows the experimental results. 10 mW mode-locked average power corresponds to ~1 nJ pulse energy. The spectrum shows the characteristic sharp peaks around its edges resembling the ANDi fiber laser modes as expected (Figure 2.10(a)). The measured dechirped pulse duration is ~220 fs (Figure 2.10(b)). The interferometric AC shows noticeable side-lobes, which arise from the steep sides and structure of the spectrum. The CPSF action of the intracavity spectral filter makes a noticeable improvement of the dechirped pulse duration. The net cavity dispersion is larger than in the gain-guided soliton fiber laser [20], yet this laser successfully creates femtosecond pulses. The demonstration of femtosecond Er-doped fiber laser operation at large net cavity dispersion is an important step to achieve femtosecond-duration and high energy pulses from Er-doped fiber lasers according to the master equation prediction [6].

## 2.4 Conclusion

In conclusion, we have demonstrated a fiber laser that generates high-quality femtosecond pulses without the use of intracavity dispersion control. The behavior and performance of the laser agree qualitatively with numerical simulations that illustrate the intended pulse-shaping mechanism by enhanced spectral filtering of chirped pulses in the cavity. Nevertheless, our picture of this mode-locking process is rudimentary, and more work will be required to obtain a systematic understanding. Improved performance should accompany better understanding of this mode-locking process.

# BIBLIOGRAPHY

[1] A. Chong, J. Buckley, W. Renninger, and F. Wise, Opt. Express **14,** 10095 (2006).

[2] R. L. Fork, O. E. Martinez, and J. P. Gordon, Opt. Lett. **9**, 150 (1984).

[3] E. B. Treacy, IEEE J. Quantum Electron. **QE-5**, 454(1969).

[4] R. Szipocs, K. Ferencz, C. Spielmann, and F. Krausz, Opt. Lett. **19**, 201 (1994).

[5] O. E. Martinez, R. L. Fork, and J. P. Gordon, Opt. Lett. **9**, 156 (1984).

[6] H. A. Haus, J. G. Fujimoto, and E. P. Ippen, IEEE J. Quantum Electron. **28**, 2086 (1992).

[7] B. Proctor, E. Westwig, and F. Wise, Opt. Lett. **18**, 1654 (1993).

[8] S. M. J. Kelly, Electron. Lett. **28**, 806 (1992).

[9] K. Tamura, E. P. Ippen, H. A. Haus, and L. E. Nelson, Opt. Lett. **18**, 1080 (1993).

[10] F. O. Ilday, J. R. Buckley, W. G. Clark, and F. W. Wise, Phys. Rev. Lett. **92**, 213902 (2004).

[11] F. O. Ilday, J. R. Buckley, H. Lim, F. W. Wise, and W. G. Clark, Opt. Lett. **28**, 1365 (2003).

[12] J. R. Buckley, F. W. Wise, F. O. Ilday, and T. Sosnowski, Opt. Lett. **30**, 1888 (2005).

[13] H. Lim, F. O. Ilday, and F. W. Wise, Opt. Express **10**, 1497 (2002).

[14] A. V. Avdkhin, S. W. Popov, and J. R. Taylor, Opt. Express **11**, 265 (2003).

[15] I. Hartl, G. Imeshev, L. Dong, G. C. Cho, and M. E. Fermann, Conference on Lasers and Electro-Optics 2005, Baltimore, MD, paper CThG1.

[16] J. Buckley, A. Chong, S. Zhou, W. Renninger, and F. Wise, J. Opt. Soc. Am. B **24,** 1803 (2007).

[17] H. Lim, F. O. Ilday, and F. W. Wise, Opt. Lett. **28**, 660 (2003).

[18] K. Tamura, and M. Nakazawa, Applied Phys. Lett. **67,** 3691-3693 (1995).

[19] L. M. Zhao, D. Y. Tang, and J. Wu, Opt. Lett. **31,** 1788 (2006).

[20] L. M. Zhao, D. Y. Tang, T. H. Cheng, and C. Lu, Opt. Lett. **31,** 2957 (2007).

CHAPTER 3

# BEHAVIOR OF ANDi FIBER LASERS[1]

This chapter describes a systematic study of the behavior of ANDi fiber laser. It is surmised based on a variety of numerical simulations that there are three main laser parameters which determine the pulse in the ANDi fiber laser. Three main parameters of the GVD, the nonlinearity and the spectral filter BW. The effect of each parameter is studied by performing numerical simulations and experiments. It is also discussed how the ANDi fiber laser can be designed to have optimal performance.

## 3.1 Introduction

It has become conventional wisdom that the compensation of group velocity dispersion (GVD) in a laser is prerequisite to the generation of femtosecond pulses. Most modern femtosecond lasers have dispersion maps, with segments of normal and anomalous GVD. The net GVD of the cavity can be normal or anomalous. With large net anomalous GVD, soliton-like pulses can be formed as a result of the balance of anomalous GVD and positive (*i.e.*, self-focusing) nonlinearity. As the net GVD approaches zero, stretched-pulse operation occurs [2]. A stretched pulse laser has breathing solutions (dispersion-managed (DM) solitons), and in fiber lasers the pulse energy can be an order of magnitude higher than in a soliton laser.

Excessive nonlinear phase shift accumulated by the pulse as it traverses the cavity generally limits the pulse energy. Theoretically, mode-locked laser operation with large net normal GVD is expected to have stable high-energy pulses [3]. Proctor *et al.* experimentally verified the master-equation prediction of highly-chirped pulses from a

---

[1] Most of the results presented in this chapter have been published in Ref [1]

solid-state laser with net normal GVD [4]. Pulse-shaping in such a laser is based on spectral filtering of the chirped pulse, which cuts off the temporal wings of the pulse.

In recent years, researchers have actively investigated mode-locked laser operations with large net normal GVD to achieve higher pulse energies directly from an oscillator. Notable among these are the self-similar laser [5] and the so-called chirped pulse oscillator (CPO) [6], which is an optimized version of the operation reported by Proctor *et al.* [4]. The self-similar laser produces highly-chirped parabolic pulses that propagate self-similarly in the laser cavity. Strong temporal breathing arises from the dispersion map and nonlinear pulse evolution. A CPO generates highly-chirped pulses with negligible breathing due to the much weaker dispersion map. Both self-similar and CPO lasers employ dispersion maps to successfully generate high pulse energies with femtosecond dechirped pulse durations [6, 7, 8, 9, 10]. In all cases, some self-amplitude modulation is needed to start and stabilize the pulses. CPO has been used to referred to solid-state lasers. The feature that all CPOs have in common is the weak temporal breathing (i.e., the pulse is approximately constant as it traverses the cavity), which contrasts with the fiber lasers with clear pulse evolution.

In the design of high-energy femtosecond lasers, the combination of anomalous GVD and positive nonlinearity in a given segment of the cavity should be avoided, as the tendency of a pulse to form a soliton in that segment may limit the pulse energy. For fiber lasers, it is technically challenging to create a dispersion map at wavelengths where the fiber has normal GVD. For single-mode fiber (SMF) this implies wavelengths below 1.3 $\mu$m, which includes the 1-$\mu$m emission band of ytterbium (Yb)-doped fiber. Microstructure fibers can provide anomalous dispersion with negligible nonlinearity, but for technical reasons the resulting lasers do not perform at the level of lasers that employ bulk diffraction gratings for dispersion control [11]. The bulk optics detract substantially from the integrated and waveguide nature of fiber lasers, and there is therefore much motivation to eliminate them from the design.

Of course, dispersion control is not required for saturable-absorber mode-locking and picosecond pulse durations. Under these conditions, dispersion and nonlinear phase modulation do not contribute appreciably to pulse-shaping. The question we address here is whether self-amplitude modulation can play a larger role in shaping femtosecond pulses, and even stabilize high-energy pulses without a dispersion map in the cavity. The approach is to extend the pulse-shaping at normal GVD observed by Proctor *et al.* to fiber lasers. The cavity dispersion will be two to three orders of magnitude larger than that of solid-state lasers, and as mentioned, we want to eliminate the anomalous-GVD segment entirely.

One step in this direction was the report by Zhao *et al.* [12] of so-called gain-guided soliton formation in a laser without a dispersion map. Theoretically, pulse-shaping in this laser is qualitatively similar to that in a CPO [4]. However, even the theoretical (numerical) results showed that pulse-shaping is dominated by self-amplitude modulation from nonlinear polarization evolution (NPE), rather than spectral filtering of a highly-chirped pulse [13]. Furthermore, pulse durations larger than 15 ps were obtained experimentally, and dispersion and nonlinear effects should be weak with such pulse durations. Buckley *et al.* demonstrated that a spectral filter could stabilize high-energy pulses in a Yb-doped fiber laser with a dispersion map and large net GVD, to produce peak powers >100 kW from an oscillator[14]. These results motivated consideration of the possibility that the spectral filter might provide enough self-amplitude modulation in a suitably-designed cavity to allow removal of the anomalous-GVD segment.

Recently, Chong *et al.* [15] reported a mode-locked Yb fiber laser in which pulse-shaping can be dominated by spectral filtering of a highly-chirped pulse in the cavity.

The cavity contained no components with anomalous GVD, and the output pulse could be dechirped to 170 fs duration. This all-normal-dispersion (ANDi) laser exhibits a variety of pulse shapes and evolutions, which distinguish it from prior mode-locked lasers [16]. The pulse energy from an ANDi laser has been scaled to the 20-nJ level [17], and higher energies may be possible.

Here we provide a more systematic description of the behavior and performance of ANDi lasers than was possible in the brief initial report [15]. A master-equation analysis [3] of this type of laser was reported [18], but it is naturally limited to static solutions, and it fails to predict the variety of operating modes such as the characteristic spectral shapes [15]. Extensive numerical simulations show that the intracavity pulse evolution and characteristics are determined by three main parameters: the nonlinear phase shift that the pulse experiences in a round trip ($\Phi_{NL}$), the spectral filter bandwidth (BW), and the GVD of the cavity. These simulations are described in Section 2 of the paper. The effect of each parameter is discussed separately, and in summary the trends exhibit some universal features. Similarities and differences between the ANDi fiber laser, CPO, and self-similar lasers are also discussed. Experimental results are presented in Section 3. Section 4 contains a discussion of pulse-shaping in ANDi lasers, and Section 5 outlines some practically-useful features of ANDi fiber lasers. Finally, conclusions are presented in Section 6.

## 3.2 Behavior of ANDi Fiber Lasers : Theory

### 3.2.1 Pulse-Shaping Mechanism

The pulse-shaping mechanism in the ANDi fiber laser can be understood by examination of the pulse evolution in a typical numerically-simulated example. The simulation is based on the experimental setup in [15]. The simulated laser consists of a long segment of SMF (3 m), a Yb-doped gain fiber (60 cm), and one more piece of SMF (1 m) in order. The pulse propagation within each section is modeled by the appropriate terms of the following equation:

$$\frac{\partial A(z,\tau)}{\partial z} + i\frac{\beta_2}{2}\frac{\partial^2 A(z,\tau)}{\partial \tau^2} = i\gamma |A(z,\tau)|^2 A(z,\tau) + g(E_{pulse})A(z,\tau). \tag{3.1}$$

$A(z,\tau)$ is the electric filed envelope, while $z$ is the propagation distance and $\tau$ is the pulse local time. The dispersion and nonlinear coefficients of SMF used in the simulation are $\beta_2 = 230\text{fs}^2/\text{cm}$ and $\gamma = 0.0047(\text{W m})^{-1}$. $g(E_{pulse})$ is the net gain function for the Yb-doped gain fiber. The pulse energy is given by $E_{pulse} = \int_{-T_R/2}^{T_R/2} |A(z,\tau)|^2 d\tau$ where $T_R$ is the cavity round-trip time.

Gain saturation is modeled according to

$$g(E_{pulse}) = \frac{g_o}{1 + E_{pulse}/E_{sat}}. \tag{3.2}$$

$g_o$ corresponds to ~ 30dB of small-signal gain. A Lorentzian gain shape with ~100 nm BW is assumed. The gain saturation energy $E_{sat}$ is set according to the pump power. In the simulation, $E_{sat}$ is varied from 0.25 nJ to 6 nJ. The fiber sections are followed by an ideal saturable absorber with monotonically-increasing transmission $T = 1 - l_o/[1 + P(\tau)/P_{sat}]$ where $l_o$=0.7 is the unsaturated loss, $P(\tau)$ is the instantaneous pulse power and $P_{sat}$ is the saturation power. Details of the mode-locked spectrum can be changed by choosing different $P_{sat}$ but overall characteristics do not change substantially. Once the transmission function deviates severely from the ideal one (*e.g.*, the sinusoidal transmission curve of nonlinear polarization evolution (NPE)) the simulation starts to show dramatically different results. We decided to eliminate the detailed effects of the saturable absorber, in order to focus on the effects of other parameters. To this end, $P_{sat}$ is adjusted within the range (0.1 - 2.4 kW) according to the pulse energy, so that the same pulse shape but with different peak powers experience the same point on the saturable absorber transmission curve.

The initial simulation work presented by Chong *et al.* assumed that the gain BW could be varied, and showed that artificially narrow values of the gain BW caused enough spectral filtering action for mode-locking [15]. In the work presented here, a Gaussian spectral filter is placed after the saturable absorber in the simulation to accurately model the real laser. The spectral filter BW is varied from 8 nm to 25 nm in the simulation. The output is coupled out between the saturable absorber and the spectral filter with a ~70% coupling ratio. Pulse evolution in each segment is solved numerically with a split-step Fourier method, until the laser reaches a steady state [19].

Figure 3.1 shows how the power spectrum typically evolves in an ANDi fiber laser. After traversing the spectral filter, the spectrum shows steep edges and a Gaussian-shaped top that follows the filter transmission curve. Gentle spectral broadening is observed in the first SMF and the gain fiber. After the gain fiber amplifies the pulse, the enhanced peak power in the SMF induces a substantial nonlinear phase shift, which produces sharp peaks at the edges of the spectrum. The spectral filter, and to a lesser

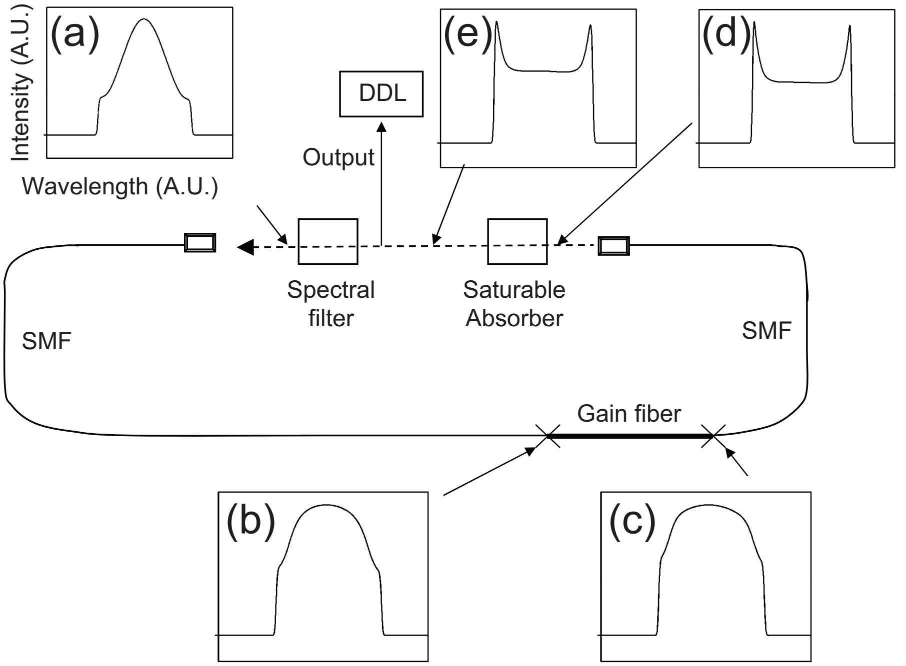

Figure 3.1: Typical numerical simulation result: (a) spectrum at the beginning of the first SMF, (b) spectrum at the beginning of the gain fiber, (c) spectrum at the end of the gain fiber, (d) spectrum at the end of the second SMF, (e) output spectrum; DDL: dispersion delay line.

degree the saturable absorber, cut off the peaks and return the spectrum to its starting shape.

The corresponding time-domain evolution is shown in Figure 3.2. The typical GVD of an ANDi fiber laser is roughly an order of magnitude higher than that of a fiber laser with a dispersion map. Because of the large normal GVD, the pulse chirp is large and positive throughout the cavity. The pulse duration increases monotonically in the segments of SMF. Self-amplitude modulation occurs in the saturable absorber and the spectral filter, but the effect of the spectral filter dominates. Therefore, the main pulse-shaping mechanism of an ANDi fiber laser can be described as chirped-pulse spectral filtering.

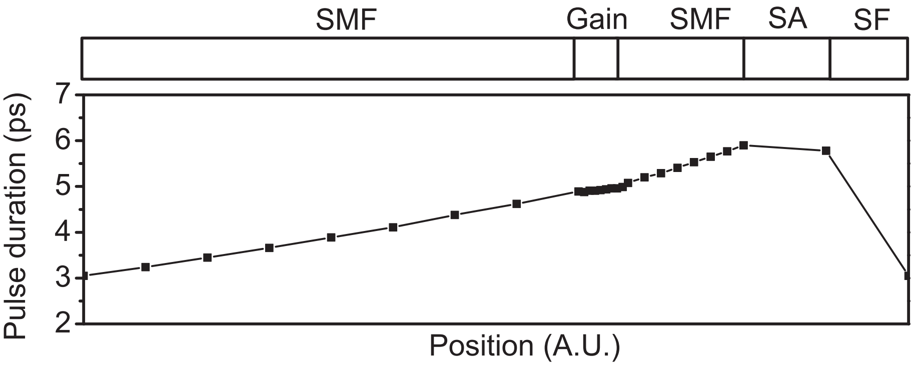

Figure 3.2: Time domain evolution of the numerical simulation result in Figure 1; SA: saturable absorber, SF: spectral filter.

### 3.2.2 Variation of Laser Parameters

From an extensive set of simulations performed with a wide range of conditions, we conclude that there are three main parameters that control the intracavity pulse evolution and characteristics. These are $\Phi_{NL}$, the spectral filter BW, and GVD. In this section, the effect of each parameter will be discussed based on simulation results. Interestingly, variation of any of these three parameters produces qualitatively similar trends in the behavior and performance.

The reference simulation condition is as follows: The fiber segment consists of 3 m of SMF, 60 cm of gain fiber, and 1 m of SMF. The resulting GVD is ~0.1 $ps^2$. All fibers have 6-$\mu$m core diameter. The spectral filter has a Gaussian transmission function with 8 nm BW. Again, the saturable absorber has a monotonically increasing transfer function. 70% of the pulse energy is coupled out of the cavity right after the saturable absorber. The pulse energy is reduced by an additional 10% to account for other losses.

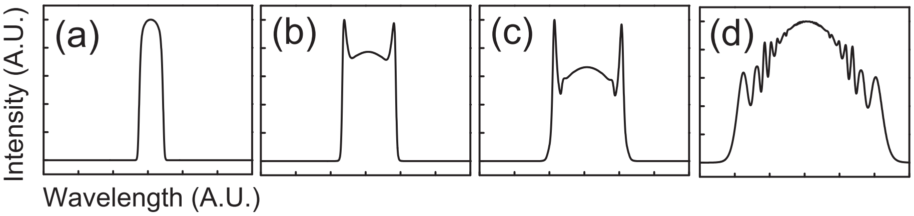

Figure 3.3: Output spectrum with $\Phi_{NL}$: (a) ~$1\pi$, (b) ~$4\pi$, (c) ~$7\pi$, (d) ~$16\pi$.

### Nonlinear Phase Shifts

The performance of the ANDi fiber laser changes extensively as $\Phi_{NL}$ varies. To investigate this effect, the pump power was increased gradually from the reference condition while holding the spectral filter BW and the GVD constant. In reality, increasing the pump power is not the only way to enhance $\Phi_{NL}$. For example, $\Phi_{NL}$ can also be varied by adjusting the output coupling ratio or the length of the SMF after the gain. However, the numerical study shows that any parameter (*e.g.*, output coupling ratio) that alters the value of $\Phi_{NL}$ produces essentially the same result. The temporal profile does not show clear trends, while the output spectra clearly display a dramatic variation. Figure 3.3 shows the trend as $\Phi_{NL}$ increases.

The output spectral BW increases with $\Phi_{NL}$. For low $\Phi_{NL}$, the spectrum appears similar to the parabolic spectrum of a self-similar laser (Figure 3.3(a)) [5]. As $\Phi_{NL}$ increases, the spectrum broadens while developing sharp peaks around its edges (Figure 3.3(b)). These features sharpen as $\Phi_{NL}$ increases up to ~$7\pi$ (Figure 3.3(c)). With larger $\Phi_{NL}$, the spectrum broadens further and eventually develops structure or fringes (Figure 3.3(d)). The output spectral BW with $\Phi_{NL}$ ~$16\pi$ is ~6 times larger than that with $\Phi_{NL}$ ~$1\pi$. Even with $\Phi_{NL}$ as large as ~$10\pi$ or more, the output pulse can be dechirped very close to the transform limit. For example, the pulse with $\Phi_{NL}$ ~$16\pi$ ($7\pi$) can be dechirped with a linear dispersive delay to only ~20% (10%) beyond the transform limit.

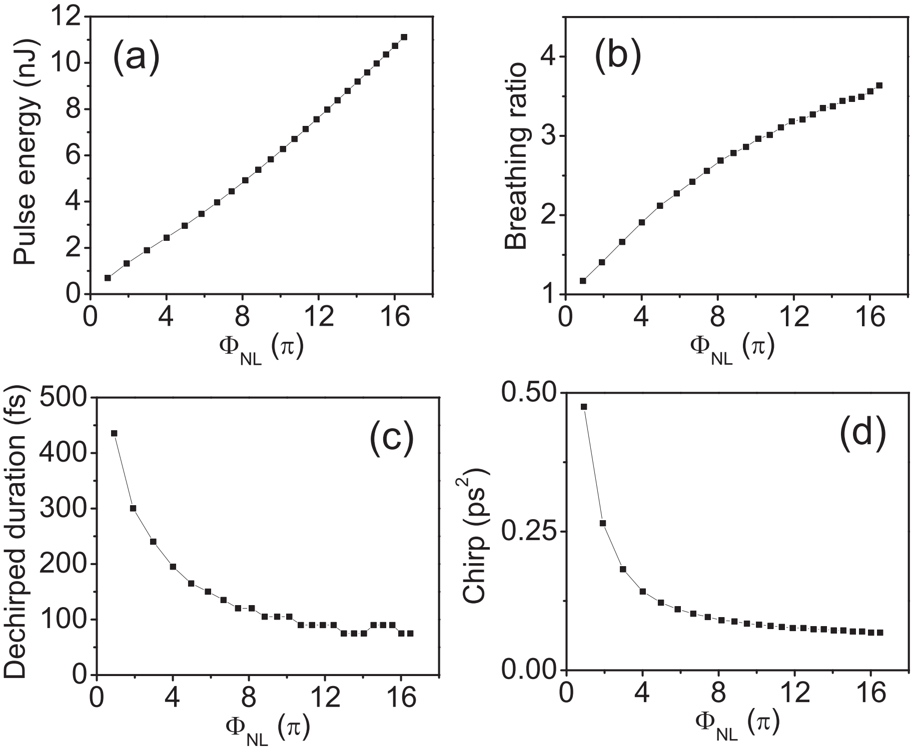

Figure 3.4: Laser performance *vs.* $\Phi_{NL}$: (a) pulse energy, (b) breathing ratio, (c) dechirped pulse duration, (d) chirp.

The dependence of the laser output parameters on $\Phi_{NL}$ is summarized in Figure 3.4. The pulse energy increases monotonically (Figure 3.4(a)). Figure 3.4(b) shows the breathing ratio, which is defined as the ratio of maximum and minimum pulse durations in the cavity. The breathing ratio increases from ~1 to ~4 as $\Phi_{NL}$ increases. The temporal breathing is large compared to that in a solid-state CPO, but small compared to that in a similariton laser. The dependence on $\Phi_{NL}$ is related to the ratio of the output spectral BW to the spectral filter BW. When the output spectrum is narrower than or equal to the spectral filter BW, the breathing ratio is ~1, as in a CPO. The spectral amplitude modulation is larger when the output spectral BW is much larger than the spectral filtering BW (*e.g.* ~5 times larger in Figure 3.3(d)). Since the pulse is highly chirped, a strong spectral amplitude modulation converts into a strong time domain amplitude modulation and thereby a large breathing ratio.

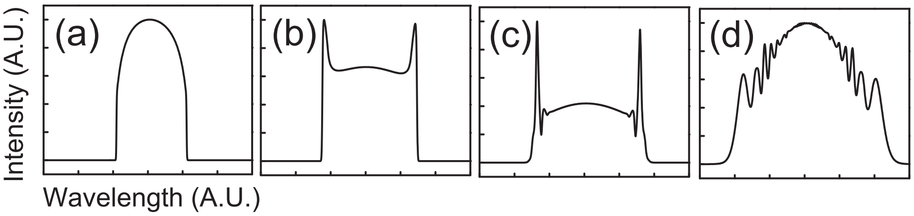

Figure 3.5: Output spectrum with spectral filter BW: (a) 25 nm, (b) 15 nm, (c) 12 nm, (d) 8 nm.

The dechirped pulse duration is inversely proportional to the spectral BW (Figure 3.4(c)). Here we define the pulse chirp as the magnitude of anomalous GVD required to dechirp the output pulse to its maximum peak power. Interestingly, the chirp decreases as $\Phi_{NL}$ increases. This indicates that the accumulation of nonlinear phase has some dechirping action against the normal GVD of the fiber.

### Spectral Filter Bandwidth

The second laser parameter that can alter the laser performance noticeably is the spectral filter BW. To survey the effect of the spectral filter BW, simulations were performed with increasing filter BW, starting from the condition used in Figure 3.3(d). Other parameters, such as $\Phi_{NL}$ and GVD were kept constant.

Figure 3.5 shows the variation of the output spectrum while the spectral filter BW is varied. Interestingly enough, reduction of the filter BW produces the same qualitative trend as increasing $\Phi_{NL}$. (Compare Figs. 3.3 and 3.5.)

The variation of the output pulse parameters *vs.* the spectral filter BW is shown in Figure 3.6. The output pulse energy is excluded because the pulse energy does not vary much with fixed pump power and output coupling ratio. The breathing ratio again covers the range from ~1 to ~4. The dechirped pulse duration and the pulse chirp increase as

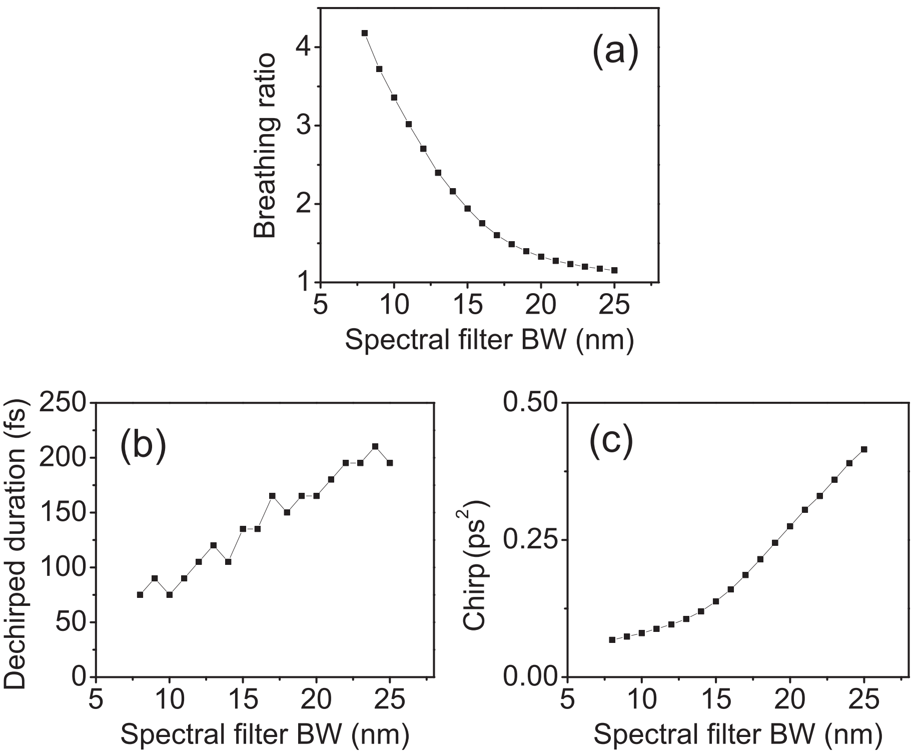

Figure 3.6: Laser performance *vs.* spectral filter BW: (a) breathing ratio, (b) dechirped pulse duration, (c) chirp.

the spectral filter increases along with decreasing output spectral BW.

### Group Velocity Dispersion

The last laser parameter to be investigated is the GVD. Numerical simulations were performed with increasing length of the first segment of SMF, starting from the condition used in Figure 3.3(d). The GVD was varied from ~0.1 $ps^2$ to ~0.5 $ps^2$ . Other parameters such as $\Phi_{NL}$ and the spectral filter BW were again held constant. Figure 3.7 shows the output spectrum as the GVD decreases. We see that decreasing the GVD produces a trend that is similar to those obtained by increasing the $\Phi_{NL}$ or decreasing the filter BW. The output energy is again omitted because it is nearly constant.

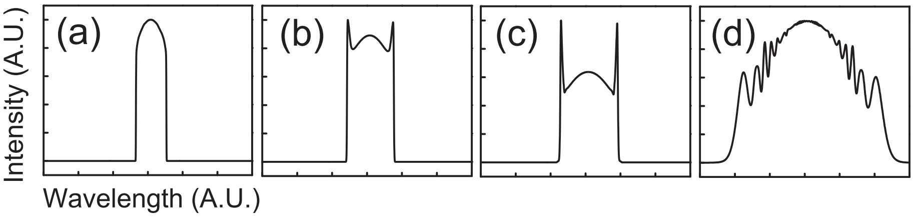

Figure 3.7: Output spectrum with GVD: (a) 0.52 $ps^2$, (b) 0.31 $ps^2$, (c) 0.24 $ps^2$, (d) 0.10 $ps^2$.

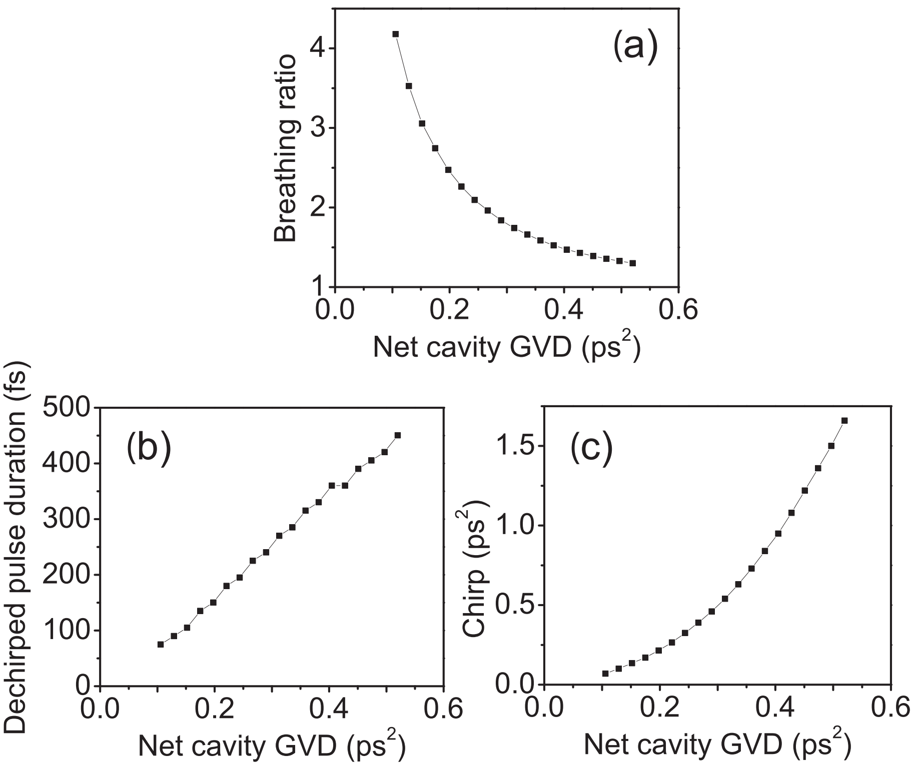

Figure 3.8: Laser performance *vs.* GVD: (a) breathing ratio, (b) dechirped pulse duration, (c) chirp.

The variation of the breathing ratio, the dechirped pulse duration, and pulse chirp are shown in Figure 3.8. The chirp increases rapidly with GVD. Other output parameters show trends similar to those observed by variation of the parameters discussed above.

Figure 3.8(b) shows that shorter pulses are obtained as the GVD gets close to zero. This trend matches the prediction of the master equation in its range of validity [3].

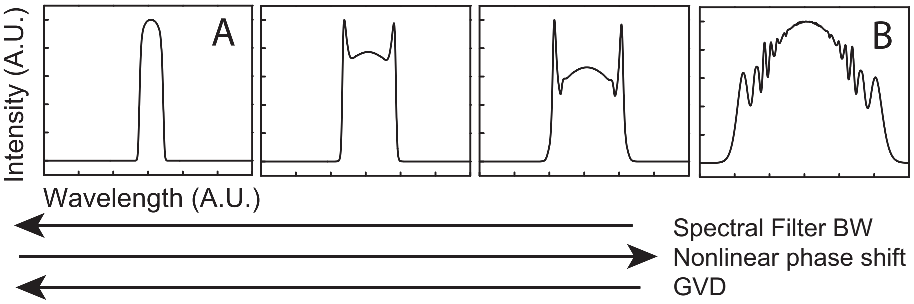

Figure 3.9: Output spectrum *vs.* laser parameters.

### 3.2.3 Summary of the Effects of Laser Parameters

The results of this section are summarized in Figure 3.9. The output spectral shape evolves gradually from the parabolic-top spectrum that is a signature of self-similar pulse evolution (Figure 3.9A) to the fringed and broadened spectrum (Figure 3.9B) with decreasing spectral filter BW, decreasing GVD, or increasing $\Phi_{NL}$. Of course, various combinations of three parameters can deliver various spectrum shapes with different characteristics. However, the shapes will still fall between spectra A and B in Figure 3.9.

Some insight also comes from looking at the temporal evolution when the breathing ratio reaches its extreme values. Other evolutions with intermediate breathing ratios will fall between these. Figure 3.10 shows the temporal evolutions that correspond to the spectra labeled A and B in Figure 3.9. The parabolic spectrum exhibits very little temporal or spectral breathing (Figure 3.10A). In that sense, the pulse propagation is similar to that in a CPO. However, there are fundamental differences between the ANDi fiber laser and a solid-state CPO. The ANDi fiber laser has GVD roughly $\sim 10^3$ times larger than that of the solid-state CPO. Furthermore, the ANDi fiber laser does not have any anomalous dispersion component, while the solid-state CPO comprises a dispersion map.

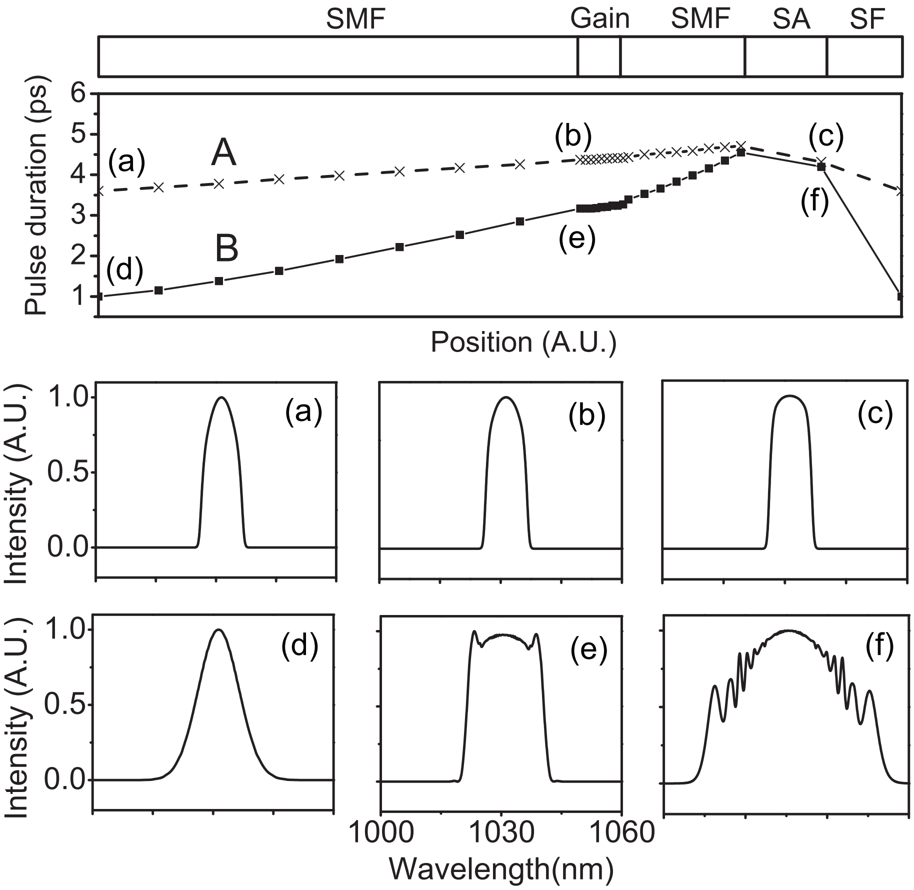

Figure 3.10: Temporal evolution of two extreme cases; top: temporal evolution of Figure 9A and 9B, middle: spectra of Figure 9A mode at various locations, bottom: spectra of Figure 9B mode at various locations.

Meanwhile, the other extreme case (Figure 3.10B) of a fringed nonlinearly-broadened spectrum has a distinct evolution. The temporal breathing ratio is ~4 and the spectrum changes significantly. The temporal evolution resembles that of the self-similar laser, where the pulse duration increases monotonically within the fiber and then decreases in the dispersive delay line with a noticeable breathing ratio [5]. The temporal evolution of Figure 3.10B is qualitatively the same as that of the self-similar laser. A major difference is that the ANDi fiber laser's self-amplitude modulation occurs mainly in the spectral filter. Furthermore, the output spectrum of the ANDi fiber laser in Figure 3.10B is not parabolic at all.

### 3.2.4 Design of ANDi lasers

It is desirable to convert the observations of this section into the design of ANDi lasers with specific performance parameters. Although explicit design formulas cannot be provided, we can give some guidelines and an overall algorithm. The GVD is the decisive parameter for mode-locked spectral BW and hence the dechirped pulse duration. As the GVD increases, the output spectral BW decreases significantly. In practice, the GVD may be decided by the desired repetition rate. Once the GVD is fixed, one can choose an appropriate spectral filter. The choice of a proper spectral filter BW is critical for the stability and the performance of the laser. Roughly, the filter BW should be chosen to match the expected pulse BW. A narrower filter will tend to generate a broad, structured output spectrum such as spectrum B in Figure 3.9. As the filter BW increases, the output spectrum will become cleaner and narrower. If the filter BW is too large, the filter will not contribute to pulse-shaping and stable operation becomes difficult to achieve.

Once the GVD and the spectral filter BW are determined, $\Phi_{NL}$ can be optimized easily by adjusting the pump power. By choosing the three main laser parameters appropriately, the output spectral BW and therefore the pulse energy can be scalable. For example, spectra in Figure 3.5(a) and Figure 3.3(a) have similar shapes, but the spectrum in Figure 3.5(a) has ~3 times larger BW, with a ~2 times shorter dechirped pulse duration and a ~17 times larger pulse energy. Remarkably, only the spectral filter BW and the pump power were adjusted to scale the energy over the stated range.

For example, the ANDi fiber laser in [15] with GVD ~0.1 $ps^2$ was mode-locked optimally with ~10 nm spectral filter BW. Pump power was set at ~350 mW to produce ~3 nJ pulse energy. With a filter BW of ~8 nm, mode-locking was easy but the output spectrum was prone to structure. Meanwhile, with a ~15 nm filter, mode-locking was difficult. In practice, we find it useful to start with a narrow spectral filter BW to obtain stable mode-locking. Then we increase the BW to obtain a desired performance. The design rationale described here can provide approximate values of the lasers parameters. For more detailed and quantitative design, numerical simulations are required.

## 3.3 Experimental

Figure 3.11 shows the experimental setup for a Yb-doped ANDi fiber laser. The experimental setup matched the simulated arrangement except for the saturable absorber and the spectral filter. In the experiments, the NPE port takes the role of a saturable absorber. NPE constitutes an approximately sinusoidal intensity transfer function, while the saturable absorber in the simulation was assumed to be an ideal monotonically increasing transfer function. Therefore, a pulse with high enough peak power may experience saturable gain due to the sinusoidal transfer function of the NPE. The output pulse is taken from the NPE port. As a result, the output coupling depends on the NPE parameters, while it was assumed to be constant in the simulation. A birefringent plate between polarization-dependent components constitutes a spectral filter. The birefringent plate was inserted roughly at Brewster's angle to minimize loss. The birefringent filter used in the experimental laser has a sinusoidal spectral transfer function, while it was assumed to be a perfect Gaussian in the simulation. The output pulse was dechirped by a grating pair external to the cavity.

Independent control of the parameters of a laser is generally challenging, and two of the three key parameters are difficult to control individually in the ANDi laser. The spectral filter BW can be changed by inserting a birefringent plate with a different thickness. However, insertion of a new component within a cavity may introduce perturbations in the laser efficiency and therefore fluctuations in $\Phi_{NL}$. Variation of the GVD by cutting

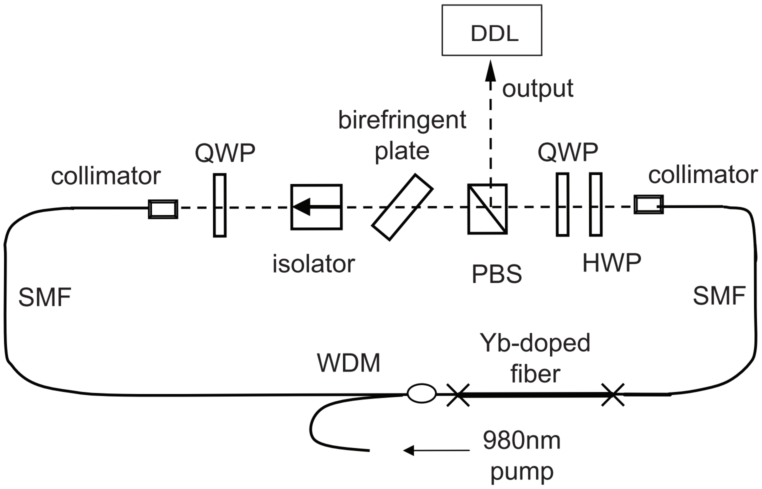

Figure 3.11: Schematic of the experimental setup; PBS: polarization beam splitter; HWP: half waveplate; QWP: quarter waveplate; WDM: wavelength division multiplexer; DDL: dispersion delay line.

or splicing a desired length of a SMF may cause the same problem. Changing the length of the cavity influences not only the GVD, but also the NPE characteristics, which will eventually perturb the value of $\Phi_{NL}$. With the given experimental setup, the only parameter that can be altered continuously without seriously affecting other parameters is $\Phi_{NL}$, which can be adjusted by controlling the pump power. Controlling the output coupling ratio at the NPE port by adjusting the waveplates also affects $\Phi_{NL}$ significantly.

A variety of stable mode-locked states can be observed by adjusting the orientation of the waveplates. By adjusting the pump power and the waveplates, $\Phi_{NL}$ can be increased gradually. The spectra recorded for increasing $\Phi_{NL}$ are presented in Figure 3.12 along with the measured autocorrelations of the dechirped pulses. The range of spectral shapes agrees fairly well with the numerical results shown in Section 2. The sharp peaks at the edges of the spectrum are a signature of chirped-pulse spectral filtering; such spectra have not been observed systematically in any prior mode-locked laser to our knowledge. The steep sides and sharp peaks in the spectra imply that the temporal profiles will have some secondary structure, and this is observed in the auto-

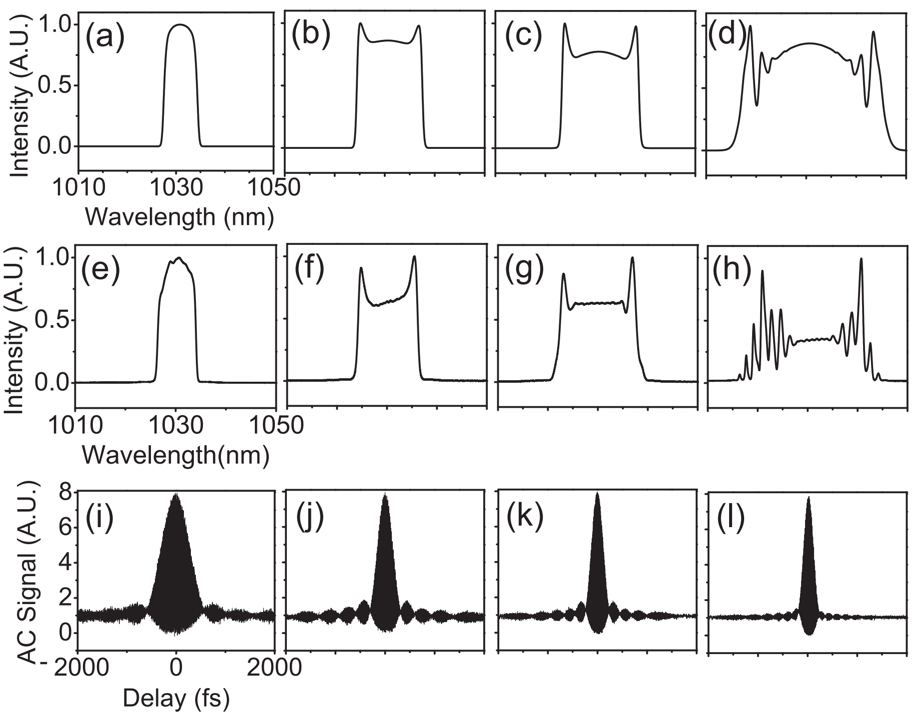

Figure 3.12: Experimental results; Top: simulated output spectrum with $\Phi_{NL}$: (a) ~$1\pi$, (b) ~$3\pi$, (c) ~$4\pi$, (d) ~$8\pi$; middle: experimental output spectrum with approximated $\Phi_{NL}$: (e) ~$1\pi$, (f) ~$3\pi$, (g) ~$4\pi$, (h) ~$8\pi$; bottom: corresponding experimental dechirped interferometric ACs.

correlations (AC). The secondary lobes in the time domain contain from ~4% (Figure 3.12(e)) to ~7% (Figure 3.12(g)) of the pulse energy. The highly-structured spectra (Figure 3.12(h)) yield small secondary pulses ~3 ps from the main pulse as verified by the AC trace.

To investigate the scaling of the important pulse parameters with $\Phi_{NL}$, we recorded the laser performance at different pulse energies, and then estimated the corresponding values of $\Phi_{NL}$. We assume for simplicity that the temporal profile is constant in the three fiber segments, and approximate the nonlinear phase as

$$\Phi_{NL}\text{approx} = \sum_{n=1}^{3} \gamma_n (\mathrm{I}_{\text{peak}})_n L_n. \tag{3.3}$$

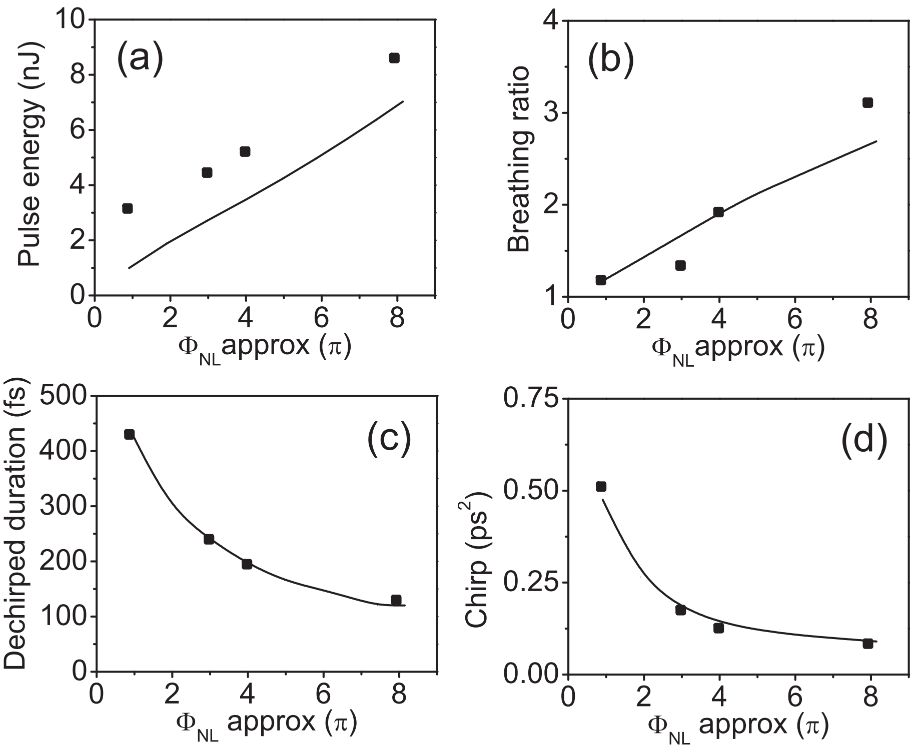

Figure 3.13: Experimental and numerically simulated laser performance *vs.* approximated $\Phi_{NL}$; dots: experiment, lines: numerical simulation; (a) pulse energy before the NPE port, (b) breathing ratio, (c) dechirped pulse duration, (d) chirp.

The peak power in the gain fiber and SMF following the gain fiber was assumed to be equal to that before the NPE port. The peak power in the SMF before the gain is approximated after the spectral filtering and attenuating the peak power according to the measured output coupling ratio. The value of $\Phi_{NL}$ for the simulated pulse is calculated by applying the same equation for the pulse at each step used in the split-step Fourier method. The measured pulse parameters are plotted *vs.* the resulting values of $\Phi_{NL}$ in Figure 3.13.

Given the uncertainty in the estimation of the $\Phi_{NL}$, the apparently excellent quantitative agreement between the measured and simulated results should be considered fortuitous. The important point is that the measured trends in all four parameters agree with those of the numerical simulations. As a result, we conclude that we have a satisfactory understanding of pulse-shaping in ANDi lasers.

The numerical simulations that model the NPE as a monotonic saturable absorber and the filter as a gaussian transmission account for all of the modes of operation of the ANDi lasers presented here. We do find in experiments that the laser can produce a limited number of modes with spectral shapes that are not matched well by these simulations. For example, a very highly chirped mode-locked operation with a narrow (~2 nm) Lorentzian-shaped spectrum is experimentally observed. However, it is not predicted by the current model. A more-sophisticated model of the NPE that explicitly includes the two polarization components with cross-phase modulation accounts not only for those pulses but also for modes in Figure 3.12. We will not discuss those further here, as the purpose of this paper is to lay out the main features of ANDi lasers that are independent of the implementation of the saturable absorber, rather than to discuss modes of operation that are specific to NPE. A systematic investigation of the saturable absorber and the spectral filter will be conducted in the near future.

## 3.4 Discussion

It is generally useful to classify mode-locking regimes that involve nonlinear phase modulations according to the net cavity GVD, as in Figure 3.14. With only anomalous dispersion, soliton formation can occur for any value of the GVD, at least in principle. With a dispersion map, the solutions are generally DM solitons. For large net anomalous GVD, the pulses approximate static solitons, but as the net GVD approaches zero the solutions breathe. These regimes are based on some balance of anomalous GVD and positive nonlinearity. DM solitons can even exist at small net normal GVD. In soliton-

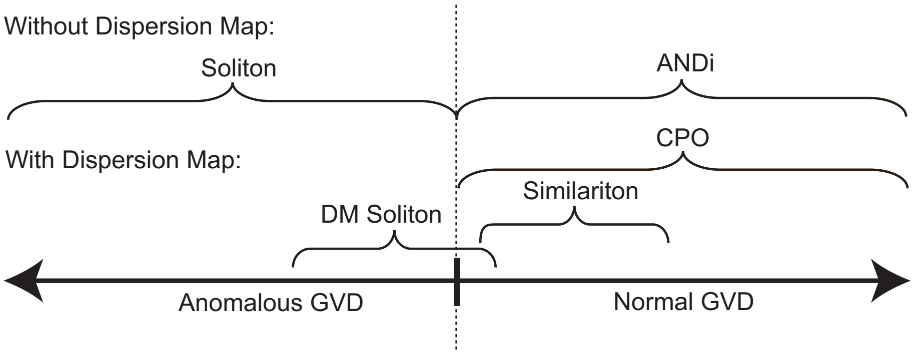

Figure 3.14: Laser operating regimes according to the net cavity dispersion and the existence of a dispersion map.

like pulse-shaping, self-amplitude modulations mostly play a secondary role, namely starting and stabilizing the mode-locking. As the net cavity GVD changes sign from anomalous to normal, different pulse-shaping mechanisms take over. With a dispersion map, self-similar operation can appear. Finally, stable pulse-shaping can occur with normal cavity GVD without a dispersion map in the ANDi laser.

The mode-locking regimes at large normal GVD rely on dissipative processes such as spectral filtering to fundamentally shape the pulse, not just to start and stabilize it. Stable pulses that form due to the balance of GVD, nonlinearity, and dissipative processes such as temporal and spectral amplitude modulation are referred to as dissipative solitons. The complex quintic Ginzburg-Landau equation (CQGLE) is used to model the average pulse in mode-locked lasers. We have recently found that a generalization of the Hocking and Stewartson solution [21], which is an exact analytic solution of the CQGLE, predicts the pulse shapes and trends observed experimentally [20]. Pulse-shaping in the ANDi laser thus seems to exhibit the essence of dissipative soliton formation, and we will pursue this connection in the future.

We can set the ANDi laser in context with related devices such as the CPO and gain-guided soliton laser. As mentioned above, these all exploit pulse-shaping processes that are conceptually and qualitatively the same as those described by the master equation [3] and first observed by Proctor et al. in a Ti:sapphire laser [4]. However, there are clear differences in operation and implementation. Fundamentally, the pulse evolutions differ. All work to date on CPOs has considered only static solutions, while the temporal breathing ratio varies from ~1 to ~4 in ANDi lasers, as shown in Figure 3.10. CPOs have been modeled with the master-equation theory, which cannot account for the spectra with sharp peaks (*e.g.* Figure 3.12 (b)-(d)). Kalashnikov *et al.* calculate so-called M-shape spectra, which bear some resemblance to the spectra produced by the ANDi lasers [22]. Nevertheless, the origin of the spectral shape is clearly different. Kalashnikov *et al.* had to add relatively large fourth-order dispersion to create the M-shape spectrum. In contrast, the simulations described here were performed with zero fourth-order dispersion, so the spectral shape is solely due to the GVD, $\Phi_{NL}$, and the spectral filtering effect. Spectral filtering plays a role in pulse-shaping in CPOs and in gain-guided soliton formation [12]. The relatively weak and constant spectral filtering action of the gain limits the range of mode-locked operations. As a consequence, the gain-guided soliton laser tends to exhibit the mode presented in Figure 3.9A, which occurs with weak spectral filtering and relatively low $\Phi_{NL}$ [12, 13]. The ANDi lasers are the first to include a controllable filter and to optimize the performance with respect to the filter parameters. Finally, CPOs to date have been constructed experimentally with elements that provide anomalous GVD, such as prism pairs and chirped mirrors. The ANDi laser has no components with anomalous GVD. Quantitatively, the cavity dispersion is 2-3 orders of magnitude larger in the fiber laser, simply because the laser contains meters of fiber, compared to ~1 cm of gain crystal in a solid-state CPO.

## 3.5 Analytic theory of ANDi fiber lasers

This section describes the analytic theory for ANDi fiber lasers briefly. It is found that the dissipative solitons of CQGLE match the pulses in the ANDi fiber lasers. This is the first decisive demonstration of dissipative solitons in a fiber system with strong dissipative processes such as a strong spectral filtering. The demonstration of dissipative solitons of CQGLE in a laser cavity shows that ANDi fiber lasers can be research tools for dissipative solitons of the Ginzburg-Landau equations. The theoretical work is done by Will Renninger in collaboration with Andy Chong.

A dissipative soliton is a localized structures which exists for an extended period of time, even though parts of the structure experience gain and loss of energy and /or mass [23]. Again as described in chapter 1, the fiber lasers have been conventionally modeled by static dissipative soliton solutions (Equation 1.13) of the CGLE which is traditionally referred as the master equation (Equation 1.12) [3]. Of course, the first natural attempt is to model the ANDi laser with the CGLE. However, the CGLE solutions failed to model a characteristic spectrum with sharp peaks around its edges. The solution of the CGLE is a chirped hyper-secant (Equation 1.13). As the chirp increases its magnitude in Equation 1.13, the corresponding spectrum becomes rectangular [4] but characteristic sharp spectral peaks do not appear at any chirp value. In contrast, it was found that a CQGLE, which is a combination of a real quintic saturable absorbing term and the CGLE, is more appropriate model to ANDi fiber lasers. By adding a quintic saturable absorbing term, a CQGLE is obtained (Equation 3.4).

$$\frac{\partial A}{\partial z} = gA + (\frac{1}{\Omega} - i\frac{D}{2})\frac{\partial^2 A}{\partial t^2} + (\alpha + i\gamma)|A|^2 A + \delta|A|^4 A. \tag{3.4}$$

In Equation 3.4, all coefficients are averaged parameters that the pulse experiences in a round trip of the cavity. $g$ is the net gain which is the combination of the gain from the gain fiber and the loss due to the laser output coupling. $\Omega$ is related to the spectral amplitude modulation such as the gain BW or the intracavity spectral filter. $\alpha$ is the cubic intensity dependent amplitude modulation term which is related to the SA. $\delta$ is the freshly added quintic amplitude modulation term. The general solution of Equation 3.4 is not known. A particular solution is given in Equation 3.5.

$$A[t, z] = \sqrt{\frac{A_o}{\cosh\left(\frac{t}{\tau}\right) + B}}\, e^{-i\frac{\beta}{2}\ln\left(\cosh\left(\frac{t}{\tau}\right)+B\right)+i\theta z}. \tag{3.5}$$

The most important parameter which governs the pulse character is the parameter $B$. For $|B|$ <1 the pulse has an temporal profile close to a hyper-secant profile. As $B$ >1 increasing in the positive direction, the pulse becomes more and more rectangular with a flatted top. For the range -1 < B < 1, the spectrum exhibits a variety of shapes resembling the spectra from ANDi fiber lasers (Figure 3.15).

To observe dissipative soliton solutions of the CQGLE in a fiber laser, a experimental setup in Figure 2.6 is used. In the experiment, a variety of modes are obtained by adjusting the NPE port and the pump power. By carefully adjusting the pump power and waveplates, modes resembling the analytic solutions in Figure 3.15 are found.

Comparing Figure 3.15 and 3.16 indicates that qualitatively the CQGLE is quite successful to model such a laser. The strong qualitative agreement between the analytic solutions and the experimental results suggest that the pulse shaping in the ANDi fiber laser can be appropriately modeled by the CQGLE. The modeling of the ANDi laser with CQGLE is quite beneficial not only for understanding the normal dispersion laser behavior but also for designing fiber lasers with a desired performance. Furthermore, the successful demonstration of dissipative solitons in a fiber system is quite significant

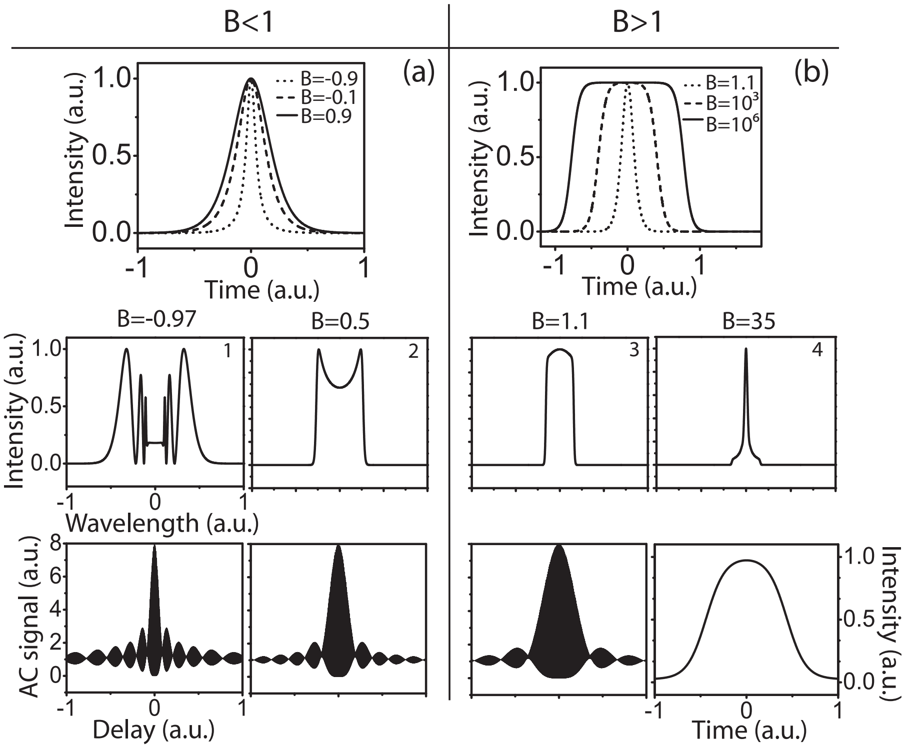

Figure 3.15: Pulse solutions categorized by the value B. Top: temporal profiles, Middle: representative spectral shapes for the indicated values of B, Bottom: corresponding ACs of the respective dechirped analytical solutions. The intensity profile is shown for B=35. From [20]

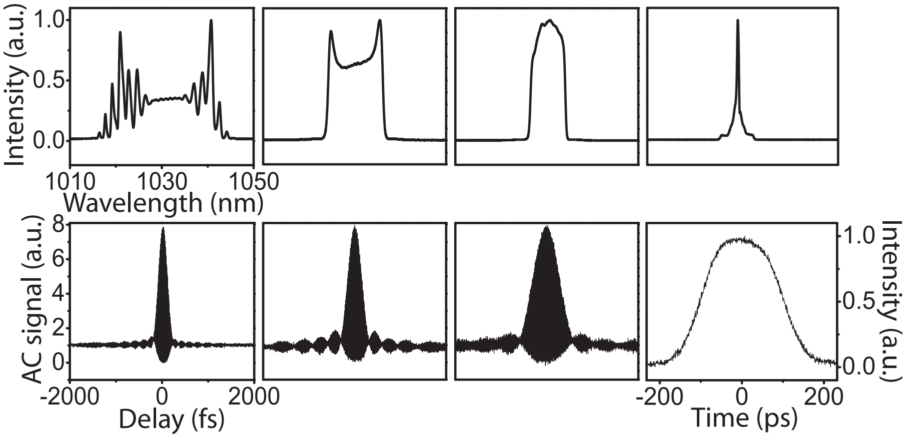

Figure 3.16: Top: representative experimental spectra corresponding to the theoretical pulses in Figure 3.15, Bottom: ACs for the corresponding dechirped pulses. The rightmost pulse is the respective output intensity profile. From [20]

scientifically.

## 3.6 Useful Features of ANDi Fiber Lasers

ANDi fiber lasers have some practically-useful features, in addition to the immediate advantage of removal of the anomalous-dispersion segment. One remarkable feature of the ANDi fiber laser is its continuous tunability without losing mode-locking. It is quite possible to go continuously among the spectra of Figure 3.12 without losing mode-locking, by rotating the waveplates in a laser. In the given experimental setup in Figure 3.11 but with 12 nm spectral filter BW, the dechirped pulse duration can be continuously tuned from ~270 fs to ~150 fs.

The pulse chirp also can be tuned continuously. Experimentally, the chirp can be varied controllably and continuously over the wide range from ~0.44 $ps^2$ to ~0.14 $ps^2$. High pulse energy lasers usually produce chirped pulses, which can be dechirped externally to the laser. In most cases, the dispersive delay is designed to be flexible to accommodate the unknown chirp of the laser output. The situation can be reversed with ANDi fiber lasers: the chirping can be tuned to generate transform-limited pulses after dechirping in a fixed dispersive delay. The tunable chirp will be a practical advantage for optical systems that include components with fixed GVD such as fiber Bragg gratings, volume Bragg gratings, and photonic crystal fibers. The tunable pulse chirp can be used as an additional degree of freedom in a chirped-pulse amplifier, *e.g.*

Finally, the center wavelength can be tuned easily by adjusting the spectral filter center wavelength. Experimentally, the center wavelength is tunable with ~20 nm range, which is close to the free spectral range of the birefringent filter. While the center wavelength is tuned, the mode-locking is sustained without perturbing the pulse shape.

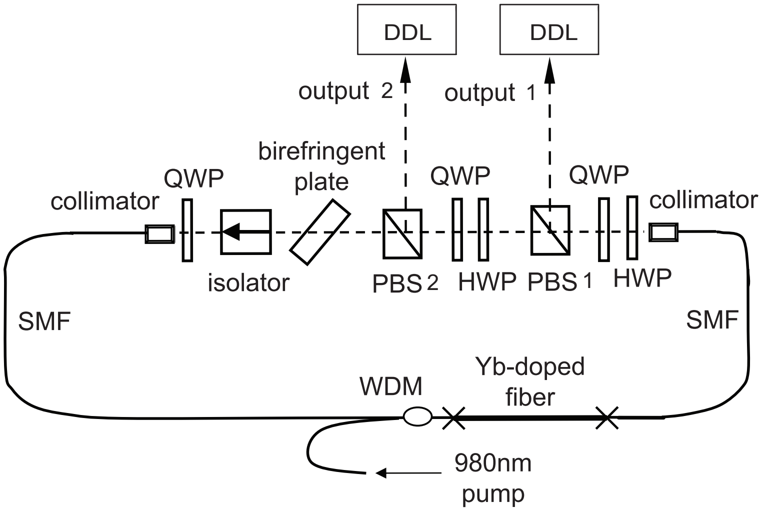

Figure 3.17: Schematic of the experimental setup with two output ports; PBS: polarization beam splitter; HWP: half waveplate; QWP: quarter waveplate; WDM: wavelength division multiplexer; DDL: dispersion delay line.

Mode-locked pulses with noticeable temporal side lobes may not be suitable for applications demanding clean pulses. One can obtain better pulse quality (sometimes with tradeoffs in pulse energy and duration) by taking the output at different points in the cavity. For example, the circulating pulse in a soliton laser is cleaner than the pulse ejected at an NPE port [24]. Figure 3.17 shows an experimental setup to demonstrate the improvement of pulse quality by coupling out at different cavity locations. Waveplates before PBS 2 are solely to adjust the output 2 coupling ratio. The spectral filter BW is set to 12 nm.

The waveplates were adjusted to optimize the pulse energy at output 2. Figure 3.18 demonstrates that a cleaner pulse can be obtained after the NPE port. The pulse from the NPE output (output 1) has a sharply-peaked spectrum with significant major side lobes after dechirping (Figure 3.18(a),(b)). By coupling the laser output right after the NPE port, clean pulses are obtained. The spectrum and the dechirped interferometric AC (Figure 3.18(c),(d)) demonstrate the dramatic improvement. Output 2 produced 3-

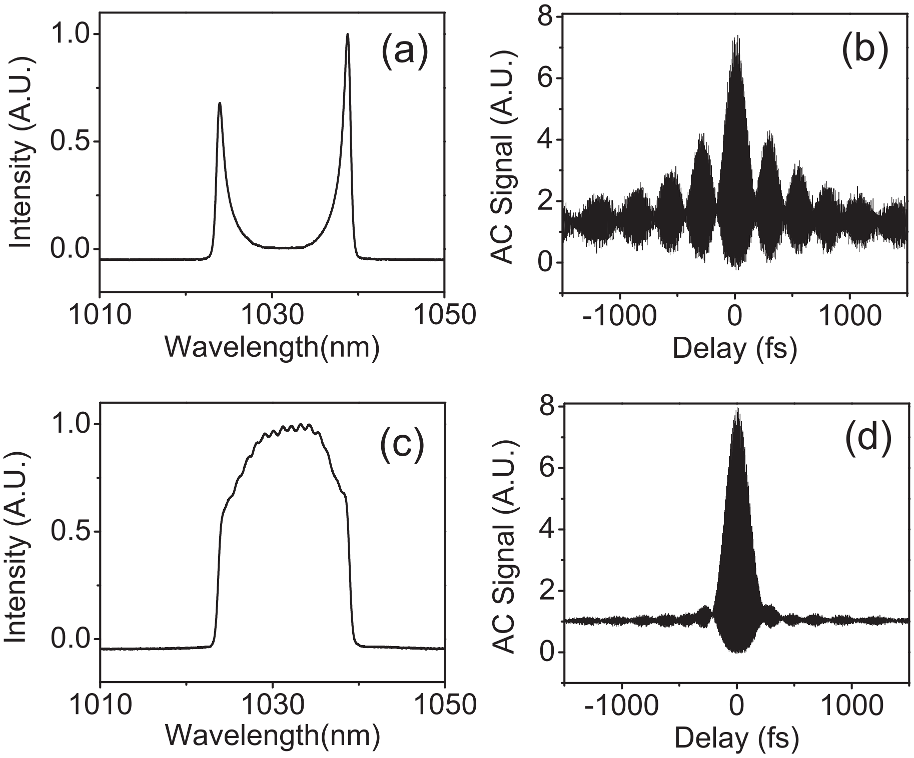

Figure 3.18: Experimental result of the laser with two output ports; output 1: (a) spectrum, (b) dechirped interferometric AC; output 2: (c) spectrum, (d) dechirped interferometric AC.

nJ that could be dechirped to ~150 fs duration. The pulse energy was sacrificed a bit since the NPE ejected pulse (output 1) still contained ~1 nJ energy. In this case, the ”pulse” from output 1 is probably useless for most applications, and really appears to be the interference of the two wave packets that make up the spectrum. We chose this example simply to illustrate the flexibility in pule shape that is available with this kind of laser.

## 3.7 Conclusion

The results of a systematic numerical and experimental study of all-normal dispersion femtosecond fiber lasers have been presented. A key contribution to pulse-shaping in these lasers arises from the spectral filter, which converts frequency chirp to self-amplitude modulation. The behavior and performance of the lasers with variations in the key parameters have been summarized. In contrast to most modern femtosecond lasers, dissipative processes such as the spectral filtering can play a crucial role in pulse formation. The ANDi fiber laser can support a wide variety of pulse shapes and evolutions, which include the CPO and the self-similar laser as limiting cases. The ANDi fiber laser is a robust pulse source capable of high-energy ultrashort pulses, with significant tunability of the pulse duration and chirp.

This work has focused on fundamental determinants of the laser performance. It should be reasonably straightforward to extend the ANDi lasers to higher pulse energies by technical approaches such as the use of large-mode-area fibers; with larger mode area, higher energy is reached at fixed nonlinear phase shift. Higher average powers will be obtained with double-clad gain fibers pumped by broad-area emitters. Order-of-magnitude increases in the pulse energy and average power should be possible. Such a level of performance would make these lasers even more attractive in short-pulse applications. Finally, lasers that are mode-locked by spectral filtering of a chirped pulse can be constructed entirely of fiber-format components to yield integrated, and eventually environmentally-stable, sources of femtosecond pulses.

# BIBLIOGRAPHY

[1] A. Chong, W. Renninger, and F. Wise, J. Opt. Soc. Am. B **25,** 140 (2008).

[2] K. Tamura, J. Jacobson, H. A. Haus, E. P. Ippen, and J. G. Fujimoto, Opt. Lett. **18,** 1080 (1993).

[3] H. A. Haus, J. G. Fujimoto, and E. P. Ippen, J. Opt. Soc. Am. B **8**, 2068 (991).

[4] B. Proctor, E. Westwig, and F. Wise, Opt. Lett. **18,** 1654 (1993).

[5] F. Ö. Ilday, J. R. Buckley, W. G. Clark, and F. W. Wise, Phys. Rev. Lett. **92,** 213902 (2004).

[6] A. Fernandez, T. Fuji, A. Poppe, A. Frbach, F. Krausz, and A. Apolonski, Opt. Lett. **29,** 1366 (2004).

[7] V. L. Kalashnikov, E. Podivilov, A. Chernykh, and A. Apolonski, Appl. Phys. B **83,** 503 (2006).

[8] A. Fernandez, A. Verhoef, V. Pervak, G. Lermann, F. Krausz, and A. Apolonski, Appl. Phys. B **87,** 395 (2007).

[9] J. R. Buckley, F. Ö. Ilday, T. Sosnowski, and F. W. Wise, Opt. Lett. **30,** 1888 (2005).

[10] M. J. Messerly, J. W. Dawson, J. An, D. Kim, and C. P. J. Barty, in *Conference On Lasers and Electro-Optics*, 2006 OSA Technical Digest Series. (Optical Society of America, Washington, D.C., 2006), paper CThC7.

[11] H. Lim, and F. Wise, Opt. Express **12,** 2231 (2004).

[12] L. M. Zhao, D. Y. Tang, and J. Wu, Opt. Lett. **31,** 1788 (2006).

[13] L. M. Zhao, D. Y. Tang, H. Zhang, T. H. Cheng, H. Y. Tam, and C. Lu, Opt. Lett. **32,** 1806 (2007).

[14] J. Buckley, A. Chong, S. Zhou, W. Renninger, and F. Wise, J. Opt. Soc. Am. B **24,** 1803 (2007).

[15] A. Chong, J. Buckley, W. Renninger, and F. Wise, Opt. Express **14,** 10095 (2006).

[16] A. Chong, W. H. Renninger, and F. W. Wise in *Conference On Lasers and Electro-Optics*, 2007 OSA Technical Digest Series. (Optical Society of America, Washington, D.C., 2007), paper CMU4.

[17] A. Chong, W. H. Renninger, and F. W. Wise, Opt. Lett. **32,** 2408 (2007).

[18] P. A. Bélanger, Opt. Express **15,** 11033 (2007).

[19] F. Ö. Ilday, Ph.D. dissertation (Cornell University 2004).

[20] W. H. Renninger, A. Chong, and F. W. Wise, Phys. Rev. A **77**, 023814 (2008).

[21] L. Hocking, and K. Stewartson, Proc. R. Soc. London A **326,** 289 (1972).

[22] V. L. Kalashnikov, E. Podivilov, A. Chernykh, S. Naumov, A. Fernandez, R. Graf and A. Apolonski, New J. Phys. **7,** 217 (16p) (2005).

[23] *Dissipative Solitons*, edited by N. Akhmediev and A. Ankiewics (Springer, Berlin, 2005).

[24] K. Tamura, and M. Nakazawa, Applied Phys. Lett. **67,** 3691-3693 (1995).

CHAPTER 4

# GENERATING HIGH PULSE ENERGY FROM ANDi FIBER LASERS[1]

In this chapter, the investigation of high pulse energy generation in ANDi fiber lasers is presented. Since the net GVD of ANDi fiber lasers are much larger than conventional fiber lasers, high-energy pulses are predicted. Furthermore, unique pulse shaping mechanism of chirped-pulse spectral filtering provides a stable mode-locked operation even with a substantially large nonlinear phase shift ($>10\pi$). By selecting appropriate GVD, spectral filter and proper pump power, ~25 nJ pulse energy with ~150 fs pulse duration is achieved.

## 4.1 Introduction

Fiber lasers have the practical advantages of better stability, greater efficiency, lower sensitivity to alignment and a more compact design than solid-state lasers. However, applications of short-pulse fiber lasers have been limited by the lower pulse energies available from fiber lasers. Most femtosecond fiber lasers employ segments of normal and anomalous group velocity dispersion (GVD) within the cavity. Different operating regimes are found according to the net cavity dispersion. By increasing the net cavity GVD from large and anomalous to large and normal, soliton, stretched pulse [2] and self-similar [3] regimes are found in sequence. To date, self-similar lasers have produced the largest pulse energies. Buckley *et.al.* demonstrated a self-similar ytterbium (Yb) doped fiber laser with a pulse energy above 10 nJ [4]. Above 20 nJ was achieved by increasing the mode area and thereby reducing self-phase modulation (SPM) [5].

Recently, a femtosecond-pulse laser without anomalous GVD in the cavity was

---

[1] Most of the results presented in this chapter have been published in Ref [1]

demonstrated [6]. Self-amplitude modulation in such an all-normal-dispersion (ANDi) fiber laser occurs through spectral filtering of a highly-chirped pulse in the cavity. The pulse can be dechirped to the transform-limit outside the cavity. Pulse energy as high as 3 nJ was achieved in the initial demonstration. The simplicity of an ANDi laser makes it attractive for applications, and it is natural to ask whether the pulse energy can be scaled to larger values.

Two features of an ANDi laser suggest that this design will be compatible with high-energy pulses. First, ANDi lasers can be mode-locked with the net (normal) cavity GVD an order of magnitude higher than that of fiber lasers with dispersion maps. Pulse energy is theoretically expected to increase rapidly with increasing GVD [3]. Second, the pulse-shaping mechanism requires SPM, and gets stronger with increasing pulse intensity and nonlinear phase shift. Thus, an ANDi laser may be more tolerant of large nonlinear phase shifts than prior lasers.

In this chapter, we report the results of an investigation into high-energy operation of an ANDi laser. Numerical simulations indicate that femtosecond pulses with energies in the vicinity of 50 nJ should be possible. Experiments are constrained by the pump power available from single-mode diodes, but pulse energies above 20 nJ are still achieved. The experimental results agree reasonably well with the numerical calculations, and represent an order-of-magnitude increase over the pulse energy of the initial ANDi laser [6]. After dechirping to 150-200 fs duration, peak powers in the 100-kW range are possible. The pulse energy and peak power are comparable to the highest-reported values for femtosecond fiber oscillators.

## 4.2 Numerical simulations and experimental results

The available pump power impacts the design of the laser in several ways. By pumping a segment of gain fiber with two single-mode diodes, up to 800 mW power is available in-core. The efficiency of the ANDi laser can be 30-40% which implies a maximum average output-power of ~300 mW. To access the 10-30 nJ energy range, the repetition rate must be reduced to ~10 MHz, which corresponds to >10 m of fiber in the cavity. The large normal GVD provided by such fiber lengths is desirable, but it also reduces the output spectral bandwidth [7]. The spectral filter that shapes the pulse must be chosen appropriately.

Numerical simulations were performed to assess these issues and explore the high-energy limit of operation [8]. Here we summarize the results obtained with 8- and 16-m cavities, which correspond to 25- and 12.5-MHz repetition rates, respectively. The fiber is followed by a lumped saturable absorber, which represents nonlinear polarization evolution (NPE), and a gaussian filter in a ring cavity (see top of Figure 4.1). Based on initial trials, a filter bandwidth (BW) of 8 (6) nm was chosen for the 25 (12.5) MHz repetition rate laser.

Stable solutions are found for a wide range of pulse energies, up to ~50 nJ. Results that are representative of pulse energies > 10 nJ are shown in Figure 4.1. Specifically, the result for the laser with a 25 (12.5) MHz repetition rate and 12- (26)-nJ output pulse energy is shown. The pulse duration increases monotonically in the long segment of SMF. It decreases owing to NPE, but the self-amplitude modulation is dominated by filtering in the gain segment and the spectral filter. The approximately gaussian spectrum (Figure 4.1, middle and bottom panels) broadens in the SMF segments, and eventually develops the steep and structured edges characteristic of SPM. The filter restores the

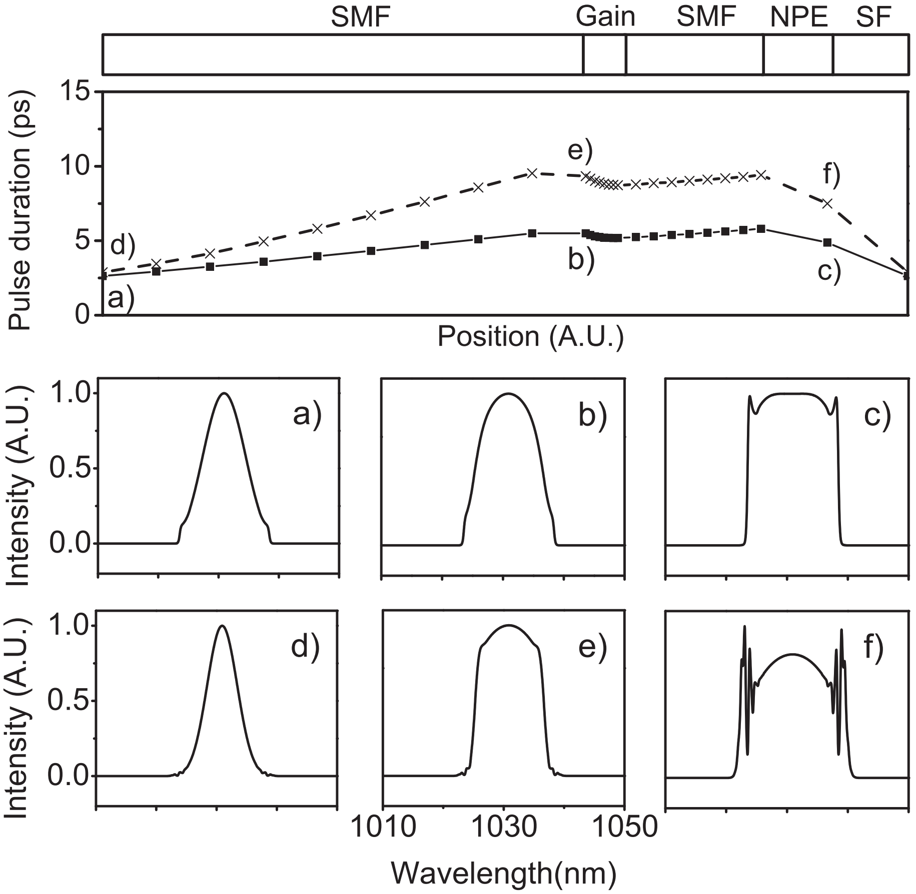

Figure 4.1: Numerical simulation results: Top: pulse duration evolution for lasers with 25 MHz (solid line, 12 nJ pulse energy) and 12.5 MHz (dashed line, 26 nJ pulse energy) repetition rates; Middle / Bottom: 25 MHz / 12.5 MHz laser spectra at a)/d) beginning of the first SMF, b)/e) beginning of the gain fiber and c)/f) output; NPE: nonlinear polarization evolution; SF: spectral filter

roughly-gaussian spectrum on each traversal of the cavity. The temporal and a spectral breathing ratios increase to accommodate higher pulse energy and nonlinear phase shift ($\Phi_{NL}$). For the 26-nJ pulse, e.g., $\Phi_{NL} \sim 12\pi$. However, the pulse can be dechirped to within 15% of the transform limit with a linear dispersive delay. Pulse-shaping based on chirping and spectral filtering is remarkably effective in producing output pulses with nearly-linear chirp.

Based on the results of the simulations, an ANDi laser was built with Yb-doped gain

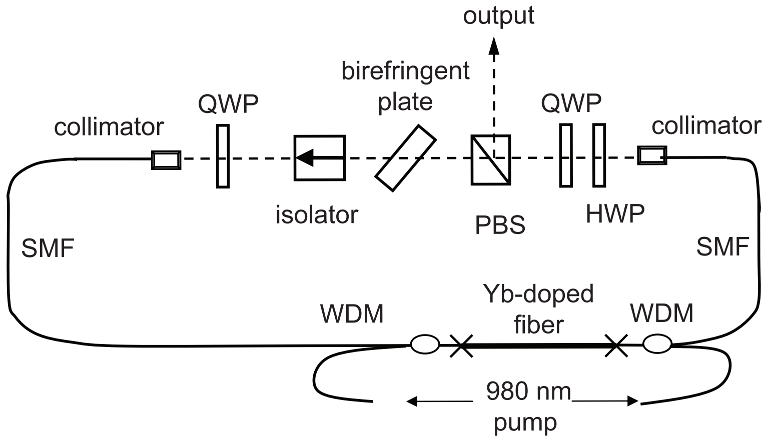

Figure 4.2: Schematic of ANDi fiber laser: QWP: quarter-waveplate; HWP: half-waveplate; PBS: polarizing beam-splitter; WDM: wavelength-division multiplexer.

fiber (Figure 4.2). The total cavity length can be adjusted to give a ~25 (12.5) MHz repetition rate. The fiber section consists of 7 (15) m of SMF followed by 20 (50) cm of Yb fiber with another ~1 (0.5) m segment SMF attached at the end of the gain fiber. All fibers have a 6-$\mu$m core diameter. The total cavity dispersion is ~0.19 (0.38) $ps^2$. Two 980-nm diodes supply ~800 mW maximum pump power. To optimize the output pulse energy, the output is taken directly from the polarizing beam splitter, acting as the NPE ejection port[9]. A birefringent plate with suitable thickness, inserted between the beam splitter and the isolator, provides a sinusoidal spectral transmission. A filter bandwidth of 8 (6) nm is chosen for the 25 (12.5) MHz repetition rate laser. These setups produce a variety of mode-locked states as the waveplates are rotated. The output pulse train is monitored with a photodetector/sampling oscilloscope combination with a bandwidth of 30 GHz. The interferometric and intensity autocorrelations are monitored for delays up to ~100 ps.

For the 25-MHz laser, single-pulse and self-starting mode-locking occurs for many settings of the waveplates. The mode-locked average power is 300 mW with 660-mW pump power. The maximum pulse energy is 12 nJ. With the corresponding waveplates

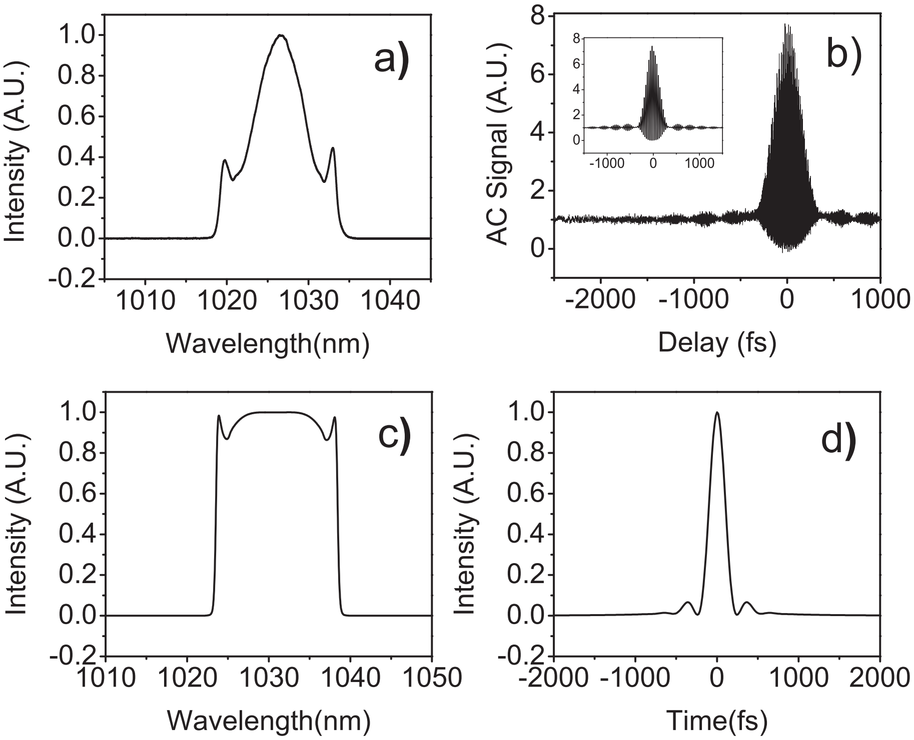

Figure 4.3: Output of the 25 MHz laser at 12 nJ energy: a) spectrum, b) dechirped autocorrelation (~240 fs) and the autocorrelation of the zero-phase Fourier-transform of the spectrum (~210 fs, inset), c) simulated spectrum, d) simulated dechirped pulse (~225 fs).

setting, ~80% of the incoming pulse energy is coupled out at the NPE ejection port. As shown in Figure 4.3, the measured spectrum exhibits the main features of the simulation at the same energy. The 12-nJ pulses can be dechirped to 240-fs duration (Figure 4.3(b)), which is close to the transform limit, as predicted. Despite the structured spectrum, the experimental output pulse quality is high: only 1% of the pulse energy is in the secondary temporal lobes.

With the repetition rate reduced to 12.5 MHz, stable single-pulsing operation is obtained with low pump power (< 200 mW). As the pump power increases, the laser tends to multi-pulse. With pump power above 200 mW, only the mode with the broadest output spectrum is single-pulsing. The highest pulse energy that was obtained directly and in single-pulsing operation is 22 nJ (275 mW average power). However, with the waveplates oriented to produce the 22-nJ pulses, the pump power can then be increased, increasing the pulse energy up to 26 nJ (325 mW average power obtained with 750 mW pump power. ~70% of the incoming pulse energy is coupled out at the NPE ejection port.) The 26-nJ pulses are not self-starting, although they are self-sustaining. This behavior is an indication of over-driving the NPE. The characteristics of the 26-nJ pulses are shown in Figure 4.4 along with the corresponding simulation results. The dechirped pulse duration is 165 fs, which is again close to the transform-limited value. In this case the side-lobes in the time domain contain ~4% of the energy. The spectrum exhibits the strong fringes seen in the simulation. A small pulse that contains ~0.5% of the total pulse energy occurs ~4 ps from the main peak, which is the time interval expected from the spectral fringe spacing. As demonstrated previously [9], the experimental result shows the NPE ejected output pulse quality is worse than that of the cavity circulating pulse. The transmitted spectrum (Figure 4.4(a) dotted) of the NPE port is cleaner than the ejected spectrum with only ~2% of the energy in the side lobes and negligible small remote pulses.

The pulse quality is significantly improved from the previously reported result [6]. In the initial demonstration, an interference filter was used. Numerical simulations consistently show that a Gaussian-shaped filter is highly desirable, and in the present work we implement such a shape by the use of a birefringence filter. We believe that higher pulse energies are possible with ANDi fiber lasers. As mentioned above, numerical simulations show that 50-nJ pulses are stable with an appropriate saturable absorber. By replacing NPE with a semiconductor saturable absorber, e.g., it should be possible to reach higher energies at lower repetition rates. However, the results presented here are probably approaching the margin of multi-pulsing and acceptable pulse quality. Our future effort will be focused not only to increase the pulse energy but also to improve

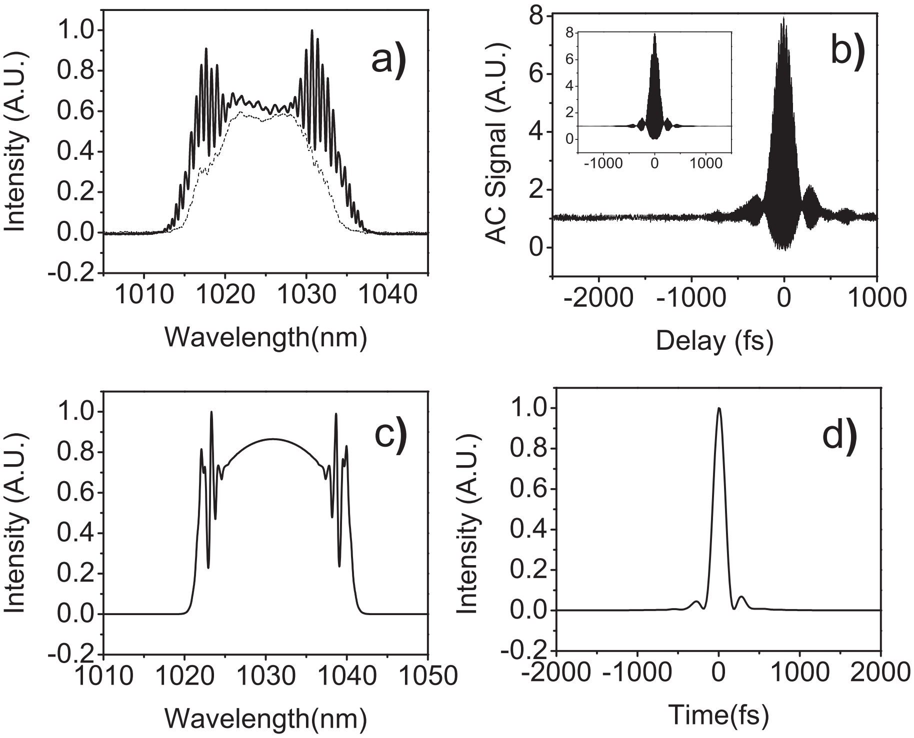

Figure 4.4: Output of the 12.5 MHz laser at 26 nJ energy: a) spectra transmitted (dotted) and rejected (solid) from the NPE port, b) dechirped autocorrelation (~165 fs) and the autocorrelation of the zero-phase Fourier-transform of the spectrum (~140 fs, inset), c) simulated spectrum, d) simulated dechirped pulse (~195 fs).

the pulse quality and stability against multi-pulsing. This work demonstrates that stable, high-quality pulses in the range of 10-20 nJ can be obtained with this class of laser.

## 4.3 Conclusion

To summarize, we have shown that an ANDi fiber laser can generate stable pulses despite the accumulation of nonlinear phase shifts greater than 10 $\pi$. Strong pulse-shaping by spectral filtering of the chirped pulse in the cavity supports stable pulses with 20 nJ energy, and these can be dechirped to ~200 fs duration. Experimental results agree reasonably well with numerical simulations of the laser behavior and performance. Higher energies may be reached by further development of the effective or real saturable absorber in the laser.

# BIBLIOGRAPHY

[1] A. Chong, W. H. Renninger, and F. W. Wise, Opt. Lett. **32,** 2408 (2007).

[2] K. Tamura, J. Jacobson, H. A. Haus, E. P. Ippem, and J. G. Fujimoto, Opt. Lett. **18,** 1080 (1993).

[3] F. O. Ilday, J. R. Buckley, W. G. Clark, and F. W. Wise, Phys. Rev. Lett. **92,** 213902 (2004).

[4] J. R. Buckley, F. O. Ilday, T. Sosnowski, and F. W. Wise, Opt. Lett. **30,** 1888 (2005).

[5] M. J. Messerly, J. W. Dawson, J. An, D. Kim, and C. P. J. Barty, in *Conference On Lasers and Electro-Optics*, 2006 OSA Technical Digest Series. (Optical Society of America, Washington, D.C., 2006), paper CThC7.

[6] A. Chong, J. Buckley, W. Renninger, and F. Wise, Opt. Express **14,** 10095 (2006).

[7] B. Proctor, E. Westwig, and F. Wise, Opt. Lett. **18,** 1654 (1993).

[8] F. O. Ilday, Appendix A in the Ph.D. dissertation, Cornell University (2004).

[9] K. Tamura, and M. Nakazawa, Applied Phys. Lett. **67,** 3691 (1995).

## CHAPTER 5

## PULSE DURATION LIMITATION OF ANDi FIBER LASERS

In this chapter, the investigation of short pulse generation in ANDi fiber lasers is presented. According to the numerical simulations, very short pulse durations compatible to those of stretched pulse fiber lasers can be generated. The pulse shaping mechanism to generate a short pulse duration is fundamentally different from that of the stretched pulse fiber laser. The numerical simulation result shows the possibility of ~10 cycle pulse generation in ANDi fiber lasers. In the experiment, a ~10 cycle pulse was not realized due to the limited pump power but reasonably short pulse durations of 70~80 fs are obtained.

### 5.1 Introduction

Fiber lasers have the practical advantages over solid-state lasers. However, applications of fiber lasers have been limited by the lower pulse energies and the longer pulse durations. The design of a short pulse fiber laser was heavily influenced by the master equation approach [1]. The shortest pulse duration is reachable around zero net cavity group velocity dispersion (GVD) according to the master equation approach. Guided by the master equation prediction, building a stretched pulse fiber laser [2] with a dispersion map targeting near zero net GVD was a common sense to obtain very short pulses.

Most distinguished short pulse results are as follows. Ilday *et al.* demonstrated 36-fs pulses from a Ytterbium (Yb)-doped fiber laser [3]. The higher-order dispersions were huddles for even shorter pulses. By compensating third-order dispersion (TOD) of Yb-doped fiber laser with a grating-prism pair, Buckley *et al.* demonstrated 33-fs pulses with outstanding pulse quality [4]. For Erbium (Er)-doped fiber lasers, Tang *et* *al.* demonstrated 47-fs pulses [5]. These are accomplishments of short pulses based on the stretched pulse operations at near zero net GVD. Stretched pulse operations was believed to be essential for generating short pulses (*i.e.* <100 fs) with possible higher-order dispersion compensation to enhance the pulse duration and quality.

Recently, an all-normal dispersion (ANDi) femtosecond laser with an intracavity spectral filter was demonstrated [6]. Self-amplitude modulation in such a laser occurs through spectral filtering of a highly-chirped pulse. Chong *et al.* demonstrated an interesting mode of ~150 fs pulses from a ~16 m Yb-doped ANDi fiber laser cavity which was ~ 45 times of the dispersion length [7]. It indicates that shorter pulses may be possible at very large GVD by choosing laser parameters properly. Generating short pulses with a simple ANDi laser without an anomalous GVD segment will be attractive for various applications. Moreover, since the pulses are always highly chirped in ANDi lasers, higher-order dispersion may have negligible effects.

In this chapter, we report an investigation into the pulse duration limitation of Yb-doped ANDi fiber lasers. Numerical simulations indicate that ~30 fs pulses are possible at a large normal GVD. Experiments are constrained by the available pump power, but 70~80 fs dechirped pulse durations were still obtained at a large normal GVD (0.03~0.05 $ps^2$).

## 5.2 Numerical simulation and experimental results

A guide for generating short pulses was provided by the systematic study of the ANDi laser [8]. The output pulse is a strong function of the laser cavity GVD, $\Phi^{NL}$, and the spectral filter BW. The mode-locked spectrum tends to be broadened with decreasing GVD, decreasing spectral filtering bandwidth (BW), or increasing $\Phi^{NL}$. To see the effect of parameters, numerical simulations were performed. The cavity was consisted of a segment of SMF, and ~60 cm Yb-doped gain fiber with another ~1 m SMF fiber segment. After the fiber segment, a spectral filter with ~12 nm BW was set. Numerical simulations were performed for various combinations of the GVD and the $\Phi^{NL}$ by adjusting the length of the first SMF segment and the pump power.

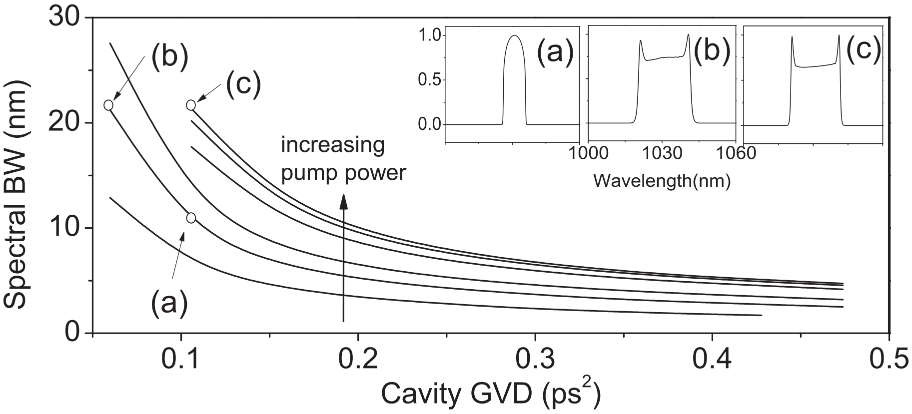

Figure 5.1: Numerical simulation result summary of an ANDi fiber laser: Mode-locked spectral BW *vs.* GVD

The numerical simulation results are summarized in Figure 5.1. The spectral BW increases as the cavity GVD decreases. Increasing the pump power and therefore the $\Phi^{NL}$ also has the similar effect. Figure 5.1(a)-(c) show how the mode-locked spectra with various combinations of GVD and the pump power. Starting from a mode of Figure 5.1(a), decreasing GVD while holding the pump power constant develops a more structured but wider spectrum (Figure 5.1(b)). Meanwhile, increasing the pump power while holding GVD constant has a similar effect. Dechirped pulse durations of Figure 5.1(b) and (c) are quite close. However, Fig 5.1(c) spectrum is more structured (higher peaks around its edges) with a degraded pulse quality. The trend shows that the larger $\Phi^{NL}$ broadens the spectrum and but the pulse quality is degraded with structures in the spectrum. Meanwhile, less GVD again broadens the spectrum with improved pulse quality. Based on the simulation trend, the strategy to generate short pulses is to design a cavity with smallest possible GVD while pump the gain fiber as high as possible to generate substantial $\Phi^{NL}$. Controlling GVD and $\Phi^{NL}$ separately is tough especially for Yb-doped laser since the ratio of the GVD coefficient and the nonlinearity coefficient of the commercially available SMF is not flexible unless cumbersome photonic crystal fibers are used. In this paper, we will focus on Yb-doped fiber lasers with only regular which is the most practical case.

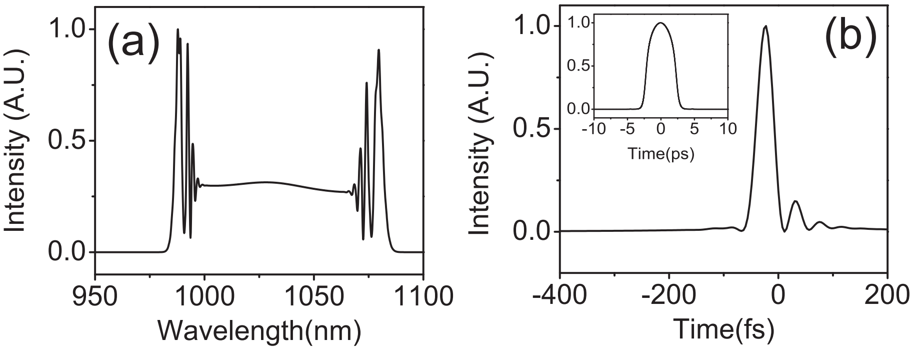

Figure 5.2: Numerical simulation results of an ANDi fiber laser: a) mode-locked output spectrum, b) externally dechirped time profile (~34 fs)(inset: chirped pulse directly from the laser cavity (~4.3 ps))

For core pumped Yb-doped fiber lasers, the pump power and the net GVD are practically limited. Nevertheless, to verify that the laser can generate very short pulses, numerical simulations were performed with a realistically short cavity and ideal unlimited pump power. The cavity was consisted of 50 cm of SMF, and 20 cm gain fiber (40 nm gain BW) with another 50 cm SMF fiber segment. After the fiber segment, a 40 nm BW spectral filter was set. Numerical simulations were performed for various $\Phi^{NL}$ by adjusting the pump power.

The numerical simulation result with the shortest dechirped pulse duration is shown in Figure 5.2. The spectrum develops sharp structures near its edges (Figure 5.1(a)) and as the consequence, the dechirped pulse shows strong sidelobes (Figure 5.1(b)). However, the spectrum was broad enough to have ~34 fs dechirped pulse duration. The pulse energy was ~44 nJ which corresponds to ~7 W average power. Same numerical simulation without TOD was performed but the spectrum and the dechirped pulse duration were not altered significantly. It is believed that highly chirped pulses of ANDi lasers are impervious to higher-order dispersions. It implies that the strategy of generating short pulses from ANDi lasers is essentially different from that of stretched pulse lasers. For stretched pulse lasers, the compensation of higher-order dispersions is desirable. Moreover, the pulse energy from the stretched pulse laser is moderate. In contrast, the compensation of higher-order dispersions in ANDi lasers does not affect the laser performance noticeably. The simulation also indicates that the ANDi fiber laser can generate very high pulse energies since the pulse shaping mechanism requires substantial $\Phi^{NL}$. To predict the real performance of the laser, we performed a numerical simulation with realistic pump power to have 2~3 nJ (200~400 mW average power) pulse energies. The dechirped pulse durations, which are expected to be observed experimentally with available pump power, were 70~80 fs.

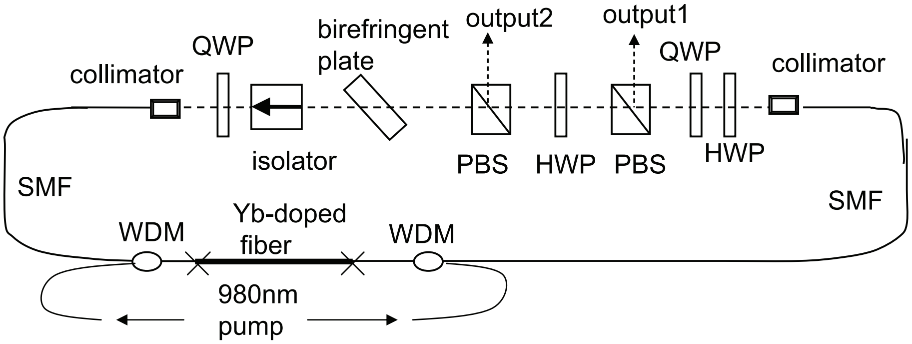

Figure 5.3: Schematic of ANDi fiber laser: QWP: quarter-waveplate; HWP: half-waveplate; PBS: polarizing beam-splitter; WDM: wavelength-division multiplexer.

Based on the simulation results, an ANDi laser was built (Figure 5.3). Since the pump power is limited, we increased the SMF after the gain fiber to enhance the $\Phi^{NL}$ targeting a 80 MHz repetition rate. The fiber section consists of ~44 cm of SMF, ~17 cm of Yb-doped fiber, and ~170 cm segment SMF. The cavity GVD is ~0.053 $ps^2$. Two

980-nm diodes supply ~900 mW pump power. A set of a half, a quarter waveplate, and a polarizing beam splitter (PBS) acts as the nonlinear polarization evolution (NPE) ejection port (output 1). It is well known that the cavity circulating pulse quality is better than that of the NPE ejected [9]. To obtain quality pulses, we setup a second PBS to couple out the cavity circulating pulse as the main output (output 2). A birefringent filter with 15 nm BW was set after the second PBS. The output pulse train is monitored with a photodetector/sampling oscilloscope combination with a bandwidth of 30 GHz. The autocorrelation (AC) signal is monitored for delays up to ∼100 ps. The laser is mode-locked for various self-starting modes by adjusting waveplates. The shortest duration result is shown in Figure 5.4.

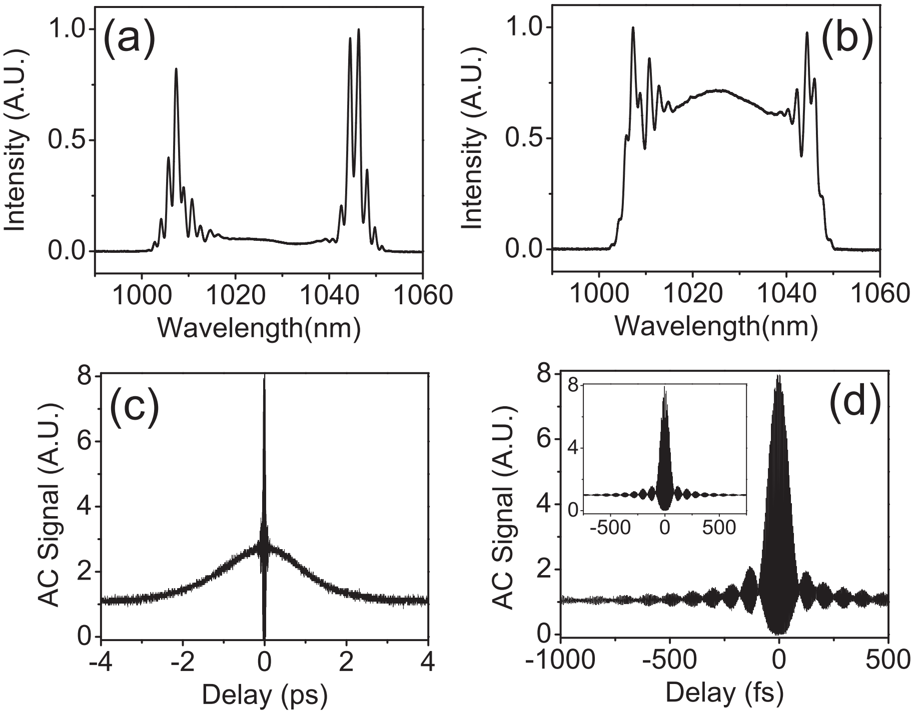

Figure 5.4: Output of the 80 MHz laser : a) output1 spectrum, b) output2 spectrum, c) chirped autocorrelation (∼1.7 ps), d) dechirped autocorrelation (∼68 fs) and the autocorrelation of the zero-phase Fourier-transform of the spectrum (inset).

The structured spectrum of output 1 (Figure 5.4(a)) is similar to the simulation result (Figure 5.2(a)). However, the cavity circulating spectrum is much cleaner (Figure 5.4(b)) which was dechirped to ~70 fs pulse duration (within ~7 % of the transform limited). The output 2 has 172 mW average power which corresponds to ~2 nJ pulse energy. Even though the output 2 spectrum is less structured, the time profile has some sidelobes as the consequence of remaining spectral fringes and steep edges. The role of the spectral filter is crucial. Without it, no stable mode-locking is obtained. One can improve the pulse quality further while keeping the pulse duration by decreasing GVD and nonlinearity properly. This process is equivalent to moving from the condition of Figure 5.1(c) to that of Figure 5.1(b). While keeping the same pump power, the segment of SMF after the gain fiber in Figure 5.4 was reduced to ~75 cm (GVD ~0.033 $ps^2$, 130 MHz repetition rate). The best result was presented in Figure 5.5.

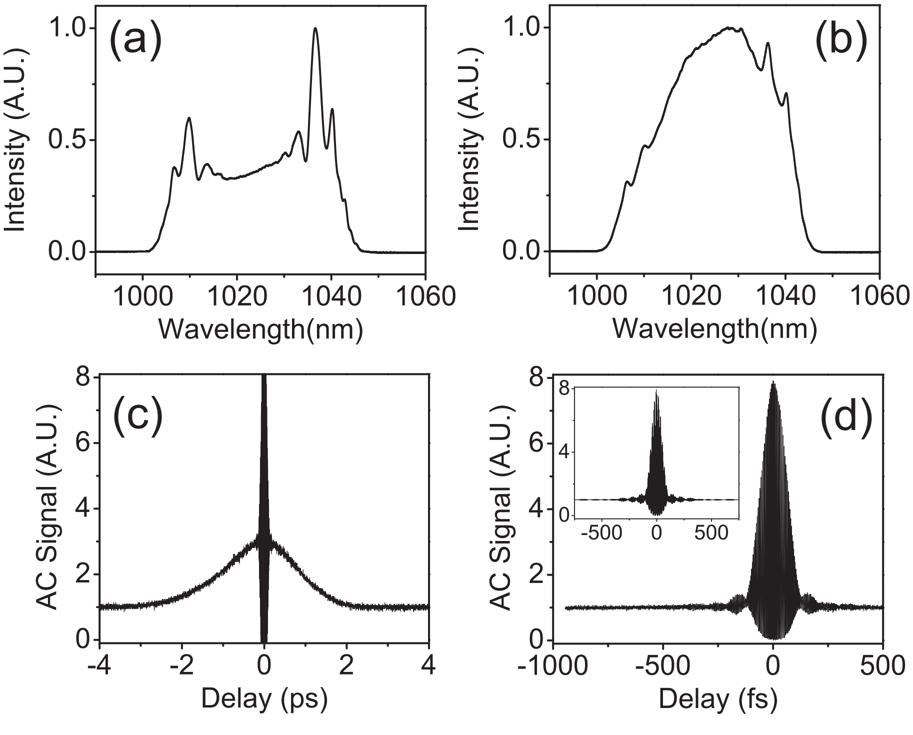

Figure 5.5: Output of the 130 MHz laser : a) output1 spectrum, b) output2 spectrum, c) chirped autocorrelation (~1.4 ps), d) dechirped autocorrelation (~77 fs) and the autocorrelation of the zero-phase Fourier-transform of the spectrum (inset).

The mode-locked spectrum (Figure 5.5(a)) is much smoother as expected. The cavity circulating pulse has a noticeably clean spectrum (Figure 5.5(b)). AC (Figure 5.5(d)) shows a clean ~80 fs dechirped pulse with very small sidelobes (within 7% of the transform limited). 155 mW average power corresponds to ~1.2 nJ pulse energy. Without a spectral filter, some modes were stably mode-locked. However, those modes were always narrower in spectral BW. It indicates that the spectral filter is crucial to stabilize the mode with a broadened spectrum by substantial $\Phi^{NL}$. The experimental results agree with the numerical simulation with realistic pump power. Recently, Ruehl *et al.* demonstrated ~75 fs from a high normal GVD Er-doped fiber laser [10]. Even though the result in this paper looks similar to the work of Ruehl *et al.*, the pulse shaping mechanism is quite different. Ruehl *et al.*'s laser relied on a wide Raman gain BW while the short pulse generation in this paper is based on balancing of GVD, $\Phi^{NL}$, and an appropriate spectral filtering BW.

## 5.3 Conclusion

To summarize, we report an investigation of the pulse duration limitation of Yb-doped ANDi fiber lasers. Experimental results agree with numerical simulations. By adjusting laser parameters properly and coupling out the cavity circulating pulse, pulse quality can be improved noticeably. The experiment demonstrated clean pulses with energies of 1~2 nJ and 70~80-fs dechirped duration. The experiment is limited by the available pump power and the numerical simulation suggests that ~30 fs duration is quite possible from a very simple ANDi fiber laser with a proper pump power.

# BIBLIOGRAPHY

[1] H. A. Haus, J. G. Fujimoto, and E. P. Ippen, J. Opt. Soc. Am. B **8**, 2068 (991).

[2] K. Tamura, J. Jacobson, H. A. Haus, E. P. Ippen, and J. G. Fujimoto, Opt. Lett. **18,** 1080 (1993).

[3] F. Ilday, J. Buckley, L. Kuznetsova, and F. Wise, Opt. Express **11,** 3550 (2003).

[4] J. R. Buckley, S. W. Clark, and F. W. Wise, Opt. Lett. **31,** 1340 (2006)

[5] D. Y. Tang and L. M. Zhao, Opt. Lett. **32,** 41 (2007).

[6] A. Chong, J. Buckley, W. Renninger, and F. Wise, Opt. Express **14,** 10095 (2006).

[7] A. Chong, W. H. Renninger, and F. W. Wise, Opt. Lett. **32,** 2408 (2007).

[8] A. Chong, W. Renninger, and F. Wise, J. Opt. Soc. Am. B **25,** 140 (2008).

[9] K. Tamura, and M. Nakazawa, Applied Phys. Lett. **67,** 3691 (1995).

[10] A. Ruehl, V. Kuhn, D. Wandt and D. Kracht, Opt. Express **16,** 3130 (2008).

# CHAPTER 6

# ENVIRONMENTALLY STABLE ANDi FIBER LASERS[1]

Chapter 6 describes the demonstration of environmentally stable version of ANDi fiber lasers utilizing polarization maintaining fibers. Two cavity designs are presented in this chapter along with experimental results for each one. The first one is the sigma cavity design and the second one is the Fabry-Perot linear cavity. The self-starting is initiated by the semiconductor saturable absorber in both cases. The unique pulse shaping mechanism of chirped pulse spectral filtering generates femtosecond pulses at very large normal GVD.

## 6.1 Introduction

Femtosecond fiber lasers are attractive short-pulse sources because of their stability, high efficiency, low sensitivity to alignment, compact design and low production cost. There were notable achievements of the pulse energy and the pulse duration in high-energy ytterbium (Yb)-doped fiber lasers recently. However, wide adoption of fiber lasers beyond the laboratory environment is discouraged because the mode-locked operation can be disrupted by external perturbations. Thermal and mechanical perturbations to the fiber can induce random birefringence, which can substantially alter the laser performance.

Ideally, linearly-polarized light along the slow axis of a polarization-maintaining (PM) fiber is robust against such perturbations. Researchers have devoted substantial efforts to development of environmentally-stable mode-locked fiber lasers, in many configurations. Although PM fibers were successfully employed in a variety of laser configurations, building femtosecond Yb-doped PM fiber lasers was challenging. Fiber lasers

---

[1] Most of the results presented in this chapter have been published in Ref [1]

typically contain an intracavity anomalous group velocity dispersion (GVD) segment, which has been considered a prerequisite to the generation of femtosecond pulses. For Yb-doped fiber lasers, components that introduce anomalous GVD (grating pairs, photonic crystal fibers (PCF), fiber Bragg gratings, higher-order-mode (HOM) fibers, etc.) tend to introduce complications and/or increase cost. The nonlinear polarization evolution (NPE) mode-locking technique, which exploits the cross phase modulation between two polarization modes, is not conveniently applicable to PM fibers.

Various mode-locking mechanisms and means of introducing anomalous GVD into PM Yb-doped fiber lasers have been proposed. A sigma-type cavity utilizing an anomalous dispersion photonic bandgap fiber as a PM fiber was demonstrated [2]. Nielsen *et al.* reported a femtosecond PM linear fiber laser with a semiconductor saturable absorber mirror (SESAM) and a grating pair [3], and a fiber Bragg grating can replace the bulk grating pair [4]. A clever way to implement NPE in a PM fiber laser was also demonstrated [5]: a linear cavity with a Faraday mirror was successfully mode-locked utilizing NPE in the PM fiber. This work established the possibility of NPE in the PM fiber, but the pulse duration was in the picosecond range.

Recently, a femtosecond fiber laser without an intracavity anomalous GVD segment was demonstrated [6]. Self-amplitude modulation in such an all-normal-dispersion (ANDi) laser occurs through spectral filtering of a chirped pulse. A simple environmentally-stable femtosecond fiber laser is anticipated by replacing all fiber components with PM versions and adding a suitable saturable absorber (SA), such as a SESAM. The self-amplitude modulation is dominated by the contribution of the filtering in ANDi lasers, but a significant contribution from NPE has also been required for stable operation. Thus, it is not clear *a priori* that a SESAM will be adequate to stabilize pulses formed by the spectral filtering mechanism. Ortaç *et al.* reported a laser based on single-polarization large-mode-area (LMA) PCF and a SESAM, which generated 750-fs pulses with 25 nJ energy [7]. Pulse shaping in this laser is attributed to saturable absorption, with minimal effects from spectral filtering. The LMA fiber offers intriguing potential for high pulse energies, but since the fiber cannot be bent, lasers with LMA fibers lose the advantage of the flexible optical fiber. Therefore the laser integration remains complicated and expensive. With free-space pumping, inflexible gain fiber and the laser cavity largely defined by bulk optics, birefringence of the fiber is not likely to be the primary limit to stability of this kind of laser.

We demonstrate an environmentally-stable ANDi Yb-doped fiber laser that employs only PM fibers. We present two different fiber laser configurations for the environmentally-stable ANDi fiber lasers. For the sigma laser configuration, the unique pulse-shaping mechanism of the ANDi fiber laser provides stable mode-locked operation at large normal net cavity GVD ($\sim 0.1ps^2$). The linear cavity configuration with PM fiber and very large normal GVD ($\sim 0.17ps^2$) is also demonstrated. For both cases, the pulse-shaping is dominated by the spectral-filtering mechanism, and self-starting operation is ensured by the inclusion of a SESAM. Strong spectral filtering can enhance the mode-locked spectrum and hence the dechirped pulse duration [9]. Even with such large GVD, the laser generates ~300-fs pulses. Once the mode-locked operation was obtained, the laser was stable against external perturbations to the fiber due to the environmentally-stable nature of the PM fiber.

## 6.2 Numerical simulations and experimental results for a sigma cavity

The experimental setup is shown in Figure 6.1. The fiber section contains only PM fiber components. The fiber section consists of ~3 m of PM single-mode fiber (SMF) followed by ~60 cm of PM Yb-doped fiber with another ~1 m segment PM SMF attached at the end of the gain fiber. The PM wavelength division multiplexer couples a maximum of 300 mW of 980-nm pump power to the core of the gain fiber. The total cavity dispersion is ~0.1 $ps^2$. All PM fiber components were carefully spliced with extinction ratios over 35 dB. After the fiber section, the laser output 1 is coupled out at the ejection port consisting of a half-waveplate (HWP), a quarter-waveplate (QWP) and a polarizing beam splitter (PBS). A combination of waveplates and a PBS does not induce an amplitude modulation even though it resembles an NPE port. The role of it is simply to provide a fully flexible output coupling ratio in the experiment. The waveplates and PBS setup can be replaced by fiber integrated devices such as a PM variable coupler and a PM circulator. The SESAM is commercially available with a ~35% modulation depth, a ~40-nm spectral bandwidth (BW) and a ~500-fs relaxation time constant. A 10× microscopic objective lens was used to focus the beam on the SESAM.

The beam propagates through another ejection port to couple out at output 2 through PBS 2. The purpose of the second ejection port is to obtain cleaner pulses owing to the SESAM's saturable noise suppressing action. Again, the second ejection port can be replaced by a PM variable coupler for a fiber integrated laser design. The remaining beam travels through an ~8 nm BW birefringence filter consisting of PBS 2, a birefringent plate and a polarization dependent isolator. A HWP adjusts the linear polarization to match the slow axis of the PM fiber. Coupling into the PM fiber requires careful

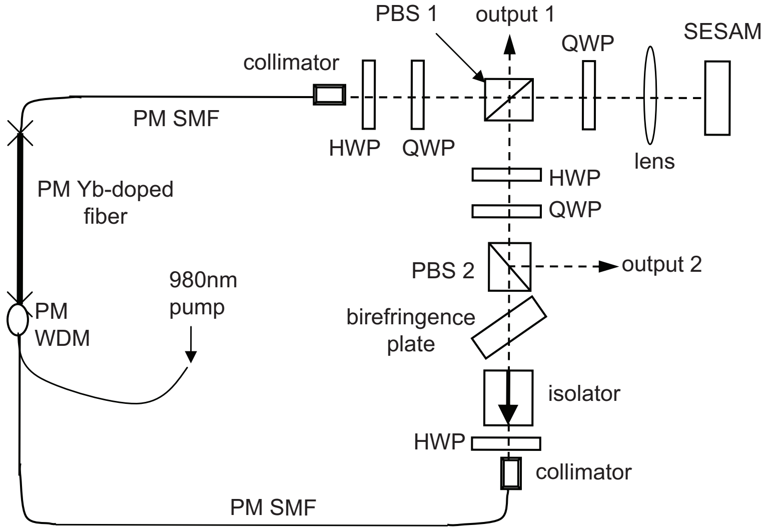

Figure 6.1: Schematic of environmentally-stable ANDi fiber laser: QWP: quarter-waveplate; HWP: half-waveplate; PBS: polarizing beam-splitter; WDM: wavelength-division multiplexer.

treatment to suppress energy in the wrong (fast) polarization axis. If the polarization coupling into the PM fiber or the splicing between PM components are not perfect, spectral ripples and fringes can appear on the top of the spectrum due to small energy in the PM fiber's wrong polarization axis[3]. Reducing fringes is highly desirable because fringes on the spectrum usually indicate the time-domain pulse quality degradation with possible small remote pulses. In practice, we could not find the perfect alignment condition and some fringes on the top of the spectrum always showed up at output 1. To circumvent the difficulty, it was decided to take the main output after the SESAM (output 2).

The laser cavity is similar to a sigma-type cavity [2] but there is no fiber in the linear segment. The linear segment was created solely to insert a reflective SESAM in an effectively ring-cavity configuration. The laser produced a variety of mode-locked states as the waveplates were adjusted. The output pulse train was monitored with a fast detector with a ~300 ps response time. The interferometric and intensity autocorrelations

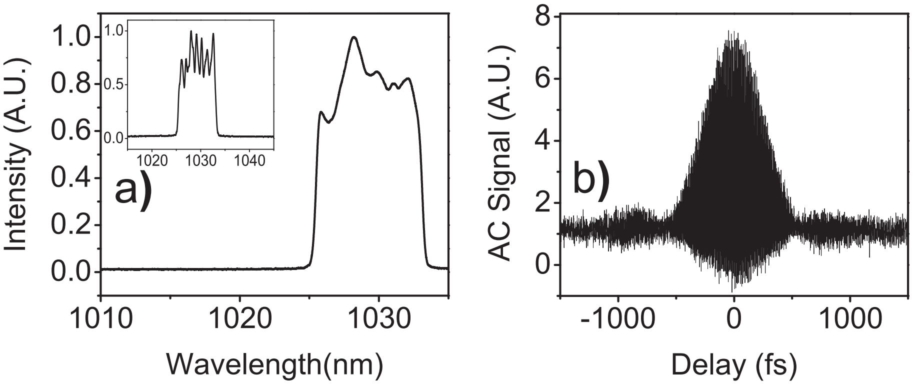

Figure 6.2: Output of the environmentally-stable ANDi laser a) main output spectrum (inset: output 1 spectrum), b) dechirped autocorrelation (~400 fs).

(AC) were monitored for delays up to ∼100 ps.

The ejection ports were adjusted to suppress output 1 while output 2 was maximized as much as possible. By adjusting the waveplates carefully, a stable self-starting mode-locked operation was obtained. As the pump power passed beyond 200 mW, the operation quickly evolved into multi-pulsing.

Figure 6.2. shows a typical output of the laser under single-pulsing operation. The spectrum (Figure 6.2(a)) resembles the similariton's characteristic spectrum [10]. This spectrum shape was also observed in a non-PM ANDi Yb-doped fiber laser [8]. The pulse energy was ~0.5 nJ with 200-mW pump power. Pulses were externally dechirped by a grating pair to ~400-fs pulse duration which is within 3% of the transform limit. The spectrum of output 1 (Figure 6.2(a) inset) shows spectral fringes. The spectral fringes (~1-nm spacing) indicate a small remote pulse with a ~3.5-ps delay, which roughly matches the polarization mode group delay due to the total fiber birefringence. However, the spectrum of output 2 (Figure 6.2(a)) was much smoother since the SESAM suppresses the small remote pulse caused by excessive energy in the PM fiber's wrong polarization axis. The operation was unvaried due to external mechanical perturbations

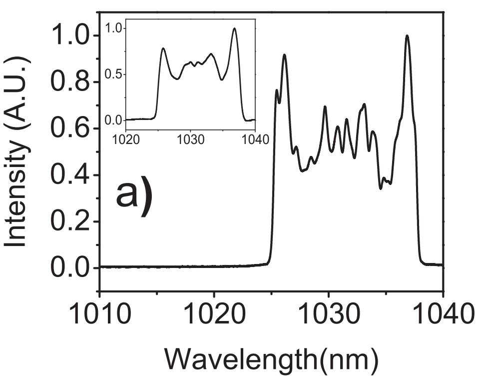

Figure 6.3: Output of the modified environmentally-stable ANDi laser a) main output spectrum (inset: spectrum), b) dechirped autocorrelation (~270 fs).

such as moving, shaking and twisting of the fiber. The mode-locked operation was unchanged and sustained for three days until intentionally interrupted.

We attempted to create each of the operating modes seen in the non-PM ANDi fiber laser [8]. However, the laser described above could not produce modes accompanied by spectra with sharp peaks which are to be generated from high nonlinearity. To verify that the PM ANDi fiber laser exhibits the same features as the non-PM ANDi fiber laser, the laser cavity was slightly modified. To enhance the cavity efficiency and therefore the induced nonlinearity in the fiber, one of the output ports was removed while the pump power was increased to its maximum. Since PBS 1 was essential to composing a sigma cavity, the second output port was the only one that could be removed. We simply pulled out PBS 2 to eliminate the second output port. After removing PBS 2, by adjusting the waveplates, a stable single-pulsing mode-locked operation with the desired spectrum shape was achieved.

Figure 6.3 shows the typical output for the modified laser. The spectrum shows sharp peaks around its edges as observed in non-PM ANDi fiber lasers [6, 8]. Since there was only one output ejection port right after the fiber section, we could not exploit the SESAM's saturable noise suppression. The beam coupling into the PM fiber was carefully adjusted to reduce the spectral fringes as much as possible but some spectral fringes still appeared. Again, there is presumably a small pulse 3.5-ps away from the main envelope. A small pulse was verified by the zero-phase Fourier-transform of the spectrum but it was in the noise of the AC measurement. The SESAM's saturable noise suppression action could be monitored by measuring the spectrum reflected on the surface of the birefringence plate (Figure 6.3(a) inset). 0.8-nJ pulse energy with ~300-mW pump power was achieved. The dechirped pulse duration of ~270-fs was much shorter than that of the mode in Figure 6.2 as expected. The dechirped pulse duration was only ~15% beyond the transform limit.

Interestingly, the mode presented in Figure 6.3 could support stable single-pulsing operation with enhanced output pulse energy and higher pump power. Considering that the first version of the laser (which produced the data of Figure 6.2) was limited by multi-pulsing, it is surprising that stable single-pulse mode-locking is achieved at higher energies. This counter-intuitive trend is observed in non-PM versions of the ANDi laser [9], and will be addressed systematically elsewhere. Future efforts will be focused on further understanding multi-pulsing in this kind of laser.

Likewise, the operation was environmentally-stable to external perturbations. However, the laser lost the mode-locked operation within several hours due to the SESAM's surface damage. It is believed that choosing an appropriate SESAM with a suitable focusing lens will solve the SESAM damage problem. Nevertheless, we failed to stop the SESAM surface damage with available components in the laboratory. The SESAM damage problem will be investigated systematically in the future. The typical pulse energy was much lower than that of non-PM ANDi fiber lasers due to the low efficiency (~12% mode-locked efficiency) caused by a complicated sigma cavity structure. We believe a ring-cavity with a transmission SESAM will have a higher laser efficiency with a pulse energy comparable to a non-PM ANDi fiber laser.

## 6.3 Numerical simulations and experimental results for a linear cavity

In this section, we report an environmentally-stable ANDi laser utilizing a Fabry-Perot cavity. The design is a linear cavity with PM fiber and very large normal GVD ($\sim 0.17ps^2$). The pulse-shaping is dominated by the spectral-filtering mechanism, and self-starting operation is ensured by the inclusion of a SESAM. Strong spectral filtering can enhance the mode-locked spectrum and hence the dechirped pulse duration [9]. Even with such large GVD, the laser generates 300-fs pulses.

A numerical simulation with realistic parameters was performed to understand the detailed operation of a linear ANDi fiber laser. Figure 6.4 shows the cavity schematic with numerically simulated spectra at various locations. The SA is assumed to saturate monotonically, and to have an infinitely fast response. The fiber section consists of 1 m of single-mode fiber (SMF) followed by 60 cm of Yb-doped gain fiber and another 40 cm of SMF. After the fiber segment, is a Gaussian filter with 12 nm bandwidth (BW). The pulse traverses the filter twice in each round trip. The output is coupled out with 70% coupling ratio right after the pulse passes the spectral filter in the forward direction, as shown in Figure 6.4. Pulse evolution in each segment was solved numerically using a split-step Fourier method until it reaches a steady state.

After reflection from the SESAM, the spectrum exhibits a parabolic top, with steep edges (Figure 6.4(a)). Weak spectral broadening occurs in the first segment of SMF

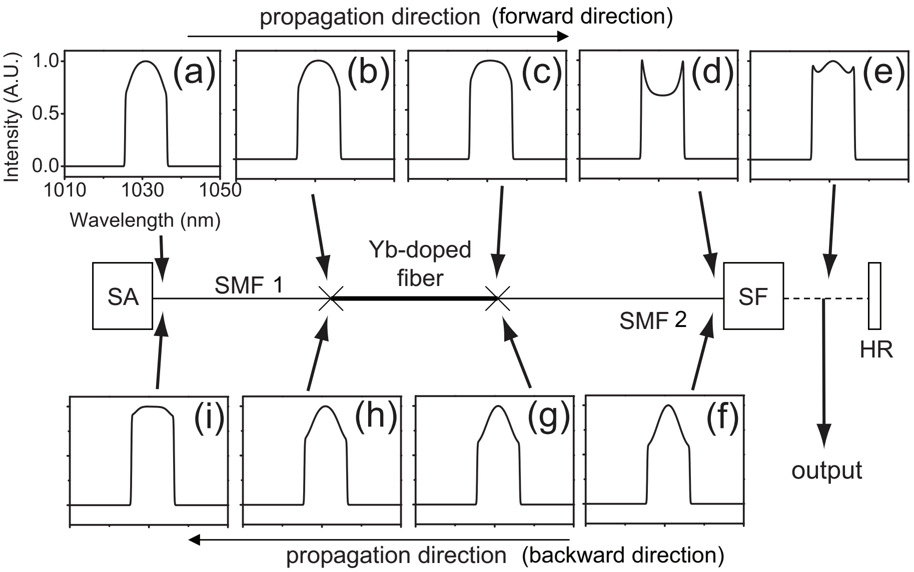

Figure 6.4: Linear ANDi fiber laser simulation setup with simulated spectra at various locations: SA: saturable absorber; SF: spectral filter; HR: high reflection mirror; SMF: single mode fiber.

(Figure 6.4(b),(c)). The amplified pulse undergoes substantial self-phase modulation in the following SMF segment, and the spectrum develops sharp peaks near its edges (Figure 6.4(d)). These peaks are diminished by the two passes through the filter (Figure 6.4(e and f), and the spectrum mimics the filter characteristic. The spectrum gently broadens on propagation in the backward direction (Figure 6.4(g),(h),(i)), and the SA restores the spectrum to that in Figure 6.4(a). The self-amplitude modulation is predominantly (~80% of the total) from the spectral filtering, similar to what was found in ring cavities [6, 8]. The simulated main output pulse has 2 nJ energy with ~5 ps duration.

The experimental setup is shown in Figure 6.5. The SESAM (from BATOP GmbH) has ~35% modulation depth, ~40 nm spectral bandwidth (BW) and a relaxation time constant ~500 fs. The fiber segments are as in the numerical simulations described above. All PM fiber components were carefully spliced with an estimated extinction ratio over 35 dB. PBS 1, the birefringent plate, and PBS 2 constitute a birefringent filter with ~12 nm BW. The round-trip cavity dispersion is ~0.17 $ps^2$. The experimental

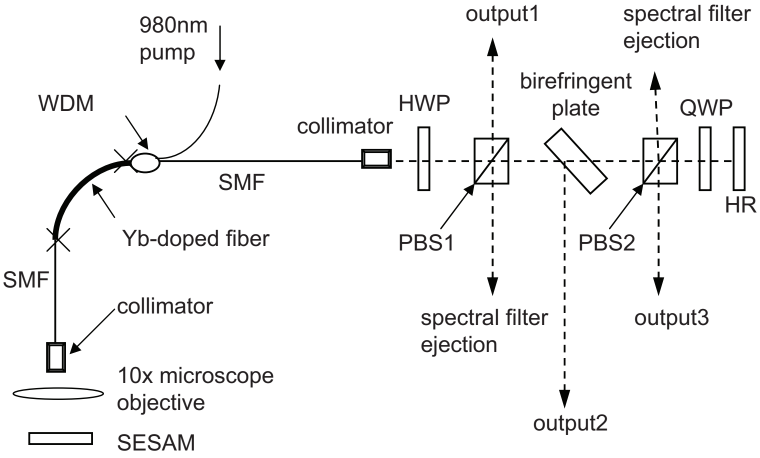

Figure 6.5: Schematic of environmentally-stable linear ANDi fiber laser: QWP: quarter-waveplate; HWP: half-waveplate; PBS: polarizing beam-splitter; WDM: wavelength-division multiplexer; HR: high reflection mirror. All components are PM components.

setup is designed to allow maximum flexibility in studies of pulse formation, which is provided by the bulk optics. However, the cavity could be simplified and integrated by replacing all components with fiber-format versions, which are commercially available. The ejection from the PBS1 (output 1), was monitored to observe the spectrum right after the fiber segment. The reflection from the birefringent plate (output 2) allows us to monitor any modulation on the spectrum transmitted through PBS 1. The double pass through the quarter-waveplate (QWP) rotates the polarization to adjust the coupling ratio of output 3, from PBS 2. Output 3 is the main laser output. Two other outputs from the laser are energy ejected by the filtering action. Energy ejected at the birefringent filter is not useful for most applications due to the low pulse quality. The mode-locked spectra indicates some residual energy in the fast polarization axis of the PM fiber.

If the polarization coupling into the PM fiber or the splicing between PM components is not perfect, some ripples on the top of the spectrum can be observed [3]. Such ripples indicate degradation of the pulse temporal profile or the existence of secondary pulses. PBS 1 can relieve the problem by ejecting residual pulses in the wrong polarization axis of the PM fiber. It also ensures that a linear polarization matching the slow axis of the PM fiber goes back into the fiber segment.

By carefully adjusting the waveplates, a clean mode-locked spectrum without fringes can be obtained at the main output. The SESAM and the spectral filter were both essential for mode-locking. Although only PM fiber components were used, some residual NPE action due to energy in the wrong polarization axis might contribute to mode-locking. However, without a SESAM, stable mode-locked operation did not occur for any orientation of the waveplates. This indicates that the NPE action alone was not strong enough to start the laser.

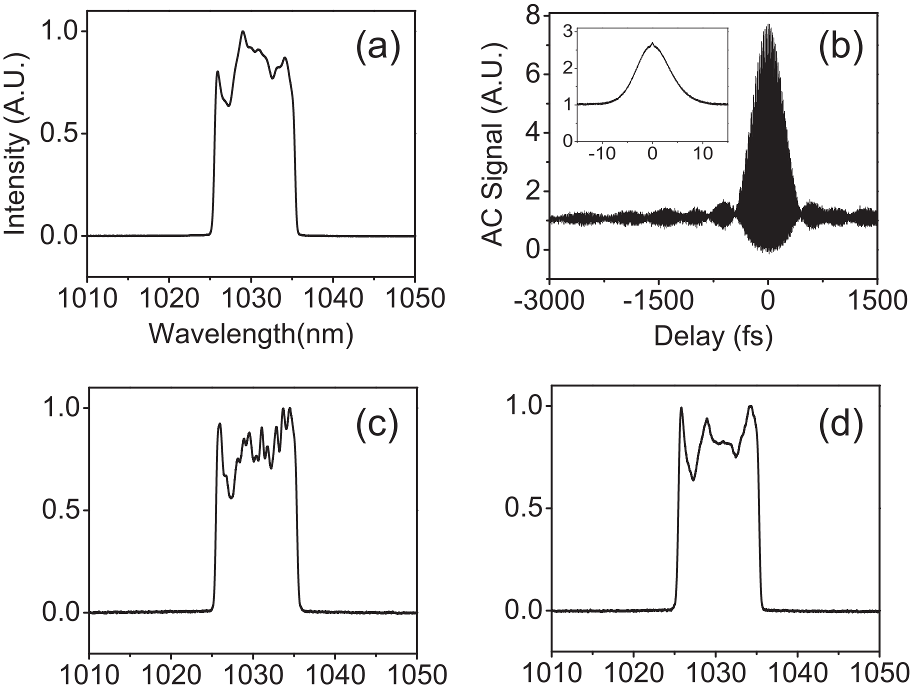

Figure 6.6: Output of the environmentally-stable linear ANDi laser (a) output 3 spectrum (74 mW), (b) output 3 dechirped autocorrelation (~310 fs) (inset: chirped autocorrelation), (c) output 1 spectrum (3.6 mW), (d) output 2 spectrum (4 mW).

The output pulse train was monitored with a detector with 300 ps response time, and the autocorrelation (AC) was monitored for delays up to ~100 ps. Figure 6.6 shows the output. The spectrum from output 1 (Figure 6.6(c)) has sharp peaks near its edges, as predicted by the numerical simulations. Spectral fringes with ~0.7-nm spacing indicate possible remote pulses located ~5 ps from the main pulse, which roughly matches the polarization mode group delay due to the total linear birefringence. However, the spectrum transmitted by PBS 1 (Figure 6.6(d)) is much smoother. It is believed that PBS 1 ejects the energy in the wrong polarization axis of the PM fiber. Even though the transmitted spectrum is less structured, the overall shape does not vary much from the spectrum ejected by PBS 1. The SA modulates the amplitude of the chirped pulse, which in turn produces spectral modulation. The similar spectra transmitted and ejected by PBS 1 also indicate that the NPE only makes a weak contribution to the overall amplitude modulation.

The main output (output 3) spectrum (Figure 6.6(a)) has lower peaks due to the spectral filtering. The average power of output 3 was ~74 mW with 33 MHz repetition rate, which corresponds to ~2.2 nJ pulse energy. The coupling ratio was ~80%. The pulse duration was ~6 ps (Figure 6.6(b) inset) which was dechirped by a grating pair to 310 fs (Figure 6.6(b)), which is within 10% of the Fourier-transform limit. The spectral shape, spectral BW, pulse energy, and pulse duration not only qualitatively but also quantitatively match the numerical simulation results. The operation was unvaried due to external mechanical perturbations to the fiber. The mode-locked operation was unchanged and sustained for ~3 days until intentionally interrupted. Improvement of the laser performance by optimization of the parameters is anticipated. For example, the numerical simulation indicates that the pulse energy can be improved by 50% by simply increasing the pump power. Previously-reported ring cavity ANDi lasers with NPE could operate in a wide variety of modes [8, 9]. In contrast, only limited modes are observed with the PM cavity, all similar to that of Figure 6.6. It is not understood what restricts the lasing modes in the PM cavity. Currently, we conjecture that the fixed saturation curve and long relaxation time of the SESAM restrict the laser to a narrow range of pulse parameters.

## 6.4 Conclusion

To summarize, we demonstrate an environmentally mode-locked femtosecond ANDi fiber laser with a linear and a sigma cavity design comprising only PM fibers. Experimental results agrees well with the numerical simulation predictions. Filtering of a chirped pulse, along with the saturable absorption of a SESAM combine to generate stable, self-starting mode-locked femtosecond pulses at very large GVD.

# BIBLIOGRAPHY

[1] A. Chong, W. Renninger, and F. Wise, Opt. Lett. **33,** 1071 (2008).

[2] H. Lim, A. Chong, and F. W. Wise, Opt. Express **13,** 3460 (2005).

[3] C. K. Nielsen, B. Ortac, T. Schreiber, J. Limpert, R. Hohmuth, W. Richter, and A. Tunnermann, Opt. Express **13,** 9346 (2005).

[4] I. Hartl, G. Imeshev, L. Dong, G. C. Cho, and M. E. Fermann, in *Conference on Lasers and Electro-Optics/Quantum Electronics and Laser Science and Photonic Applications Systems Technologies*, Technical Digest (CD) (Optical Society of America, 2005), paper CThG1.

[5] C. K. Nielsen, and S. R. Keiding, Opt. Lett. **32,** 1474 (2007).

[6] A. Chong, J. Buckley, W. Renninger, and F. Wise, Opt. Express **14,** 10095 (2006).

[7] B. Ortaç, C. Lecaplain, A. Hiduer, T. Schreiber, J. Limpert, and A. Tnnermann, Opt. Express **16,** 2122 (2008).

[8] A. Chong, W. Renninger, and F. Wise, Opt. Lett. **32,** 2408 (2007).

[9] A. Chong, W. Renninger, and F. Wise, J. Opt. Soc. Am. B **24,** 1815 (2007).

[10] F. O. Ilday, J. R. Buckley, W. G. Clark, and F. W. Wise, Phys. Rev. Lett. **92,** 213902 (2004).

CHAPTER 7

# CONTROLLING MULTIPULSING STATES IN ANDi FIBER LASER WITH SPECTRAL FILTERING

This chapter describes the observation of high-harmonic mode-locked operations of ANDi fiber lasers. Interestingly, the operation is tunable from a soliton bunch state to a high-harmonic mode-locked state by adjusting the spectral filtering. The theoretical understanding of the phenomena and the experimental results are discussed.

## 7.1 Introduction

The fiber lasers with NPE mode-locking mechanism generate a variety of mode-locked operations. Among those modes, multipulsing operations are a commonly observed phenomena. The fiber lasers can operate either with a single pulse or in multiple pulses in a cavity round trip. The cause of multipulsing operations is connected to the pulse energy quantization in a laser cavity. The pulse energy quantization in soliton fiber lasers is theoretically understood based on the soliton area theorem of the NLSE. Motivated by readily available NLSE treatment with fully known soliton solutions, multipulsing operations in soliton fiber lasers were studied experimentally and theoretically extensively [1, 2, 3]. The pulse energy quantization is theoretically understood based on the soliton area theorem of the NLSE.

In case of a normally dispersive fiber lasers, the pulse energy quantization can be understood based on dissipative solitons in a dispersive medium with a gain and a spectral filtering (*i.e.* CGLE without a SA term) [7]. In fact, Bélanger *et al.*'s model is not quite suitable to describe fiber lasers. However, the idea of the multipulsing due to the pulse energy limitation is same for more complicated systems such as the energy limitations of dissipative solitons in the CGLE. In all cases, the multipulsing is explained as the energy distribution into multiple numbers of pulses not to violate the pulse energy limit of the system.

The fascinating aspect of the multipulsing phenomena is the interaction between multiple pulses. When pulses attract, bounded solitons can be formed. The bound solitons in soliton fiber lasers were extensively studied experimentally and theoretically [4, 5, 6]. When a long distance stabilization occurs (even though the mechanism of it is not fully understood theoretically), pulses may be distributed periodically to have a repetition rate which is a multiple of the resonator round trip repetition rate [8]. This phenomenon is referred as a harmonically mode-locked operation. When the interaction between pulses is somewhat intermediate (*i.e.* the repulsion between pulses is short-ranged), a soliton bunch can appear in soliton fiber lasers [10]. In contrast, the burst of pulses from normally dispersive fiber lasers is different from a traditional soliton bunch since the pulse is not the NLSE soliton. However, since the pulses from normally dispersive fiber lasers can be categorized as dissipative solitons, the burst from the normally dispersive fiber lasers is still referred as a soliton bunch in this thesis. So far, it is not fully understood what determines the interaction between pulses. However, based on theoretical study of the complex Swift-Hohenberg equation (CSHE), it was shown that the spectral filtering is important to determine the interaction between pulses [9]. The CSHE, which is an important equation to understand the fiber laser, is an extension of the CGLE. The details of the CSHE is covered not in this chapter but in chapter 11.

Recently, Komarov *et al.* theoretically showed that the interaction between multiple pulses in an ANDi fiber laser with a NPE can be adjusted by introducing a narrow tunable spectral filter [11]. In this chapter, we demonstrate the multipulsing management experimentally utilizing a tunable spectral filter in ANDi fiber lasers. By introducing a subtle detuning of the spectral filter, a harmonically mode-locked state converts into a soliton bunch and vice versa in ANDi fiber lasers. Controlling the multipulsing state with a simple spectral filter is surely an interesting physics and it may find some applications immediately.

## 7.2 Theory

The schematic in Figure 7.1 was used in the theoretical study of the controlling multipulsing states in a normally dispersive fiber laser [11].

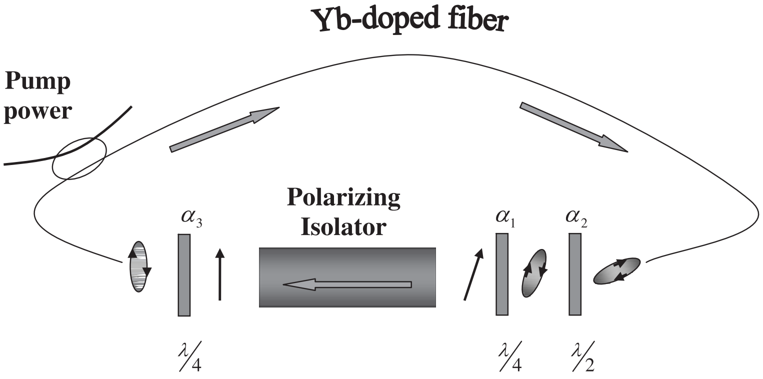

Figure 7.1: Schematic representation of the investigated laser. The ring laser resonator consists of the fibre gain medium, the polarizer, two quarter-wave plates and one half-wave plate. $\alpha 1$, $\alpha 2$ and $\alpha 3$ are the orientation angles of the phase plates. From [11].

The Figure 7.1 is a fiber laser with a NPE mode-locking mechanism with the fiber segment only consists of a normally dispersive gain fiber. Instead of introducing a symmetric spectral filtering, Komarov *et al.* introduced a spectral filtering effect with a peculiar shape (Figure 7.2). Once the physical intracavity spectral filter is introduced, the laser becomes an ANDi fiber laser.

Figure 7.2 shows the net spectral gain-loss profile used in the simulation. Without a

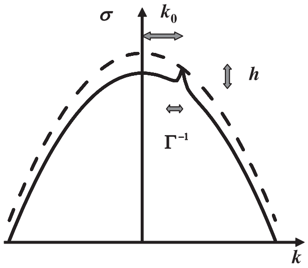

Figure 7.2: Net spectral gainloss profile with (solid line) and without (dashed line) additional frequency-dependent narrow band loss. From [11].

spectral filter, the pulse in the cavity only faces the gain spectral filtering effect (dashed line in Figure 7.2). When an extra Lorentzian spectral filer with a narrow BW is introduced in the cavity, the pulse faces the spectral gain-loss profile of the solid line in Figure 7.2. $\Gamma^{-1}$ is the BW of the spectral filter while $k_o$ is the frequency detuning of the spectral filter from the gain center wavelength. $h$ is the height of the spectral filter.

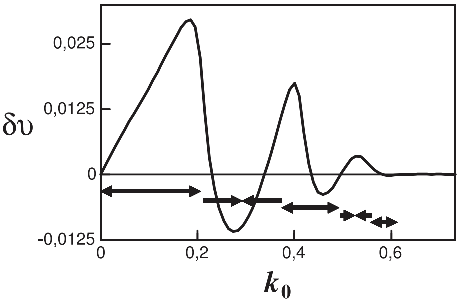

Figure 7.3: Dependence of the change in the soliton velocity on the frequency detuning $k_o$ of the additional narrow spectral selector. Arrows ← → and → ← identify the regions of $k_o$ where the interaction is either repulsive or attractive, respectively. From [11].

By performing numerical simulations with a variety of combinations, Komarov *et al.* found that the interaction between pulse can be changed from the attraction to the repulsion by adjusting the frequency detuning of the spectral filter. Figure 7.3 shows the relative velocity ($\delta\upsilon$) between pulses. Pulses are repulsive ($\delta\upsilon > 0$) or attractive ($\delta\upsilon < 0$) according to $k_o$. Therefore, it is conveniently tunable by the spectral filter frequency detuning for the pulses to form a soliton burst with the attraction or to repulse each other to fill up the available time space forming a high-harmonically mode-locked state.

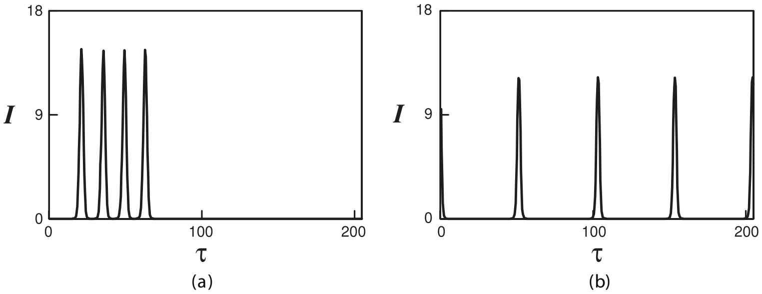

Figure 7.4: Modeling of the regime of harmonic passive mode-locking due to soliton repulsion. (a) Initial distribution of radiation in the ring cavity. (b) Final stationary distribution. From [11].

The final stationary results of the soliton bunch (Figure 7.4(a)) and the harmonically mode-locked state (Figure 7.4(b)) are shown in Figure 7.4.

## 7.3 Experimental

### 7.3.1 Converting from a high harmonically mode-locked state to a soliton bunch

Motivated by the theoretical achievement, an experiment is conducted to demonstrate the controlling the multipulsing state in ANDi fiber lasers. A experimental setup is shown in Figure 7.5.

The total cavity length gives a ~12.5 MHz repetition rate. The fiber section consists of ~15 m of SMF followed by ~50 cm of Yb fiber with another ~50 cm segment SMF attached at the end of the gain fiber. All fibers have a 6-$\mu$m core diameter. The total

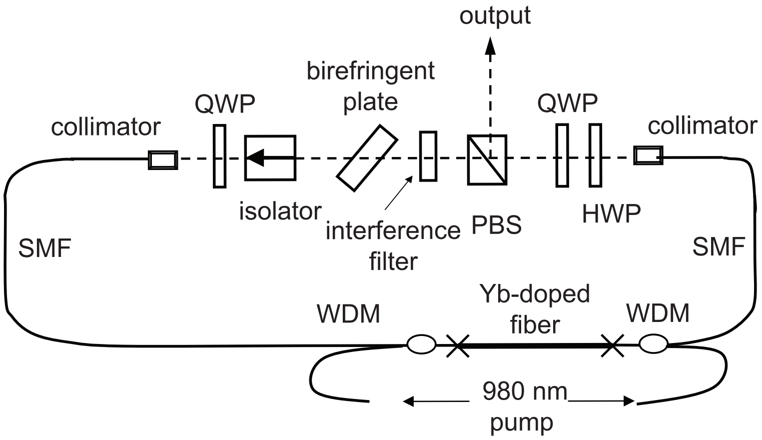

Figure 7.5: Schematic of the experimental setup

cavity dispersion is ~0.38 $ps^2$. Two 980-nm diodes supply ~800 mW maximum pump power. The output is taken directly from the polarizing beam splitter, acting as the NPE ejection port. The ANDi fiber laser has two spectral filters. The first one is the birefringence filter with ~12 nm BW and the second one is the interference filter with ~4 nm BW. In the experiment, the center wavelength of the interference filter is fixed. By adjusting the center wavelength of the birefringence filter, one can introduce a subtle filter frequency detuning.

By adjusting waveplates, the laser is harmonically mode-locked with ~165 MHz repetition rate (Figure 7.6). Each pulse has ~1.7 nJ energy. From this mode-locked operation, by adjusting the center wavelength of the birefringence filter to induce a subtle frequency detuning, the harmonically mode-locked operation slowly converts into the soliton bunch. The soliton bunch is shown in Figure 7.7.

In this particular case, 10 pulses are bunched up with a ~50 ps separation. Each pulse contains ~2.1 nJ energy. The soliton bunch (Figure 7.7) converts back to the harmonically mode-locked (Figure 7.6) by moving the frequency detuning in the opposite direction. The experimental result verifies the theoretical prediction of the controlling

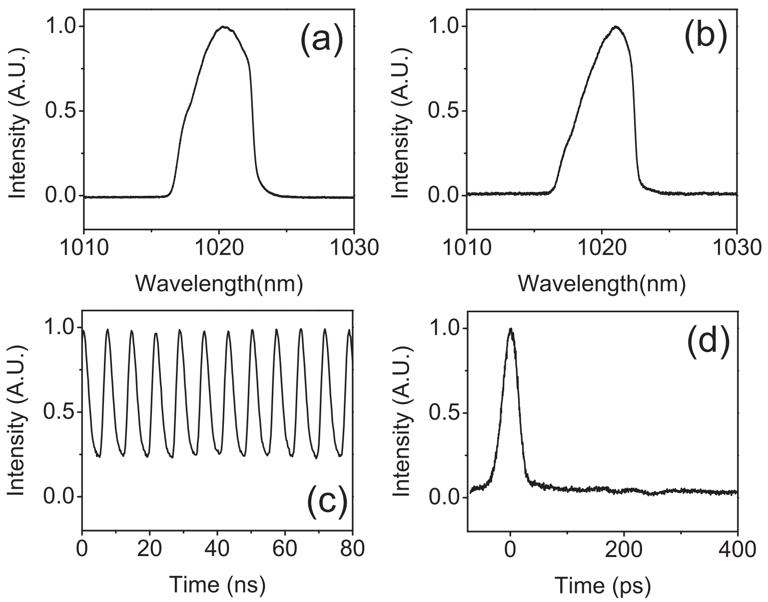

Figure 7.6: Harmonically mode-locked spectrum and pulse train : a) output1 spectrum, b) spectrum after the NPE port, c) long range pulse train, d) short-range pulse train.

the multipulsing states by the spectral filtering in ANDi fiber lasers [11].

### 7.3.2 Quantization of the pulse separation

In this section, we will provide the experimental observation of the pulse separation in a dissipative soliton bunch. The experimental setup is same as Figure 7.5 except that the birefringence filter BW is chosen to be ~6 nm. It was found that several values of separations in a soliton bunch can be generated by simply adjusting waveplate in the fiber laser. Figure 7.8 shows the spectrum and the pulse train of a soliton bunch. In this particular case, the pulse separation is ~35 ps.

By adjusting waveplates, soliton bunches with different pulse separation are easily found. For example, Figure 7.9 shows a soliton bunch with a ~180 ps separation.

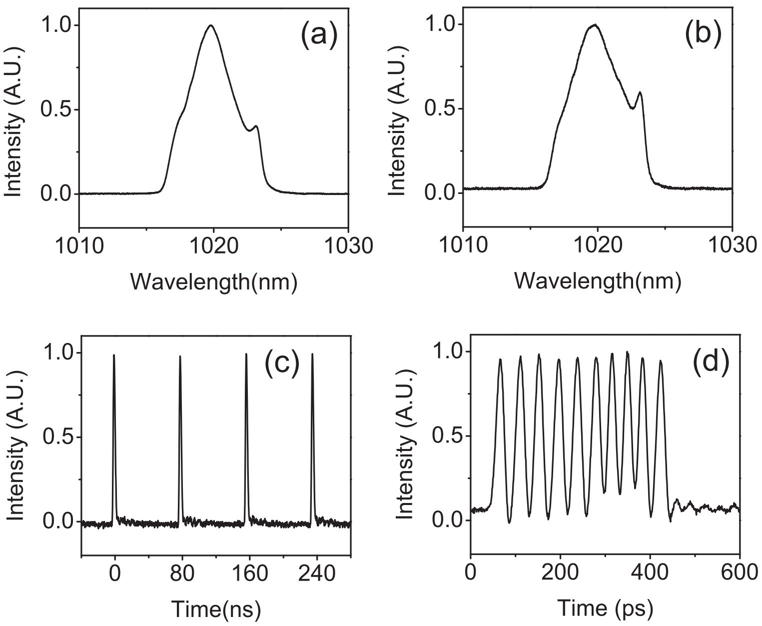

Figure 7.7: Soliton bunch spectrum and pulse train: a) output1 spectrum, b) spectrum after the NPE port, c) long range pulse train, d) short-range pulse train.

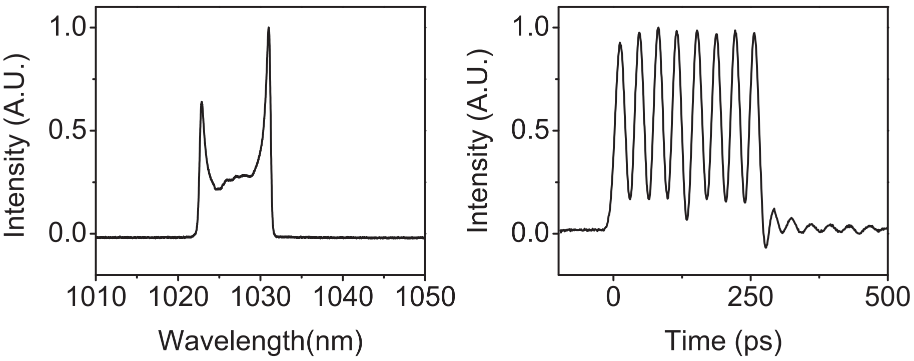

Figure 7.8: Soliton bunch with ~35 ps pulse separation.

The pulse separation between pulses is not always a constant. Figure 7.10 shows the hybrid pulse separations of ~35 ps and ~100 ps while Figure 7.11 shows the combination of ~35 ps and ~180 ps.

For any modes of this particular laser, it was found that the pulse separation between pulses is one of three separation values of ~35 ps, ~100 ps, and ~180 ps. To emphasize

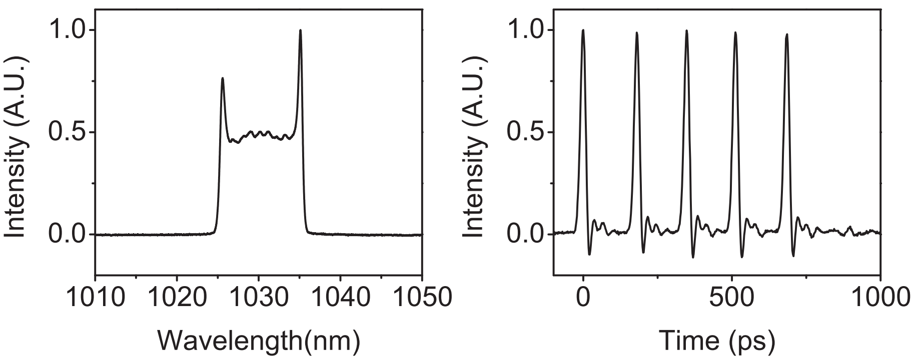

Figure 7.9: Soliton bunch with ~180 ps pulse separation.

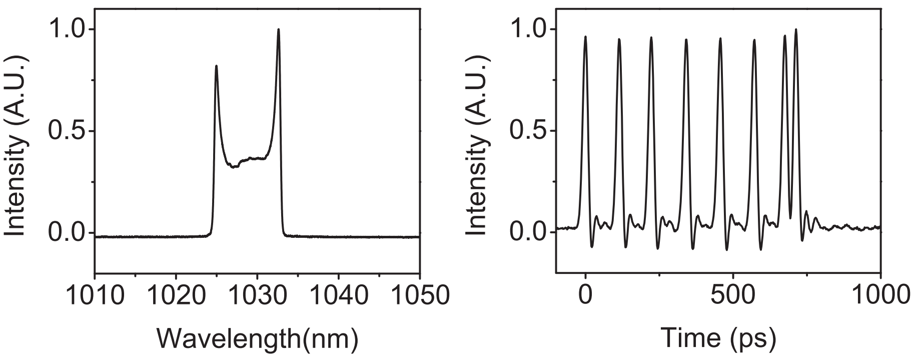

Figure 7.10: Soliton bunch with hybrid pulse separtions (~35 ps and ~100).

that the pulse separation is to be certain limited number of values, we refer the phenomenon as the quantization of the pulse separation in a soliton bunch. Even though it is not fully understood what determines the separation, it seems like the spectral filter

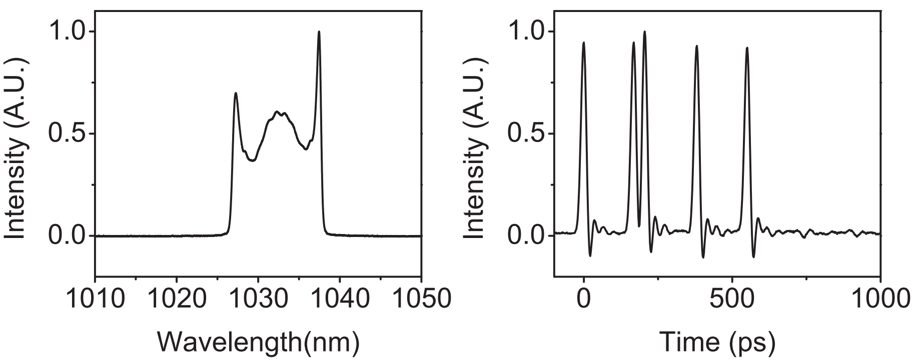

Figure 7.11: Soliton bunch with hybrid pulse separations (~35 ps and ~180).

BW surely is a factor. For example, Figure 7.7 shows a ~50 ps separation with 12 nm birefringence filter while Figure 7.8-11 exhibit different values with 6 nm birefringence filter. It is believed that other laser parameters such as the GVD, and $\Phi^{NL}$ affect the pulse separation but the systematic study was not conducted yet. Further research is necessary to address the issue in detail.

## 7.4 Conclusion

We demonstrate the multipulsing management experimentally utilizing a tunable spectral filter in ANDi fiber lasers. By introducing a subtle detuning of the spectral filter, a harmonically mode-locked state converts into a soliton bunch and vice versa in ANDi fiber lasers. Controlling the laser multipulsing state with a simple spectral filter is surely an interesting physics and a meaningful step to understand the role of the spectral filtering in multipulsing operations. The quantization of the separation between pulses is again an interesting physics and may be already significant for some applications. It is strongly believed that the fiber laser with controllable pulse numbers and separations will find a variety of applications immediately.

# BIBLIOGRAPHY

[1] D. Y. Tang, W.S. Man, and H. Y. Tam, Opt. Commun. **165**, 189 (1999).

[2] A. B. Grudinin, D. J. Richardson, and D. N. Payne, Electron. Lett. **28**, 67 (1992).

[3] A. Komarov, H. Leblond, and F. Sanchez, Phys. Rev. A **71**, 053809 (2005).

[4] D. Y. Tang, W. S. Man, H. Y. Tam, and P. D. Drummond, Phys. Rev. A **64,** 033814 (2001).

[5] N. N. Akhmediev, A. Ankiewicz, and J. M. Soto-Crespo, J. Opt. Soc. Am. B **15,** 515 (1998).

[6] B. A. Malomed, Phys. Rev. A **44,** 6954 (1991).

[7] P. A. Bélanger, L. Gagnon, and C. Paré, Opt. Lett. **14**, 943 (1989).

[8] N. Akhmediev, J. M. Soto-Crespo, M. Grapinet, and P. Grelu, J. Nonlinear Opt. Phys. Mater. **14**, 177 (2005).

[9] J. M. Soto-Crespo, and N. Akhmediev, Phys. Rev. E **66**, 066610 (2002).

[10] P. Grelu, F. Belhache, F. Gutty, and J. M. Soto-Crespo, J. Opt. Soc. Am. B **20**, 863 (2003).

[11] A. Komarov, K. Komarov, H. Leblond, and F. Sanchez, J. Opt. A: Pure Appl. Opt. **9**, 1149 (2007).

CHAPTER 8

# ANTISYMMETRIC DISPERSION-MANAGED SOLITON IN FIBER LASERS

In this chapter, the subject is changed from ANDi fiber lasers to an interesting second-order DM soliton in a dispersion mapped passive transmission line. This second-order DM soliton is referred as the antisymmetric DM (ASDM) soliton. We report the observation of the ASDM soliton in an fiber laser oscillator. The observed pulse evolution, phase difference and pulse separation agree with the ASDM soliton theory.

## 8.1 Introduction

A dispersion-managed (DM) soliton is a soliton solution of a transmission line with a periodically alternating sign of the dispersion. The DM soliton has a breathing temporal profile, which is close to a Gaussian profile rather than the sech profile of a soliton of the ordinary nonlinear Schrödinger equation [1]. The DM soliton is different from the standard soliton in many aspects. However, it was quickly recognized that the DM soliton in a dispersion map is analogous to the standard soliton in an anomalous dispersion transmission line. Scientists were inspired to search for higher-order DM solitons, which are analogous to higher-order standard solitons, to obtain complete understanding of the DM soliton.

The first prediction of a second-order DM soliton was presented by Pare [2]. The second-order DM soliton is well-approximated by a breathing, odd Hermite-Gaussian (HG) temporal profile of $E(t) = A_o\, t\, exp(-t^2/2a^2)$. The intensity profile exhibits two temporal (spectral) envelopes with $\pi$ phase difference ($\Delta\phi$) between them. Such a pulse was referred to as an antisymmetric dispersion-managed (ASDM) soliton which can also be interpreted as bounded DM solitons with $\Delta\phi = \pi$ and an appropriate separation [2].

The bounded DM solitons can be modeled as a bound pair of chirped Gaussian pulses as presented in Equation 8.1.

$$E(t) = A_o \frac{t_o}{\sqrt{t_o^2 - iD}} \left(e^{i\pi - \frac{t^2}{2({t_o}^2 - iD)}} + e^{-\frac{(t-s)^2}{2({t_o}^2 - iD)}}\right). \tag{8.1}$$

The phase difference between pulses is taken to be a step function. The component pulses are separated by $s$, and $D$ designates the group velocity dispersion (GVD). Both models are equally good approximations as they are successfully used as an ansatz of ASDM solitons in variational approximations [2]. As an odd HG pulse experiences GVD, the pulse broadens but its shape is still HG. As the result, a stretched HG intensity profile has a constant ratio of the separation between envelopes and the duration of one envelope ($s/\Delta t$)) which is $\sim$1.73. While the HG model describes the separation between two envelopes (pulses), the bounded DM solitons model does not provide the separation information. However, it is useful to understand the ASDM soliton behavior with a non-$\pi$ phase difference which cannot be analyzed conveniently in the HG model. In this letter, both models are used to analyze interesting bounded DM solitons from a fiber laser.

The bi-soliton [3] and the temporal soliton-molecule [4] are related to ASDM solitons. Distinct focuses and approaches lead to distinct terminologies, but a bi-soliton with $\Delta\phi = \pi$ and a temporal soliton molecule refer to fields that are identical in their essential features. The potential importance of the ASDM soliton in optical telecommunication was soon acknowledged. The data transmission rate and the timing jitter can be improved significantly utilizing ASDM solitons [3, 5]. Recently, the generation of ASDM solitons in a fiber laser with a strong dispersion map was predicted by numerical simulations [6].

Meanwhile, bound solitons in passively mode-locked fiber lasers have been researched extensively. Motivated by the theoretical predictions of bound solitons of the Ginzburg-Landau equation (GLE) [7, 8], Tang *et al.* demonstrated bound solitons in a mode-locked soliton fiber ring laser [9]. Since then, a variety of bound solitons have been observed in soliton fiber lasers. Bound solitons with $\Delta\phi = \pi$ would seem to be closely similar to the ASDM soliton, but they evolve in fundamentally-different ways. Bound solitons of the GLE are static solutions with constant pulse duration and separation everywhere in the cavity. Experimentally-observed pulse separations are typically $\sim$10 times the pulse duration. This phenomenon is consistent with the theoretical prediction of bound soliton pair formation with slightly-overlapping solitons [7]. In contrast, the ASDM soliton is a bound pair of breathing DM solitons. As the ASDM soliton propagates, it is quite possible for the (chirped) pulse duration to become much larger than the pulse separation. Even though chirped DM solitons overlap substantially, the temporal intensity is zero at the center of the two DM solitons owing to $\Delta\phi = \pi$. Bound solitons were also observed in a stretched pulse fiber laser [10, 11]. Although many aspects of these bound pulses were elucidated, a bound state with $\Delta\phi = \pi$ has not been reported. Furthermore, the pulse separation and/or the duration were too large to allow appreciable overlap between even the stretched pulses. To date, ASDM soliton evolution in a fiber laser has not been reported.

In this chapter, we report evidence of ASDM solitons in a passively mode-locked fiber ring laser. The pulse from the fiber laser is consistent with the ASDM soliton descriptions of bounded DM solitons with $\Delta\phi = \pi$ and an appropriate separation. ASDM solitons only occur within a narrow range of net cavity dispersion values.

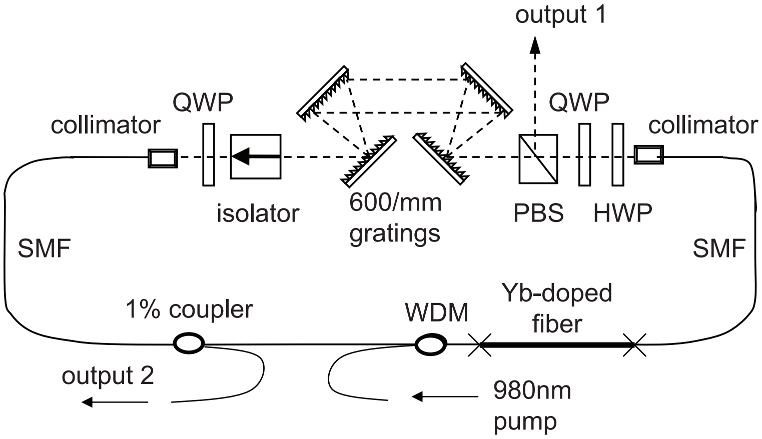

Figure 8.1: Experimental setup: QWP: quarter-waveplate; HWP: half-waveplate; PBS: polarizing beam-splitter; WDM: wavelength-division multiplexer.

## 8.2 Experimental

Experiments were performed with the soliton fiber laser shown schematically in Figure 8.1. The fiber section consists of 410 cm of SMF followed by 60 cm of Yb-doped fiber and another 130 cm of SMF. All fibers have normal dispersion with a 6-$\mu$m core diameter. After the fiber section, nonlinear polarization evolution (NPE) provides self-amplitude modulation. The main output (output 1) is taken directly from the polarizing beam splitter, which is the NPE ejection port. A double-pass 600 lines/mm grating pair provides anomalous dispersion, and the net cavity GVD is -0.038 $ps^2$. The pulse repetition rate is 30 MHz. A 1% coupler is placed at the middle of the fiber cavity (output 2) to monitor the evolving spectrum. The output pulse train is monitored with a photodetector down to ~300 ps, and the pulse autocorrelation (AC) is monitored for delays up to ~100 ps.

Fundamental DM soliton (*i.e.*, the lowest-order symmetric soliton) operation is obtained easily by adjusting the waveplates. The bound state of DM solitons, which matches the description of the ASDM soliton [2], is produced by adjusting the net GVD,

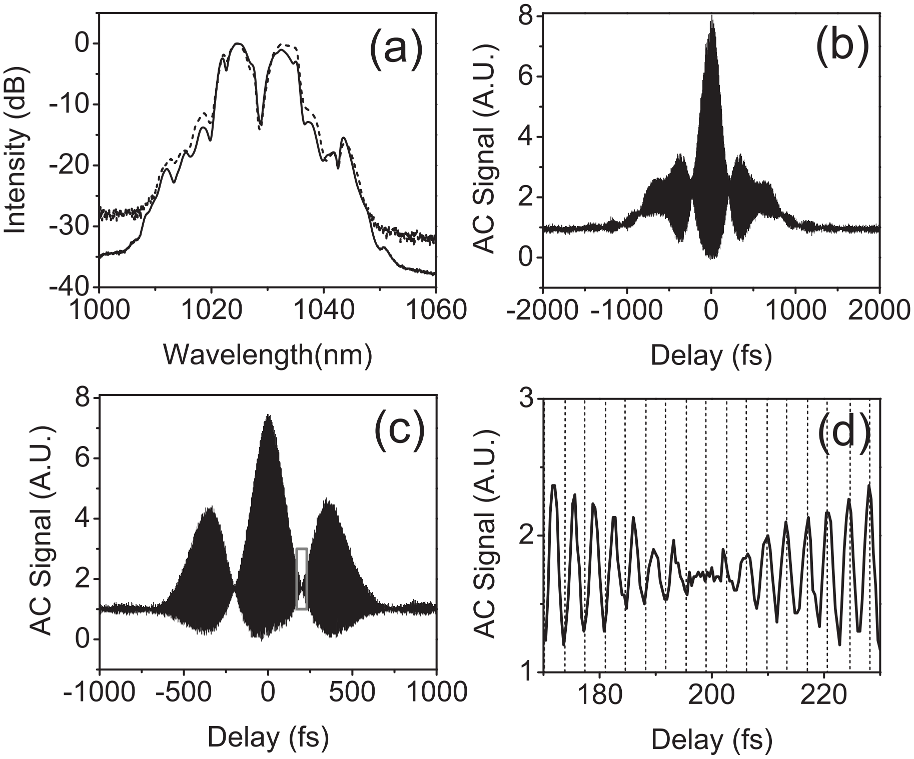

Figure 8.2: Experimental result: (a) main output spectrum (dotted: output 2 spectrum),(b) chirped interferometric AC, (c) dechirped interferometric AC, (d) dechirped interferometric AC (grey rectangular region in (c), periodic vertical lines indicate the period of fringes).

the pump power and waveplates carefully (Figure 8.2). With ~100 mW pump power, the output power is 10 mW, which corresponds to ~0.3 nJ pulse energy. The power spectrum develops a pronounced dip in the center. The pulse from the main output is positively chirped. The pulse is dechirped optimally by a grating pair that provides ~ -0.042 $ps^2$. This value implies that the pulse reaches minimum pulse duration at two points in the cavity, one in the anomalous-dispersion segment and one in the normal-dispersion segment, as expected for a DM soliton. The dechirped interferometric AC with three peaks (Figure 8.2(c)) indicates a doubly-peaked intensity profile. The component pulses are 145 fs in duration and ~350 fs apart. The power spectrum and autocorrelation would suggest $\Delta\phi = \pi$ between the pulses, and this is confirmed in the fringes of the AC (Figure 8.2(d)).

A complete characterization of the electric field of this type of pulse is desirable. In particular, verification of the $\Delta\phi$ between the bound pulses would be valuable. Second harmonic generation frequency-resolved optical grating (SHG FROG) available in our laboratory cannot resolve the $\Delta\phi$, due to the fundamental phase ambiguity in the measurement technique [12]. Hause *et al.* recently developed a technique to retrieve the intensity and phase of this kind of pulse, but a sophisticated experimental setup is required [13]. In the absence of a direct measurement, we decided to compare experimental and theoretical ACs based on bounded DM solitons model (Equation 8.1) to assess the claim of the $\Delta\phi = \pi$. Theoretical ACs are created by substituting the experimentally-observed parameters $t_o$ = 87 fs, $s$ = 350 fs and varying the GVD value in Equation 8.1. Results are shown in Figure 8.3.

The tails of the tightly-bound DM solitons overlap. The intensity in the overlapping region, which influences the AC trace, is sensitive to the phase difference. For example, ACs with $\Delta\phi = \pi/2$ (Figure 8.3(a) and (b) insets) are quite different from those with $\Delta\phi = \pi$. With $\Delta\phi = \pi$, the theoretical AC has three clear lobes, with near zero intensity between lobes. The experimentally AC, which matches very well with the theoretical AC envelope (Figure 8.3(b)), shows the expected behavior with close to zero intensity between lobes (Figure 8.2(c and d)). The temporal profile of the chirped pulse directly from the fiber cavity can be calculated. With $D = 0.042\ ps^2$ (the magnitude of dispersion needed to dechirp the pulse), pulses are stretched to ~815 fs, with ~ 350-fs separation. Even though the pulses overlap significantly, due to $\Delta\phi = \pi$, the combined temporal intensity profile shows two separate envelopes with ~355 fs durations and a ~630 fs separation. The calculated $s/\Delta t$ ~1.77 agrees very well with 1.73 of the HG model. The $s/\Delta t$ ~2.41 for the dechirped case is still reasonably close to the HG model prediction. Again, the calculated AC of bounded chirped Gaussian pulses matches very well with the measured AC trace (Figure 8.3(a)). From the good agreement between

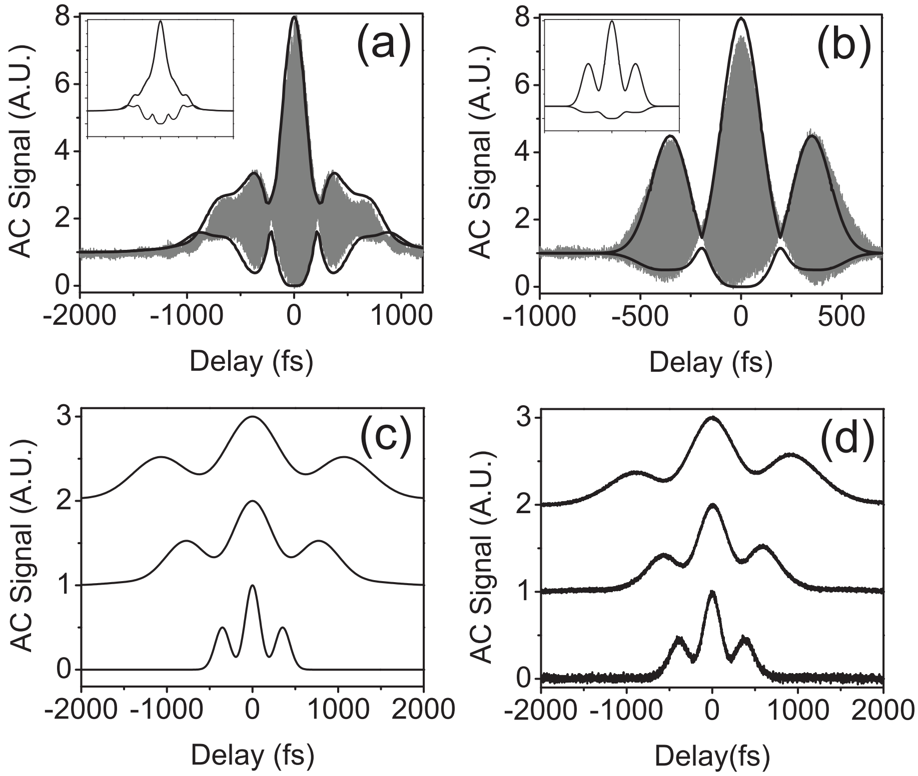

Figure 8.3: (a) Chirped interferometric AC and (b) dechirped AC; grey: experimental ACs of Figure 2, black: calculated AC envelope for bound Gaussian pulses, insets: calculated AC envelopes with $\pi/2$ phase difference, (c) calculated intensity ACs for chirped bound Gaussian pulses; bottom: $D = 0$, middle: $D = -0.05\ ps^2$, top: $D = -0.07\ ps^2$, (d) experimental intensity ACs of chirped pulses with the same GVD values as in (c).

the calculated ACs from Equation 8.1 and the measured traces (Figure 8.3(a and b)), we conclude that $\Delta\phi \sim \pi$ and the separation between pulses agrees with that of the HG pulse. The measured pulse shape, $\Delta\phi \sim \pi$, $s/\Delta t$, and observed characteristic evolution are consistent with the ASDM soliton [2]. ACs of a highly-chirped ASDM soliton (Figure 8.3(d))) still match the calculated ACs (Figure 8.3(c)) of Equation 8.1 with an ideal phase profile. This indicate that the phase difference is close to an ideal step function.

ASDM solitons are only observed with the net cavity GVD in a narrow range, within ± 0.005 $ps^2$ of -0.038 $ps^2$. In contrast, ordinary DM solitons can be observed for a wide range of anomalous dispersion. Extensive searches for the ASDM soliton pulses were made at each dispersion value, but the ASDM soliton was only found in the stated narrow range. Similar investigations were performed with other fiber lasers in our laboratory, with a similar conclusion: although solitons can be generated for a wide range of dispersions, ASDM solitons only seem to form near a single dispersion value that is particular to the details of the laser.

## 8.3 Conclusion

To summarize, we have demonstrated a ASDM soliton generation from a Yb-doped fiber laser with a strong dispersion map. The measured pulse shape, $\Delta\phi \sim \pi$, $s/\Delta t$, and the characteristic evolution are consistent with the ASDM soliton. Future work could include direct measurements of the pulse intensity and phase, as well as an investigation of the occurrence of ASDM solitons only at a fixed dispersion value. The ASDM soliton fiber laser is a realization of an interesting higher-order DM soliton in a feedback system with possible applications of ASDM solitons in optical telecommunications.

# BIBLIOGRAPHY

[1] Y. S. Kivshar, and G. P. Agrawal, *Optical Solitons from Fibers and Photonic Crystals* (Academic, 2003).

[2] C. Paré, and P. A. Bélanger, Opt. Commun. **168,** 103 (1999).

[3] A. Maruta, T. Inoue, Y. Nonaka, and Y. Yoshika, IEEE J. Sel. Top. Quantum Electron. **8,** 640 (2002).

[4] M. Stratmann, T. Pagel, and F. Mitschke, Phys. Rev. Lett. **95,** 143902 (2005).

[5] B. Feng, and B. A. Malomed, Opt. Commun. **229,** 173 (2004).

[6] X. Mao, and A. Maruta, in *The 5th International Conference on Optical Communications and Networks/the 2nd International Symposium Advances and Trends in Fiber Optics and Applications*, (ICOCN/ATFO 2006), (Chengdu and Jin-Zhai-Gou, China, 2006), No.705162

[7] B. A. Malomed, Phys. Rev. A **44,** 6954 (1991).

[8] N. N. Akhmediev, A. Ankiewicz, and J. M. Soto-Crespo, J. Opt. Soc. Am. B **15,** 515 (1998).

[9] D. Y. Tang, W. S. Man, H. Y. Tam, and P. D. Drummond, Phys. Rev. A **64,** 033814 (2001).

[10] Ph. Grelu, F. Belhache, F. Gutty and J. M. Soto-Crespo, Opt. Lett. **27,** 966 (2002).

[11] L. M. Zhao, D. Y. Tang, t. h. Cheng, H. Y. Tam and C. Lu, Appl. Opt. **46,** 4768 (2007).

[12] R. Trebino, K. W. DeLong, D. N. Fittinghoff, J. N. Sweetser, M. A. Krumbügel, B. A. Richman, and D. J. Kane, Rev. Sci. Instrum. **68,** 3277 (1997).

[13] A. Hause, H. Hartwig, B. Seifert, H. Stolz, M. Böhm, and F. Mitschke, Phys. Rev. A **75,** 063836 (2007).

## CHAPTER 9

# NONLINEAR CHIRPED-PULSE AMPLIFICATION (CPA)[1]

In this chapter, theoretical study of the chirped-pulse amplification (CPA) system with high nonlinearity and third-order dispersion (TOD) is described. Interestingly, with a substantial $\Phi^{NL}$ and proper TOD, the final amplified pulse duration and quality are improved. This chapter provides the theory to optimize the CPA system performance by manipulating the $\Phi^{NL}$ and TOD of the CPA system.

## 9.1 Introduction

It is common knowledge that nonlinear phase shifts ($\Phi^{NL}$) can lead to distortion of optical pulses. In fiber, optical pulses experience small mode field area and a long propagation distance, conditions that are conducive to the generation of large $\Phi^{NL}$. Therefore, building a high energy ($> \mu$J) femtosecond fiber amplifier is a nontrivial task.

Chirped-pulse amplification (CPA)[2] is the most effective method to date to avoid excessive $\Phi^{NL}$, and thereby produce high energy femtosecond pulses in a fiber amplifier.[3, 4] Until the last year, it was believed that residual third-order dispersion (TOD) due to any mismatch between stretcher and compressor dispersions would degrade the amplified output pulse quality. This is true in linear propagation. CPA systems were carefully designed to minimize residual TOD. As a result, a grating pair stretcher and a compressor with the same type of grating pair became a common fiber CPA configuration. Even though fiber stretchers would offer major practical advantages such as environmental stability, compactness, and trivial alignment compared to a grating stretcher, they were avoided in fiber CPA system because the residual TOD would

---

[1] Most of the results presented in this chapter have been published in Ref [1]

substantially broaden the output pulse.

Recently, Zhou *et al.*[5] and Shah *et al.*[3] showed that substantial residual TOD can help the output pulse quality in the presence of a substantial amount of $\Phi^{NL}$ in fiber CPA. According to these works, fiber CPA system design can be much more flexible by manipulating residual TOD with different combinations of stretchers and compressors. For example, the combination of a fiber stretcher and a grating compressor can improve the pulse quality, while offering major practical advantages over grating pair stretcher in case of a high gain with nonzero $\Phi^{NL}$.[5]

The so-called cubicon amplifier of Shah *et al.* is straightforward to understand.[3] Since the pulse is highly chirped in a stretcher, the power spectrum profile follows the temporal profile.[6] Therefore, the nonlinear phase shift in the frequency domain ($\Phi^{NL}(\omega)$) (accumulated mainly in the gain fiber) has the same shape as the spectrum, which is made asymmetric with a filter. As a result, substantial residual TOD can be compensated by asymmetric $\Phi^{NL}(\omega)$, and this leads to better output pulse quality. Obviously, the spectrum shape depends on the sign of the TOD. Fiber amplifiers with pulse energies of ~100 $\mu$J and pulse durations of ~650 fs have been demonstrated with the cubicon approach. [3]

The work of Zhou *et al.* is fundamentally different.[7] The compensation of $\Phi^{NL}$ by residual TOD works even with a completely-symmetric spectral profile. A highly-chirped symmetric spectrum generates a symmetric $\Phi^{NL}(\omega)$ during amplification, which cannot compensate the anti-symmetric cubic phase of residual TOD. However, higher peak power is achieved by manipulating the residual TOD and $\Phi^{NL}$ only. This process applies to arbitrary spectral shapes, so requires no filtering, and remarkably, is independent of the sign of the residual TOD. $\Phi^{NL}\sim 10\pi$ are not only tolerable, but will be desirable. These values were considered disastrous in the context of CPA prior to the works of Shah *et al.* and Zhou *et al.* In simple terms, the nonlinear phase shift implies increases in pulse energy by the same factor, i.e., ~30.

Our goal is to design fiber amplifiers that achieve maximum peak power. Optimization of a nonlinear CPA system is a complicated, multivariable problem. It would be impractical to do it through numerical simulations alone. We introduce an approximate analytical model that can be used to survey the relevant parameter space. This model also provides some insight into the compensation of nonlinearity by TOD. Once the most promising ranges of parameters are found for a given application, numerical simulations will be used to refine and quantify the conclusions. This paper is organized as follows: In section 2, the simple CPA model is introduced. In section 3, the compensation of $\Phi^{NL}$ by residual TOD in CPA is discussed. Section 4 discusses how to optimize the CPA output performance by manipulating the design parameters. Section 5 summarizes the conclusions.

## 9.2 CPA model

Since a CPA system is quite complicated, numerical simulations are usually performed to get the final theoretical output. However, we can exploit the fact that the pulse is highly chirped in the stretcher, to simplify the analysis under a range of reasonable assumptions. The model assumes the ideal conditions of CPA, which are listed below.

1) The input pulse is transform-limited

2) The input pulse peak power is not enough to induce significant $\Phi^{NL}$ in the stretcher

3) The input spectrum is not changed due to $\Phi^{NL}$ in CPA

4) GVD parameter($\beta_2$) is much larger than TOD parameter($\beta_3$) in the stretcher

5) The amplifier gain spectrum is flat (i.e. infinite gain spectrum bandwidth)

6) Raman scattering, self-steepening, and fourth- and higher-order dispersion are negligible

7) Residual GVD and residual TOD are independent parameters

Residual GVD and residual TOD are the difference between the stretcher and the compressor in the absence of nonlinearity. Of course $\Phi^{NL}(\omega)$ has a quadratic and a cubic term in a Taylor expansion, which will act just like linear GVD and TOD. However, in this paper, GVD and TOD refer to the linear dispersions from the stretcher and the compressor, not the Taylor expansion terms of $\Phi^{NL}(\omega)$. From this point on, residual GVD and residual TOD will be referred to simply as GVD and TOD, respectively. GVD and TOD can be defined mathematically in terms of $\beta_2$ and $\beta_3$ as $GVD = \int_0^L \beta_2(z)dz$ and $TOD = \int_0^L \beta_3(z)dz$ where $L$ is the total CPA propagation distance.

Most of the assumptions are to force the CPA output spectrum to be same as the input spectrum. Assumption 2 states that the linear chirping is dominant, so that substantial $\Phi^{NL}$ is not enough to induce the spectrum broadening. Of course, the validity of this assumption suffers as $\Phi^{NL}$ increases. Since the goal of a CPA system is to reduce $\Phi^{NL}$ during the amplification, the assumption can be made valid by introducing the appropriate amount of pulse stretching. In a CPA system, spectral broadening is roughly proportional to the nonlinear phase shift divided by the stretching ratio. With typical stretching ratios of ~1000 or more, even $\Phi^{NL} \sim 10\pi$ produces negligible broadening.

Assumption 5 is an ideal amplification condition, again to keep the spectrum invariant. An important consequence of assumption 5 is that the dispersion terms become significantly simpler, with zero dispersion induced by the gain. In practice, this is a good approximation when the gain spectrum is much broader than the pulse spectrum. Ytterbium (Yb) doped gain fiber has large gain bandwidth of 30~60nm[8, 9] to support ~100 fs pulse amplification.[10] However, even with a large gain bandwidth, spectrum narrowing occurs as gain increases. Therefore, the assumption also implies that gain-narrowing is negligible. This assumption also keeps the chirping linear. Therefore, the temporal profile and the spectral profile have same the same shape since the pulse is highly-chirped:

$$\Phi^{NL} \propto I(t) \propto I(\omega)\Phi^{NL}(\omega) = \Phi^{NL}\bar{I}(\omega) \tag{9.1}$$

$\bar{I}(\omega)$ is the power spectrum with the pulse peak power normalized to one. Equation 9.1 simply states that $\Phi^{NL}(\omega)$ is just the power spectrum normalized by the peak power and multiplied by $\Phi^{NL}$.

Assumption 2 precludes any $\Phi^{NL}$ which may cause the distortion of the spectrum. We assume that GVD and TOD are independent and optimize accordingly. In traditional CPA systems, GVD and TOD are coupled since the ratio of TOD and GVD parameters ($\beta_2/\beta_3$) is fixed in the stretcher and the compressor. However, stretchers and compressors can be designed for arbitrary values of the ratio of TOD to GVD. The ready availability of efficient reflection grisms based on stock components [11, 12] provides access to TOD/GVD values over a huge range, roughly from 0 to 40 fs.

Since the spectrum is constant, nonlinear and linear operators commute. Thus, pulse propagation through the CPA system can be modeled by simply adding spectral phases, without considering the order of operations. For a given input pulse, the CPA operation can be effectively represented by a single Fourier transform operation. The amplified pulse temporal profile can be expressed as

$$h(t) = \sqrt{\frac{G}{2\pi}} \int_{-\infty}^{\infty} H_i(\omega) exp(i(D_2\omega^2 + D_3\omega^3)) \times exp(i\Phi^{NL}\bar{I}(\omega)) exp(-i\omega t) d\omega \qquad (9.2)$$

In Equation 9.2, $h(t)$ is the output temporal profile, $H_i(\omega)$ is the input pulse spectral profile. $D_2$ and $D_3$ are second and third order dispersion factors defined as $D_2 = GVD/2$ and $D_3 = TOD/6$, respectively. $G$ is the intensity gain which is just a multiplicative factor due to the assumption of infinite gain bandwidth. $exp(i\Phi^{NL}\bar{I}(\omega))$ is the nonlinear phase shift term according to Equation 9.1.

Equation 9.2 is already quite simple. However, $G$ and $\Phi^{NL}$ are not totally independent since high $G$ usually implies high $\Phi^{NL}$. However, $\Phi^{NL}$ and $G$ are not directly related in CPA. The relative profile with the pulse energy normalized to the initial input pulse energy is introduced:[5]

$$h_{rel}(t) = \frac{h(t)}{PA_i \sqrt{G}} \qquad (9.3)$$

$PA_i$ is the input pulse peak amplitude. From the relative output temporal profile, one can calculate the relative peak power (RPP) which is the maximum value of $|h_{rel}(t)|^2$. In an ideal CPA with $\Phi^{NL} = 0$, flat gain spectrum, zero GVD and zero TOD, the amplified pulse will have the original input pulse shape. Therefore, for an ideal case, the output pulse RPP is one. RPP only decreases as CPA conditions deviate from the ideal conditions, unless the pulse compression which requires the spectral broadening occurs. Since spectral broadening is not considered in the model, the best possible output RPP of the CPA model is one. Therefore, the RPP is a useful indicator of how close the performance is to that of ideal CPA.

An obvious question to be considered is how the output absolute peak power (APP) can be treated theoretically. The APP is what really determines the CPA performance. It is not too difficult to handle the relationship between $\Phi^{NL}$ and $G$ theoretically to calculate the output APP. However, in this paper, we will focus on understanding RPP because it contains enough information to optimize CPA performance.

There are several natural merit function that could be chosen. RPP describes CPA performance well for applications that benefit from high peak power, regardless of the detailed pulse shape. Experimentally, RPP can also be optimized easily by maximizing the autocorrelation signal. Of course, some applications require other pulse qualities such as a clean pulse shape. The analysis in this paper does not suggest optimizing conditions for other merit functions. Several other common merit functions will be discussed briefly in later sections.

Figure 9.1 shows that the approximate model is quite accurate for a useful range of parameters of nonlinear CPA. A split-step Fourier method numerical simulation [13] with a parabolic gain approximation is used to predict the output of a Yb fiber CPA system with a fiber stretcher. For a relatively low nonlinear phase of $\Phi^{NL} = 2\pi$, the numerical simulation result and the CPA model result are almost indistinguishable. Even with a quite high nonlinear phase of $\Phi^{NL} = 10\pi$, the results are quite close.

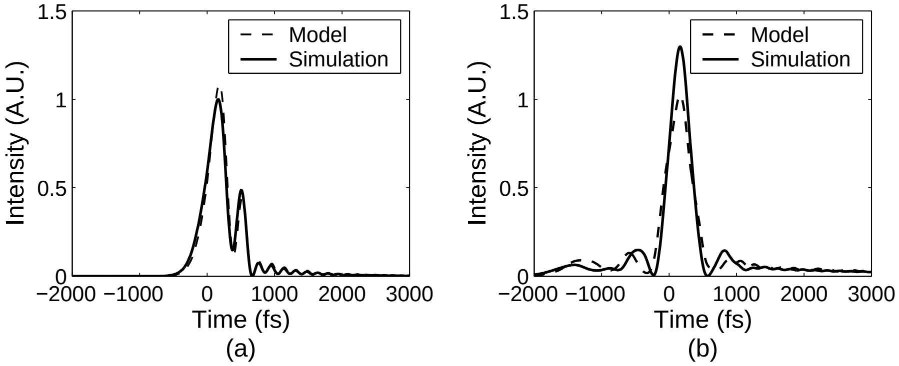

Figure 9.1: Comparison of the CPA model and the split-step Fourier method numerical simulation for $150fs$ Gaussian input. The CPA system is consisted of 2m gain fiber (60nm gain bandwidth) and 600/mm grating pair compressor. (a) 100m SMF stretcher with $\Phi^{NL} = 2\pi$, (b) 400m SMF stretcher with $\Phi^{NL} = 6\pi$.

## 9.3 Mechanism of compensation of $\Phi^{NL}$ by TOD

### 9.3.1 Pulse evolution with linear dispersion only

The compensation of $\Phi^{NL}$ by TOD, without filtering to produce an asymmetric spectrum, is counter-intuitive. It is conventional wisdom to make the spectral phase as flat as possible to achieve better pulse quality. Adding an anti-symmetric cubic phase of TOD does not make the phase flatter, but adding TOD does improve the peak power with a shorter pulse duration. The RPP definitely increases when an appropriate amount of TOD is added for given $\Phi^{NL}$ (Figure 9.2(a)). Figure 9.2(b) shows the spectral phase when TOD is added. A fully-symmetric phase spectrum produced by GVD and $\Phi^{NL}(\omega)$ is adjusted by adding anti-symmetric TOD. Around the central wavelength, the phase is flattened on the short-wavelength side, but at the expense of the long-wavelength side. Thus, the phase does not get flatter by adding TOD.

To gain insight into the compensation mechanism, linear pulse propagation will be

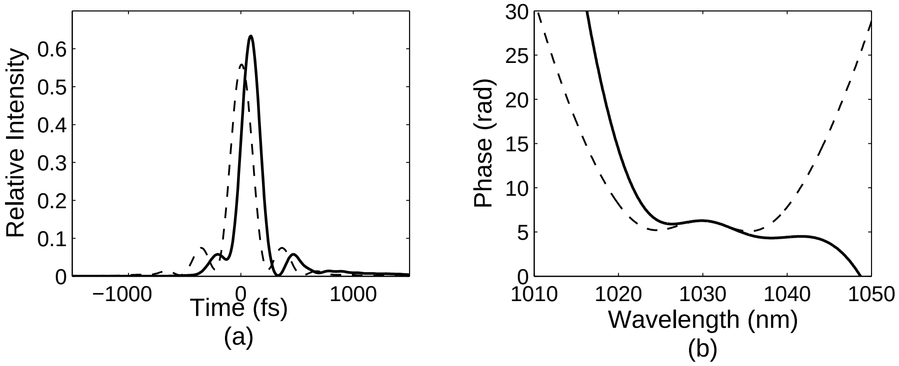

Figure 9.2: CPA output RPP improvement by adding TOD for $150fs$ Gaussian input with $\Phi^{NL} = 2\pi$ (a) Relative Intensity (b) Phase in wavelength domain Dotted line: GVD=$55,290fs^2$, TOD=0 Solid line: GVD=$55,290fs^2$, TOD=$5.09 \times 10^7 fs^3$

discussed first. The pulse evolution can be pictured as a linearly chirped pulse undergoes the TOD broadening. In the case of a Gaussian input pulse, the CPA model with $\Phi^{NL} = 0$ can be solved analytically in terms of an Airy function.[14] Figure 9.3 shows the result. Even for linear dispersion only, it shows the same phenomenon as the CPA does. The addition of the cubic phase improves the peak power of the pulse with a fully-symmetric parabolic phase due to GVD. The improvement of the peak power is quite significant and full-width half-maximum pulse width ($T_{FWHM}$) is clearly shorter as shown in Figure 9.3(a).

Some measures of pulse quality may show degrade even though the peak power is improved by adding TOD. As an example, the root-mean-square pulse width ($T_{RMS}$)is shown in Figure 9.3(b). As the TOD reshapes the pulse, the conventional $T_{FWHM}$is inadequate to characterize the pulse. However, $T_{RMS}$ can be calculated easily. Figure 3b shows that as the TOD increases, $T_{RMS}$ increases monotonically, but slowly, while the peak power improves significantly (Figure 9.3(a)). The increase in peak power and decrease in $T_{FWHM}$ are accompanied by a small sacrifice of pulse quality, as measured by $T_{RMS}$.

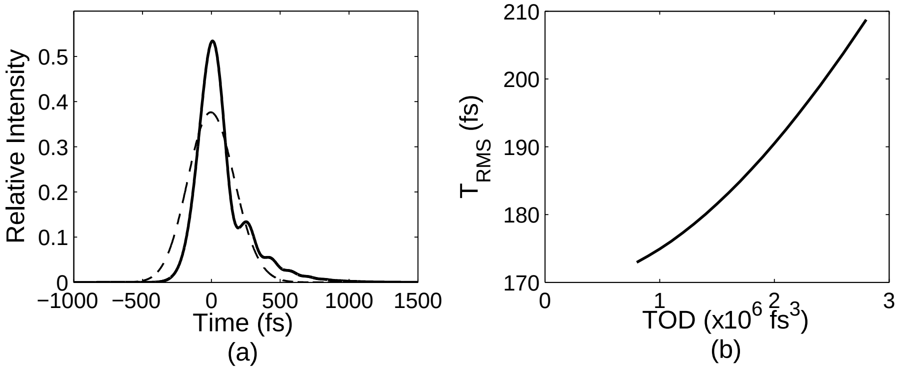

Figure 9.3: Linearly chirped pulse peak power improvement by adding TOD for $150fs$ Gaussian pulse (a) Relative (b) $T_{RMS}$ vs. TOD Dotted line: GVD=$20,000fs^2$, TOD=0 Solid line: GVD=$20,000fs^2$, TOD=$2.4 \times 10^6 fs^3$.

The physical picture of this phenomenon is therefore as follows: Even though the sign of the GVD is irrelevant, positive sign of GVD as for a CPA system is assumed. When the pulse is positively linearly chirped, it broadens with high frequencies shifted to positive time, while low frequencies to negative time. Adding positive TOD will push both high and low frequencies to positive time. Therefore, as shown in Figure 9.3, the leading edge of the pulse shrinks and the trailing edge starts to show a tail with a complicated interference pattern. This redistribution of the energy makes the peak power higher and $T_{FWHM}$ shorter. However, $T_{RMS}$ gets longer because $T_{RMS}$ is quite sensitive to the small amount of energy in the tail. Adding negative TOD will have the same effect on the peak power, but it will send the tail in the negative-time direction.

These arguments suggest that the TOD required to maximize the peak power is proportional to the GVD. The peak power improvement with TOD occurs only when the pulse is chirped with nonzero GVD. If the GVD is zero, the condition to achieve the highest peak power is zero TOD, *i.e.*, back to the original transform-limited pulse. Well-known pulse shapes such as Gaussian and hyperbolic secant definitely have maximum peak power when they are transform-limited. This is not true for all pulse shapes. For example, a pulse with a parabolic spectrum can have higher peak power with nonzero TOD, even with zero GVD, because of the temporal side lobes. One of the side lobes can be shifted toward the pulse peak with TOD, which may yield a higher peak power.

Unfortunately, the exact amount of TOD to maximize the peak power of a linearly chirped pulse is difficult to determine analytically. Even the analytically solvable Gaussian pulse evolution under GVD and TOD [14] is difficult to maximize peak power analytically owing to the complicated Airy function. However, the limiting case of a highly linearly-chirped pulse ($\frac{|GVD|}{{T_{FWHM}}^2} \rightarrow \infty$) can be analyzed approximately (Appendix A). Equation 9.4 and Table 9.1 show the relationship among GVD and TOD that maximizes the peak power when $\frac{|GVD|}{{T_{FWHM}}^2} \rightarrow \infty$ for various pulses.

$$\frac{|TOD/GVD|}{T_{FWHM}} = k \tag{9.4}$$

Table 9.1: Asymptotic $k$ of Equation 9.4 for various input pulses shapes in linear dispersive propagation

| Input Pulse | $k$ as ($\frac{|GVD|}{{T_{FWHM}}^2} \rightarrow \infty$) |
|---|---|
| Gaussian | 1.040 |
| Sech | 1.457 |
| Parabolic spectrum | 0.653 |

The absolute value sign in Equation 9.4 means that signs of GVD and TOD do not alter the pulse peak power. A Gaussian pulse evolution is studied to show the validity of Equation 9.4. Figure 9.4 is the relationship between the two dimensionless parameters ($\frac{|GVD|}{{T_{FWHM}}^2}$ and $\frac{|TOD/GVD|}{T_{FWHM}}$) that maximize the Gaussian pulse peak power.

Figure 9.4 clearly shows that the value of $\frac{|TOD/GVD|}{T_{FWHM}}$ that maximizes pulse peak power approaches $k = 1.04$ as $\frac{|GVD|}{{T_{FWHM}}^2}$ increases. The graph approaches the ideal condition

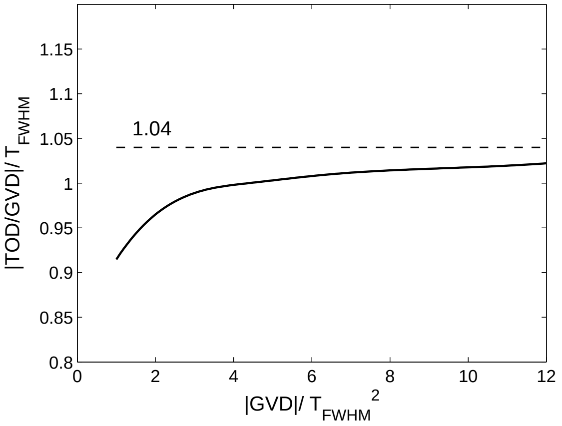

Figure 9.4: Relationship between $\frac{|GVD|}{{T_{FWHM}}^2}$ and $\frac{|TOD/GVD|}{T_{FWHM}}$ maximizing Gaussian pulse peak power

quickly even though the analysis was performed for limiting case of an the infinitely-chirped pulse. For example, at $\frac{|GVD|}{{T_{FWHM}}^2} \approx 5$, which is equivalent to $L \approx 13L_D$ (i.e. $\beta_2$ =const.), $\frac{|TOD/GVD|}{T_{FWHM}}$ is within 5% of the limiting case approximation. It is equivalent to the GVD introduced by $\sim 57m$ single mode fiber (SMF) for a 100-fs Gaussian pulse, which is quite a realistic setup in experiments.

### 9.3.2 Pulse evolution with GVD, TOD and $\Phi^{NL}$ in CPA

Extending the linear case, compensation of nonlinearity by TOD can be described as follows. With a substantial $\Phi^{NL}$, the output pulse is almost always chirped, since $\Phi^{NL}(\omega)$ and the phase from GVD rarely cancel each other perfectly. The quadratic phase of $\Phi^{NL}(\omega)$ is to be canceled by GVD from the stretcher and the compressor, but remaining higher order phase terms of $\Phi^{NL}(\omega)$ will severely chirp the pulse. Higher peak power and shorter $T_{FWHM}$ are obtained by adding appropriate amount of TOD, even though the chirp is not linear. Similar phenomena are observed in soliton-effect compression. Chan *et al.* observed that there is nonzero $\beta_3$ which optimizes higher order soliton-effect compression for given $\beta_2$.[15] The mechanism of this phenomena is exactly the same physical mechanism of compensation of $\Phi^{NL}$ by TOD.

We chose to investigate the conditions to optimize the peak power, since the peak power is enough information of pulse quality for applications requiring high peak power regardless of detailed pulse shape. It is also quite easy to optimize the peak power in the experiment by optimizing the autocorrelation signal peak power.

It is expected that the total phase shift, which is the summation of the GVD phase and $\Phi^{NL}(\omega)$, determines the required TOD to maximize the peak power. Once $\Phi^{NL}$ is included, the CPA model cannot be solved analytically, but a numerical Fourier transform has to be performed to obtain the relations among GVD, TOD and $\Phi^{NL}$ to optimize the CPA output RPP.

## 9.4 CPA performance optimization

Dimensional analysis[16]allows the results of the analytic model to be expressed in terms of five dimensionless parameters: $\frac{|GVD|}{T_{FWHM}{}^2}$,$\frac{|TOD/GVD|}{T_{FWHM}}$, $\frac{T_{FWHM} final}{T_{FWHM} initial}$, $\Phi^{NL}$ and RPP. The scaling of the results to different situations is then clear.

The complexity of the optimization is illustrated by Figure 9.5, which shows the variation of the RPP with GVD and TOD, for fixed $\Phi^{NL} = 6\pi$. It is clear that the RPP is maximized with nonzero TOD with substantial values of $\Phi^{NL}$. Another crucial point is that the RPP function has a complicated structure, with multiple local maxima. Therefore, a CPA system needs to be designed carefully to find the global maxima and exploit the full potential of compensation of $\Phi^{NL}$ by TOD.

The reduction to dimensionless parameters allows the behavior of a nonlinear CPA

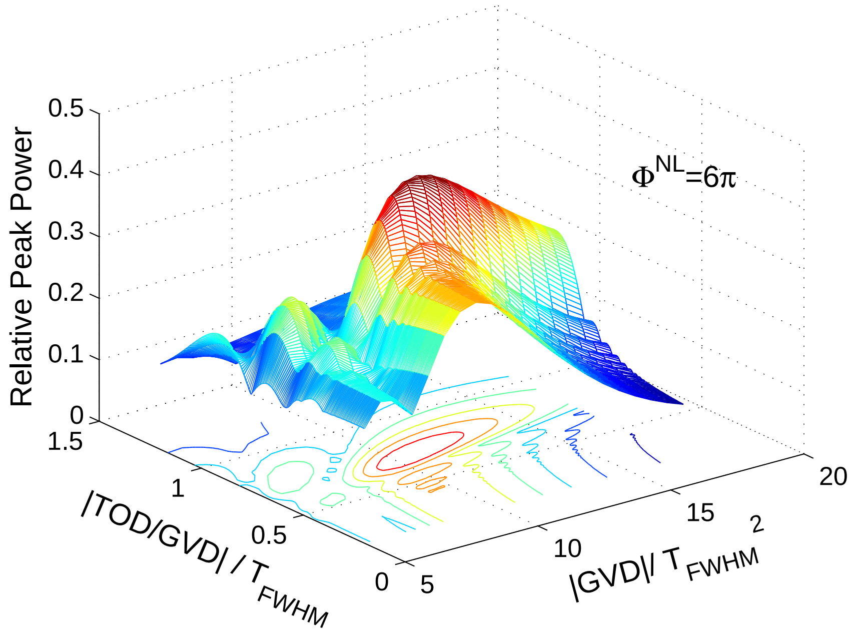

Figure 9.5: 3-D plot of CPA RPP with TOD and GVD as independent variables at $\Phi^{NL} = 6\pi$.

system to be captured in a set of universal curves, as shown in Figure 9.6.

Graphs of the optimum values of the independent (dimensionless) parameters as a function of $\Phi^{NL}$ are shown in Figure 9.6. The graphs illustrate the relationship among the four dimensionless parameters to maximize the output RPP. For example, from Figure 9.5, one can see that the RPP optimum for a Gaussian pulse with $\Phi^{NL} = 6\pi$ occurs at $\frac{|GVD|}{T_{FWHM}{}^2}$=10.79, $\frac{|TOD/GVD|}{T_{FWHM}}$=0.71. The corresponding RPP=0.45, which also can be found in Figure 9.6.

Figure 9.6(a) shows that as $\Phi^{NL}$ increases for given pulse duration, more GVD is necessary to optimize the RPP. Positive GVD is necessary to cancel the pulse-like shape of $\Phi^{NL}(\omega)$. Figure 9.6(b) shows that $\frac{|TOD/GVD|}{T_{FWHM}}$ shows asymptotic behavior similar to Figure 9.4, but with different asymptotes (Appendix B). Hence, Equation 9.4 is still applicable for nonzero $\Phi^{NL}$, but $\frac{|TOD/GVD|}{T_{FWHM}}$ approaches different $k$ values as $\Phi^{NL} \to \infty$.

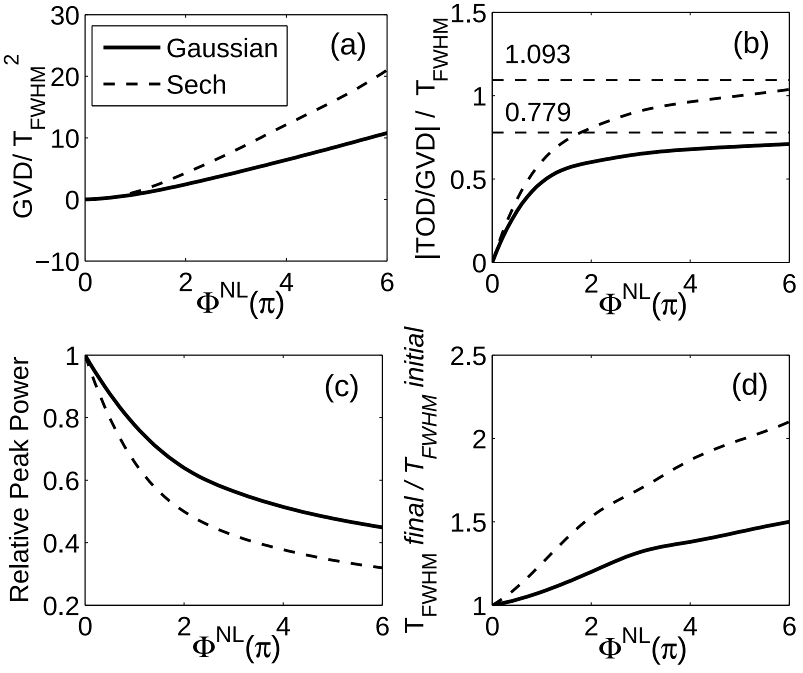

Figure 9.6: CPA dimensionless parameter relationship optimizing the output RPP

Table 9.2 shows the asymptotes for various input pulses for an ideal CPA system. Figure 9.6(c) and 9.6(d) show that the RPP and $T_{FWHM}$ degrade as $\Phi^{NL}$ increases, as expected.

Table 9.2: Asymptotic $k$ of Equation 9.4 for various input pulses shapes in an ideal CPA system

| Input Pulse | $k$ as ($\Phi^{NL} \rightarrow \infty$) |
|---|---|
| Gaussian | 0.779 |
| Sech | 1.093 |

It is important to recognize that the trends of Figure 9.6 will eventually be invalid as the model assumptions will be violated at some point. The violation may come sooner or later according to the CPA design parameters. Although the data in Figure 9.6 only goes up to $\Phi^{NL} = 6\pi$, We typically found that the model is valid up to $\Phi^{NL} = 10\pi$. However, we believe that as far as model assumptions are valid, graphs can be extended well beyond $\Phi^{NL} = 10\pi$. Since the purpose of this study is to explain the general behavior of CPA with a small number of parameters, details of the CPA design will not be covered. However, one can expect the results of Figure 9.6 to be valid as the CPA design gets close to the ideal CPA condition. Once the constant spectrum shape assumption is violated due to the finite gain spectrum shape, the CPA behavior is too complicated to be handled with a simple CPA model.[17]

From the four graphs of Figure 9.6, one can design a CPA system that optimizes the output RPP. For example, starting with a pulse with known $T_{FWHM}$ and target $\Phi^{NL}$ which can be calculated based on the available or possible stretching ratio, the target pulse energy and the gain fiber properties, one can find the required GVD from Figure 9.6(a) and the required TOD from Figure 9.6(b). One can also extract the RPP and $T_{FWHM}$ of the CPA output from Figure 9.6(c) and Figure 9.6(d), respectively when the CPA is designed with required GVD and TOD.

Figure 9.7 shows how much RPP improvement is expected with appropriate GVD and TOD combination over GVD only (i.e. TOD=0). Figure 9.7 clearly shows that manipulating TOD improves RPP and the improvement over the GVD-only case increases as $\Phi^{NL}$ increases. For example, for a Gaussian pulse with $\Phi^{NL} = 6\pi$, 30% better RPP is expected with the correct amount of TOD. Of course, the real benefit of nonlinear CPA comes from working with large nonlinear phase shift, which implies large pulse energy. In linear CPA $\Phi^{NL}$ is limited to $\sim$1, in which case the RPP $\sim$1. With $\Phi^{NL} = 6\pi$, the pulse energy is $\sim$20 times greater. The RPP is reduced to $\sim$0.4, so the APP will be increased by a factor of $20\times0.4 = 5$.

Another benefits of nonlinear CPA with TOD is the possibility of higher pulse energy with same pulse quality. It is difficult to design a CPA system for high energy pulses with very low $\Phi^{NL}$, because the stretching ratio is practically limited. The CPA system may need to accommodate $\Phi^{NL} > 1$ to reach the desired pulse energy. For example, we assume that the CPA system with a Gaussian pulse input has to accumulate $\Phi^{NL} = 2\pi$ to reach the desired pulse energy with zero TOD. Figure 9.7(a) shows that with appropriate TOD, $\Phi^{NL}$ can be increased up to $6\pi$ without sacrificing RPP. This means that the appropriate TOD increases the pulse energy ~3 times maintaining the pulse quality.

There are many choices of merit function for optimization of CPA. We chose to optimize the peak power because it is the parameter that is fundamentally limited, being directly related to the nonlinear phase shift. Experimentally, the peak power is easily and directly monitored through the autocorrelation signal, or related diagnostics such as frequency-resolved optical grating. In addition, peak power is the most important parameter in some applications, such as parametric generation of new colors.

There are other application that favor the shortest or cleanest pulses, and for those, the RPP may not be the best choice. It is reasonable to ask about the behavior of other merit functions. We will not provide a systematic answer here, but we will discuss a couple examples of alternative merit functions. When it is desirable to characterize an irregularly-shaped pulse with a single parameter, $T_{RMS}$ is often used. As mentioned above, $T_{RMS}$ increases with TOD. $T_{RMS}$ is very sensitive to even a small amount of energy in a wing or tail of a pulse, and so might be most appropriate for applications that place a premium on minimal pre- or post-pulse energy.

Another common measure of pulse quality is the fraction of the energy that resides within $T_{FWHM}$ of the pulse. This fraction is sometimes normalized to the value for a Gaussian pulse with same $T_{FWHM}$. The pulse quality is plotted verses $\Phi^{NL}$ in Figure 9.8(a). Comparison to the analogous graphs of Figure 9.7 shows that TOD provides less benefit with regard to this merit function. Although adding TOD shows less benefit

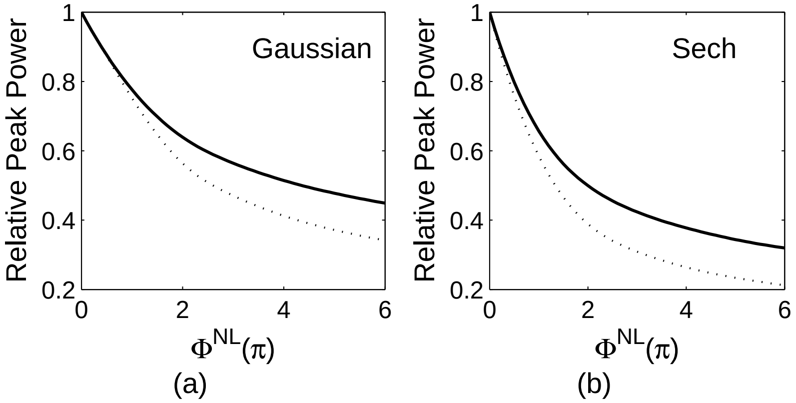

Figure 9.7: CPA RPP improvement with appropriate design parameters. Dotted line: CPA RPP optimized with GVD only(TOD=0) Solid line: CPA RPP optimized with GVD and TOD.

according to the merit function, adding TOD is definitely beneficial overall because the pulse quality is maintained while the peak power is increased. The autocorrelations of the pulses produced with $\Phi^{NL} = 6\pi$ (Figure 9.8(b)) do show the benefits of TOD: the pulse is slightly narrower, and the side lobes and pedestal are reduced significantly with the addition of TOD.

Of course, one can devise a metric that is most appropriate to a given application. A composite metric such as product of peak power and some measure of the pulse quality might also be valuable.

The benefits of mismatched stretcher and compressor dispersions may well go beyond the estimate above. With a grating stretcher, the stretching ratio is limited due to practical reasons. In contrast, with a fiber stretcher, the stretching ratio is believed to be unlimited and therefore, CPA will experience much less $\Phi^{NL}$ for given gain. Therefore, the pulse can be amplified with larger gain with substantially higher TOD, which will help to get higher RPP. As a result, much higher APP can be obtained by the use of fiber stretcher and grating compressor via compensation of $\Phi^{NL}$ by TOD. Finally, the fiber

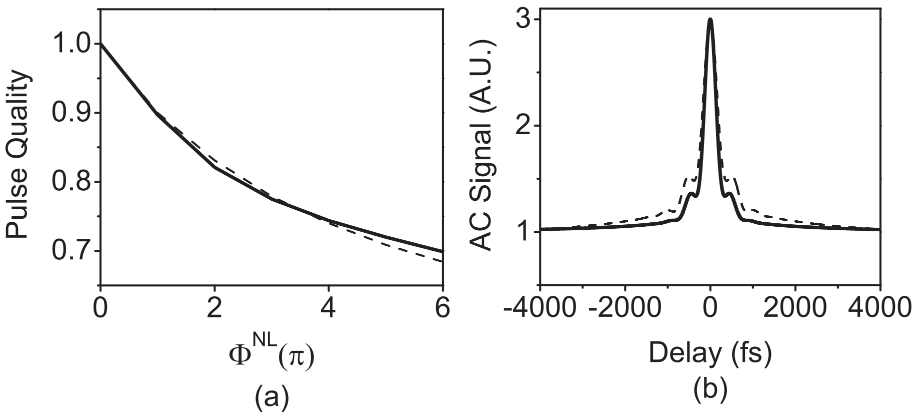

Figure 9.8: Behavior of other FOM functions for a Gaussian pulse at RPP optimization condition. a) Pulse quality FOM vs. $\Phi^{NL}$ and b) Intensity autocorrelation at $\Phi^{NL} = 6\pi$. Dotted line: CPA RPP optimized with GVD only(TOD=0) Solid line: CPA RPP optimized with GVD and TOD.

stretcher offers major benefits of ease of alignment and stability.

The choice of appropriate component to realize the theoretical design parameters from Figure 9.6 is nontrivial, since some parameters are coupled in components. For example, adjusting the distance of a grating pair compressor changes GVD and TOD simultaneously even in different directions. Therefore, multiple iterations of CPA design may be necessary to realize the target performance. In case the optimal condition is not realizable due to some practical issues, one needs to go back to Equation 9.3 to calculate the RPP using a realizable GVD and TOD combination of a CPA system. In this case, several trials may again be necessary to extract the best realizable condition. Even with sub-optimal values of GVD and TOD, it is still possible to achieve improved RPP than that of the GVD-only case. The recent emergence of grisms as practical devices will be very significant in this regard, as they allow a wide range of TOD/GVD ratios to be implemented.[12] Experiments aimed at demonstrating the enhanced performance are now being designed in our lab.

## 9.5 Conclusion

In conclusion, the mechanism of the compensation of $\Phi^{NL}$ by TOD in CPA is described based on a simple theoretical model. The model predicts the output of a CPA system under the assumption that the spectrum is not changed during the amplification process. Nonlinear CPA, with substantial residual TOD and $\Phi^{NL}$, is theoretically shown to outperform linear CPA (as judged by the peak power), by an order of magnitude under relevant conditions. The model described here is not limited to fiber devices, but is applicable to any CPA system that satisfies the model assumptions. The model is used to find the relationships between GVD, TOD and $\Phi^{NL}$ to optimize the CPA output peak power, in which the interplay of $\Phi^{NL}$ and residual TOD plays a major role. Design parameters and expected output performance of a CPA system can be extracted from four graphs with dimensionless parameters. A natural subject for the future will be extension of this model to nonlinear CPA in which substantial new spectral bandwidth is generated.

In the case of fiber CPA, the study indicates that a fiber stretcher / grating compressor CPA configuration can offer not only practical advantages but also performance improvement over a grating stretcher / grating compressor CPA configuration. We expect that the combination of fiber stretcher and grating compressor will become the standard configuration for fiber CPA.

# BIBLIOGRAPHY

[1] A. Chong, L. Kuznetsova, and F. W. Wise, J. Opt. Soc. Am. B, **24**, 1815 (2007).

[2] D. Strickland, and G. Mourou, Opt. Commun. **56,** 219 (1985).

[3] L. Shah, Z. Liu, I. Hartl, G. Imeshev, G. Cho, and M. Fermann, Opt. Express **13,** 4717 (2005).

[4] J. Limpert, A. Liem, T. Schreiber, M. Reich, H. Zellmer, and A. Tunnerman, in *Fiber Lasers: Technology, Systems, and Applications*, L. N. Durvasula, ed., Proc. SPIE volume **5335**, 245 (2004)

[5] S. Zhou, L. Kuznetsova, A. Chong, and F. W. Wise, Opt. Express **13,** 4869 (2005).

[6] A. Galvanauskas, in *Ultrafast lasers, technology and applications,* M. E. Fermann, *et al.* (Marcel Dekker, New York, NY, 2003).

[7] A. Chong, L. Kuznetsova, S. Zhou, and F. W. Wise, in *Fiber Lasers III: Technology, Systems, and Applications*, A. J. W. Brown, J. Nilsson, D. J. Harter, and A. Tnnermann, Eds., Proc. SPIE volume **6102**, 61020Y (2006).

[8] H. M. Pask, R. J. Carman, D. C. Hanna, A. C. Tropper, C. J. Mackechnie, P. R. Barber and J. M. Dawes, IEEE J. Select. Topics Quantum Electron. **1,** 2 (1995).

[9] R. Paschotta, J. Nilsson, A. C. Tropper, and D. C. Hanna, IEEE J. Quantum Electron. **33,** 1049 (1995).

[10] D. T. Walton, J. Nees, and G. Mouorou, Opt. Lett. **21,** 1061 (1996).

[11] L. Kuznetsova, F. W. Wise, S. Kane, and J. Squier, unpublished.

[12] S. Kane, R. Huff, J. Squier, E. Gibson, R. Jimenez, Ch. Durfee, F. Tortajada, H. Dinger, and B. Touzet, in *Conference on Lasers and Electro-Optics*, (Optical Society of America, Washington, D.C., 2006), CThA5.

[13] G. P. Agrawal, *Nonlinear fiber optics* 3ed. (Academic, San Diego, CA, 2001).

[14] M. Miyagi, and S. Nishida, Appl. Opt. **18,** 678 (1979).

[15] K. C. Chan, and H. F. Liu, IEEE J. Quantum Electron. **31,** 2226 (1995).

[16] G. I. Barenblatt, *Similarity, self-similarity, and intermediate asymptotics,* (Consultants Bureau, New York, NY, 1979).

[17] L. Kuznetsova, A. Chong, and F. W. Wise, Opt. Lett. **31,** 2640 (2006)

CHAPTER 10

# FUTURE DIRECTIONS

In this chapter, future possible research directions for fiber lasers and amplifiers are suggested.

## 10.1 Generating cubicons from fiber lasers with spectral filtering

Building a fiber CPA system is a nontrivial task due to the excessive $\Phi^{NL}$ and the residual TOD. As described in chapter 10, a cubicon [1] is a pulse with a specific triangular spectrum shape to circumvent the excessive $\Phi^{NL}$ and non-zero residual TOD problems in the fiber CPA system. Typical cubicon spectra are shown in Figure 10.1.

A cubicon spectrum exhibits a characteristic asymmetrical triangular shape. Utilizing cubicon CPA systems, pulses with ~100 $\mu$J pulse energies and ~650 fs pulse durations were generated [1]. Micromachining with the cubicon CPA output was also demonstrated [2]. Even though the cubicon CPA system demonstrated the robustness against the substantial $\Phi^{NL}$ and the residual TOD, the cubicon is generated by a cumbersome spectral filtering of a well known symmetrical spectrum such as a Gaussian or a hyper-secant. So far, cubicons are not generated directly from a fiber laser. Here,

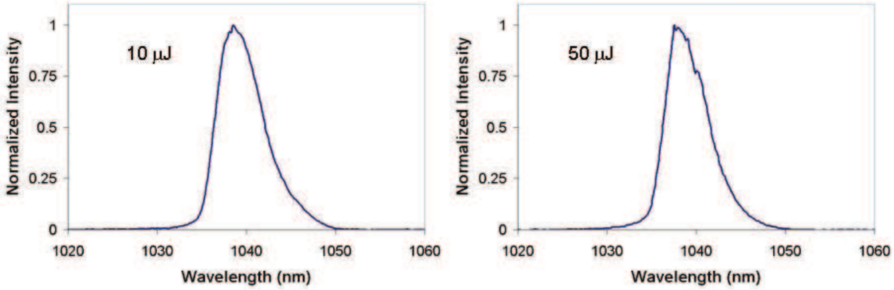

Figure 10.1: Cubicon spectra. From [1]

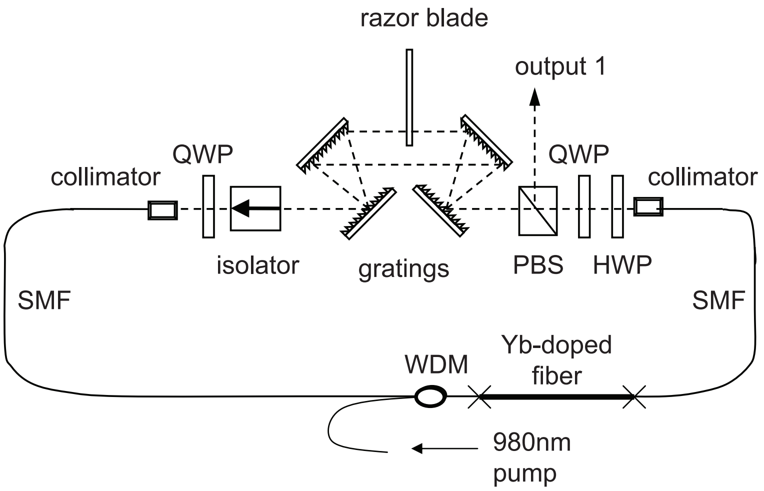

Figure 10.2: Cubicon spectrum generation experimental setup.

we suggest a future research direction of generating cubicons directly from a fiber laser with an intracavity spectral filter. By inserting an asymmetric intracavity spectral filtering component (gain narrowing + physical intracavity spectral filtering), a simple fiber laser can generate pulses with characteristic triangular spectrum shapes.

To demonstrate the idea, a simple Yb-doped fiber laser with an intracavity grating pair (Figure 10.2) is used. By inserting a razor blade to partially block the short wavelength of the intracavity laser beam, triangular spectra are generated (Figure 10.3). As the spectral filtering effect increases with more beam interception with the razor blade, the laser output spectrum intensities gets weaker but the shape gets closer to the triangular spectral shape of a cubicon.

The conventional cubicon, which is established by an external spectrum filtering, is not adjustable conveniently. Therefore, the optimal performance (highest amplified pulse energy without wave-breaking) is obtained by adjusting the pump power of the CPA [1]. However, the cubicon directly from the laser cavity can be adjusted flexibly. For example, the center wavelength and the shape of the spectrum is a function of the spectral filtering strength as shown in Figure 10.3. Hence, the optimal performance

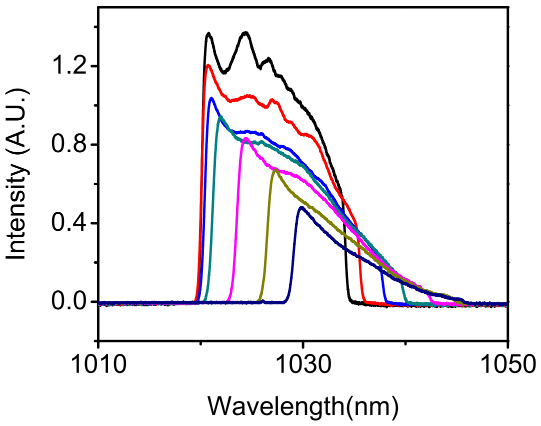

Figure 10.3: Cubicon type of spectra directly from a fiber oscillator with an intracavity spectral filter for a variety of spectral filtering strength.

can be found by adjusting the seed laser pulse shape with the maximum available CPA pump power. Even though the given example is based on a fiber laser with a dispersion map, similar spectrum shapes are also possible in ANDi fiber lasers. A CPA of cubicons directly from simple fiber lasers will be an interesting research direction. The CPA of cubicons directly from fiber lasers will be much simpler with a chance of an improved performance.

## 10.2 CPA of the pulses from ANDi fiber lasers

Besides the cubicon and the SPM TOD compensation described in chapter 9, there is another effective technique to overcome a substantial $\Phi^{NL}$ in a CPA system with the residual TOD~0 (*i.e.* a combination of a grating stretcher and a grating compressor). Once the perfectly parabolic spectrum is highly chirped, the spectrum profiled maps into the time profile. Therefore, when the highly chirped parabolic spectrum is amplified, $\Phi^{NL}$ converts into a linear chirping. Ideally, the excessive $\Phi^{NL}$ is compensated by the external

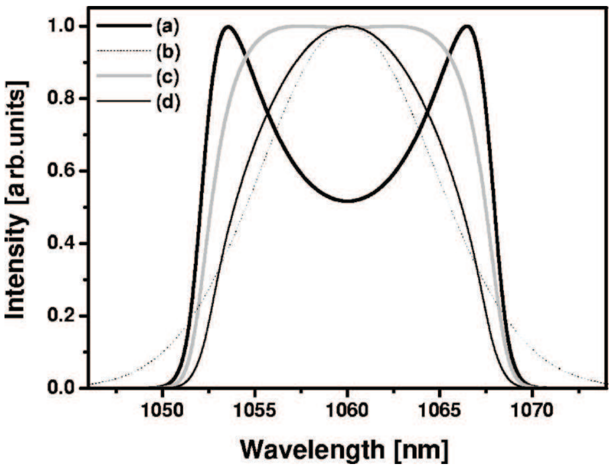

Figure 10.4: (a) Effect of the transfer function on (b) the initial Gaussian spectrum for precompensation of gain narrowing. (c) New spectrum propagates with the (d) result of an almost parabolic shape. From [3]

GVD and the amplified pulse can be dechirped to the Fourier transform limited pulse even though the $\Phi^{NL}$ that the pulse experience can be quite large. The parabolic spectrum amplification was demonstrated by Schreiber *et al.* [3]. Even though the parabolic spectrum amplification worked conceptually and also experimentally, Schreiber *et al.* pointed out there are two practical limitations in the technique. The first limitation is the practical limitation of the parabolic seed spectrum generation. The similariton spectrum is close to a parabola but it is not a perfect parabola. As the stretched similariton is amplified, the deviation from the perfect parabola will eventually cause a wave-breaking due to the non-compensable $\Phi^{NL}$ accumulation. The second limitation is the spectrum distortion due to the gain narrowing effect. Once the spectrum is deviated from a perfect parabola due to the gain narrowing, the CPA output pulse quality degrades quickly again due to the non-compensable $\Phi^{NL}$.

To overcome the limitation due to the gain narrowing, Schreiber *et al.* suggested pre-compensation of the gain narrowing [3]. The pre-compensation of the gain narrowing is illustrated in Figure 10.4. The starting Gaussian spectrum (Figure 10.4(b)) is shaped by

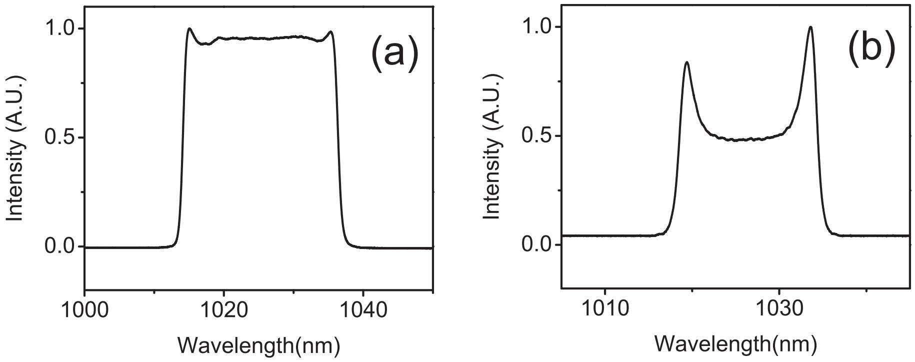

Figure 10.5: Examples of possible ANDi fiber laser spectra for pre-compensation of the gain narrowing.

the transfer function (Figure 10.4(a)). The resulting spectrum (Figure 10.4(c)), which has a flat top shape, is amplified to have a almost parabolic spectrum (Figure 10.4(d)) at the end of the gain fiber and therefore, the $\Phi^{NL}$ converts into an almost linear chirping to be compensated by the GVD. The CPA input spectrum (Figure 10.4(c)) is determined according to the details of the amplifier. For example, if the gain narrowing effect is much stronger than this particular case in Figure 10.4, the CPA input spectrum should be closer to Figure 10.4(a) to balance the strong gain narrowing effect. The pre-compensation of the gain narrowing in the CPA was demonstrated by Schimpf *et al.* [4] utilizing a liquid crystal spatial light modulator to shape the spectrum in a desired shape. A liquid crystal spatial light modulator is a cumbersome and expensive bulk optical component which is against the advantage of a fiber medium. In this section, we like to point out that the spectra from ANDi fiber laser are already close to pre-compensated spectra. Examples of ANDi fiber laser spectra are given in Figure 10.5.

The Figure 10.5(a) shows a flat topped spectrum which is close to the Figure 10.4(c). As pointed out, spectrum in Figure 10.5(b) can be a good candidate for a pre-compensated spectrum for a CPA system with a strong gain narrowing. Of course, it will be a tremendous practical benefit if a simple ANDi fiber laser can do the function of the complicated liquid crystal spatial light modulator. Applying a variety of ANDi fiber laser pulses with desired spectra as seed pulses for CPA systems will be an interesting future research.

## 10.3 Intracavity TOD compensation by a detuned spectral filtering

Building a stretched pulse fiber laser [5] with near zero net GVD is an effective strategy to generate very short femtosecond pulses. Once the net GVD approached to zero, the nonzero net TOD eventually becomes a limiting factor for the pulse duration. As the consequence, in stretched pulse fiber lasers, the compensation of the TOD and higher order dispersions is necessary if the pulse duration is desired to be further improved. Compensating higher-order dispersion in fiber lasers is a nontrivial task. Compensating the TOD in the fiber laser is already quite challenging. By compensating the TOD of the fiber with a grism (grating-prism) pair, 10-cycle pulses (~30 fs), which still is the shortest pulse duration record from fiber lasers, were obtained from a Yb-doped fiber laser [6].

Since the Yb-doped stretched pulse fiber lasers usually have a bulk anomalous dispersive segment, adding a grism pair within the cavity is not such a problem. Replacing the bulk anomalous dispersive segment by a grism pair does not effect the cavity integrity much. However, fiber lasers such as Er-doped fiber lasers can be in an all-fiber format conveniently utilizing anomalously dispersive fibers. Introducing an intracavity bulk component to compensate the TOD in such lasers is against the benefit of the laser light guided in a fiber. To overcome the practical limitation, a key question to be answered is if there is a fiber-integrated TOD compensation mechanism. Of course, specially designed fiber (*i.e.* PCF) is a good candidate but it will introduce another complication of implementing a complicated and expensive fiber within a cavity.

Here, we suggest the fiber laser cavity TOD compensation by the gain dispersion. The theoretical treatment of the gain dispersion up to the GVD term in a passive propagation is well covered in Ref [7]. In case of an ideal Lorentzian gain, the TOD effect of the gain can be conveniently expressed analytically by expanding the complex gain up to the third order. The magnitude and the sign of the gain TOD depends on the peak gain, the gain BW, and the detuning (pulse center wavelength - gain center wavelength). Of course, in a laser cavity, it is usually true that the lasing wavelength matches the peak gain wavelength. However, once a detuned spectral filter is introduced within the cavity, its effect may be significant since the filtered spectrum will face the detuned gain profile. Therefore, by adjusting the spectral filtering parameters, the magnitude and the sign of the gain TOD may be suitable to perfectly or partially cancel the cavity TOD. So far, the above discission is based on the ideal Lorentzian gain. However, for the asymmetric gain profile may be more advantageous to cancel the cavity TOD. The gain profile effect on the gain dispersion is hard to be predict analytically. However, experimental results indicates that there is some process in action in the ANDi fiber laser to compensate processes causing asymmetric mode-locked spectra. Those processes can be the TOD, higher odd order dispersions, and asymmetric nonlinear effects. Among them , it is believe that the TOD is the dominant effect causing the asymmetric mode-locked spectra.

The evidence of canceling the TOD is shown in Figure 10.6. The experimental setup is same as Figure 2.6. Without a spectral filter, a Yb-doped fiber laser usually display asymmetric mode-locked spectra which are most likely caused by the cavity TOD. Notice that the symmetry of the mode-locked spectrum changes while the lasing wavelength was tuned by the spectral filter center wavelength adjustment (Figure 10.6(a)-(c)).

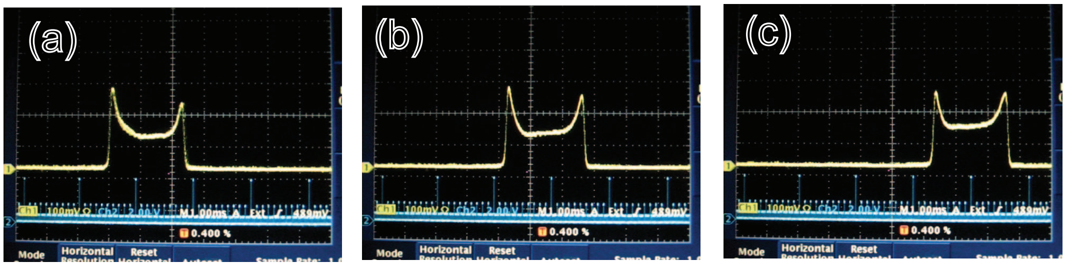

Figure 10.6: Spectrum evolution according the spectral filter center wavelength tuning.

One can look for a symmetric spectrum by tuning the spectral filter. The symmetric spectrum indicates that asymmetric dispersion terms and nonlinear effects are somehow reduced by the debunked spectral filtering action. To verify the gain TOD compensation mechanism experimentally, a capability to characterize the phase (*i.e.* SHG FROG) will be essential. Once the mechanism is verified, numerous applications are awaiting not only for oscillators but also for passive propagations. Generating short pulses from stretched pulse fiber lasers by compensating the cavity TOD is an obvious good idea. One may consider to apply this technique to reduce the residual TOD of the fiber CPA system.

## 10.4 Generation of large pulse energies with short pulse durations (<50 fs) from ANDi fiber lasers

In chapter 5, it was pointed out that the mechanism of short pulse generation from ANDi fiber lasers is fundamentally different from that of the short pulse generation from stretched pulse lasers. With a unique pulse shaping of the CPSF, a substantial $\Phi^{NL}$ is necessary to produce shorter pulses in ANDi fiber lasers. Therefore, one can conjecture that the ANDi fiber laser can produce large pulse energies with short dechirped pulse durations (i.e.<50 fs). In contrast, as the net GVD of the stretched pulse laser approaches zero, the $\Phi^{NL}$ and therefore the pulse energy have to be smaller to match the tiny net GVD. As the result, generating short pulses with large energies is extremely challenging in stretched pulse fiber lasers.

The simulation result in chapter 5 (Figure 5.2) indicates that pulses with ~40 nJ and ~30 fs dechirped durations are quite possible from ANDi fiber lasers. However, the performance of the ANDi fiber laser is currently limited by the available pump power. The laser performance is expected to be improved by providing more pump power but with a SMF pigtailed pump diodes have a power limitation (~700 mW currently).

A well known approach to overcome the pump power limitation is to use double cladding (DC) fibers with proper pump fiber couplers. Multimode fiber pigtailed pump diodes can provide tens of watts power easily. By pumping the primary cladding with a multimode fiber coupler (*i.e.* a star coupler), the DC gain fiber can be pumped even up to hundreds of watts power level. It will be an obvious good idea to build ANDi fiber lasers with DC fibers to realize the simulation prediction (Figure 5.2) or a even better performance.

## 10.5 Dissipative solitons of a Swift-Hohenberg equation in ANDi fiber lasers

In chapter 3, it is pointed out that the pulses of ANDi fiber lasers behavior resemble the dissipative solitons of the CQGLE (Equation 3.4). Even though the CQGLE approach is successful to model (Yb-doped) ANDi fiber lasers, the CQGLE has an obvious limitation. The main reason of the successful modeling by the CQGLE is the smooth Yb-

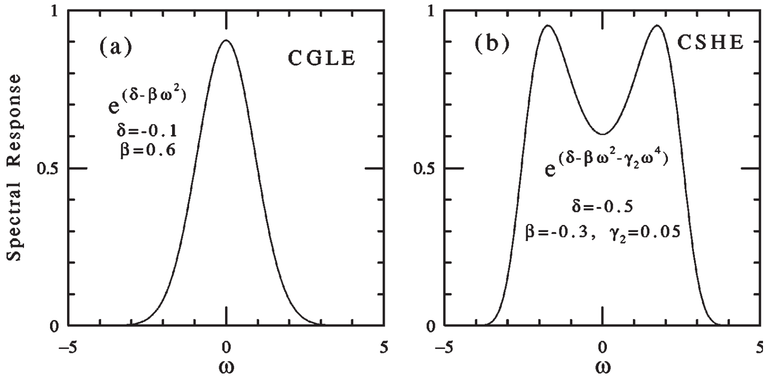

Figure 10.7: Spectral filtering in the two models of a laser: a) CGLE and b) CSHE. For parameters of the calculation, please see Ref [9]

doped fiber gain spectrum can be well approximated the second-order spectral filtering term in CQGLE. For complicated gain spectra such as a Er-doped fiber with multiple maximum gain peaks, even higher order spectral filtering effect should be considered for a proper modeling. By adding the fourth-order spectral filtering effect to the CQGLE, the equation becomes a complex Swift-Hohenberg equation (CSHE).

$$\frac{\partial A}{\partial z} = gA + (\frac{1}{\Omega} - i\frac{D}{2})\frac{\partial^2 A}{\partial t^2} + i\gamma_2\frac{\partial^4 A}{\partial t^4} + (\alpha + i\gamma)|A|^2 A + \delta|A|^4 A. \qquad (10.1)$$

The Equation 10.1 is same as the CQGLE except $i\gamma_2\frac{\partial^4 A}{\partial t^4}$ term which designates the fourth-order spectral filtering effect. The solutions of the CSHE are dissipative solitons since the soliton solutions are determined by strong dissipative processes such as the gain, the saturable absorption, and the spectral filtering. Even though some exact solutions of the CSHE are found analytically, numerical simulations seem to be the only reliable method to study the CSHE exhaustively. By solving fiber laser behaviors numerically with the CSHE model, Soto-Crespo *et al.* proposed many interesting and unique dissipative soliton solutions such as composite moving solitons and double pulses [9].

Soto-Crespo *et al.* used the spectral filtering curve in Figure 10.7(b) for numerical

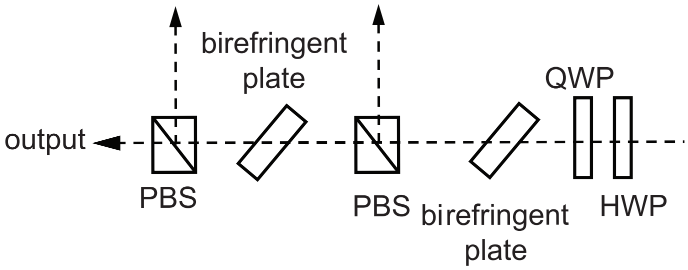

Figure 10.8: Birefringence spectral filter schematics to generate Figure 11.7(b) type of spectral transmission curve

simulations. In this particular case, the fourth-order spectral filtering introduces a center dip in the spectral transmission. Of course, it will be scientifically interesting to realize dissipative solitons of the CSHE in fiber lasers. In fact, this unique spectral filtering shape can be realized conveniently in ANDi fiber lasers with a Lyot filter setup. The spectral filter setup is shown in Figure 10.8

The first birefringence filter provides 6 nm filter BW while the second one corresponds to 12 nm spectral filtering BW. By adjusting waveplates and the orientation of birefringence plates, spectral transmission curve close to Figure 10.7(b) can be realized. The resulting spectral filtering curve is shown in Figure 10.9.

In fact, the ANDi fiber laser with the particular spectral filter was mode-locked for many interesting modes. However, unique dissipative solitons of the CSHE such as composite moving solitons or double pulses are not found yet.

## 10.6 Multipulsing characterization

Controlling the number of pulses and the separation between pulses in fiber lasers is interesting not only for the scientific aspect of it but also for practical applications such as the micromachining and the frequency comb generation. So far, the theoretical un-

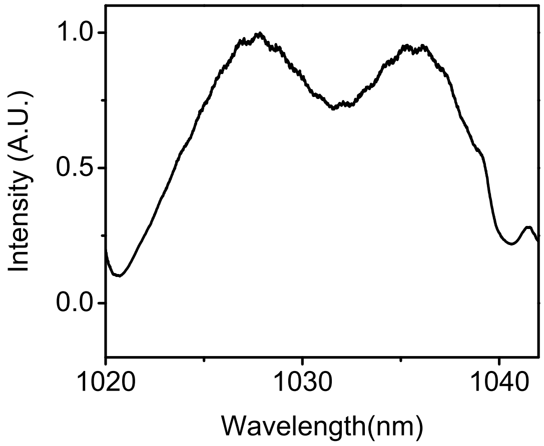

Figure 10.9: Measured spectral transmission of the experimental setup in Figure 10.8

derstanding of the multipulsing phenomena is rudimentary even for experts in lasers.

In chapter 8, an interesting aspect of controlling multipulsing states is investigated. The multipulsing state can be controlled from a soliton bunch to a harmonically mode-locked state by spectral filtering adjustment. This is a meaningful step to understand the role of the spectral filtering in multipulsing operation modes. The quantization of the separation between pulses is a quite interesting and may be already significant for some applications. It is strongly believed that the fiber laser with controllable pulse numbers and separations will find a variety of applications immediately. The mechanism which determines the separation between pulses is not understood fully. However, by performing systematic experiments with ANDi fiber lasers, it is believed that one can recognize variables (GVD, spectral filtering BW, spectral filtering detuning, etc.) which affect the multipulsing operations. The current knowledge does not provide a viable explanation of the characteristics of multipulsing operations. However, gathering systematic observations will eventually contribute in building fiber lasers with controllable multipulsing states.

# BIBLIOGRAPHY

[1] L. Shah, Z. Liu, I. Hartl, G. Imeshev, G. Cho, and M. Fermann, Opt. Express **13,** 4717 (2005).

[2] L. Shah, M. Fermann, J. W. Dawson and C. P. J. Barty, Opt. Express **14,** 12546 (2006).

[3] T. Schreiber, D. Schimpf,1 D. Müller, F. Röser, J. Limpert,1 and A. Tünnermann, J. Opt. Soc. Am. B **24,** 1809 (2007).

[4] D. N. Schimpf, J. Limpert,1 and A. Tünnermann, Opt. Express **15,** 16945 (2007).

[5] K. Tamura, J. Jacobson, H. A. Haus, E. P. Ippen, and J. G. Fujimoto, Opt. Lett. **18,** 1080 (1993).

[6] J. R. Buckley, S. W. Clark, and F. W. Wise, Opt. Lett. **31,** 1340 (2006)

[7] G. P. Agrawal, *Nonlinear Fiber Optics, 2nd Ed.* (Academic, New York, 1995).

[8] M. Hofer, M. E. Fermann, and L. Goldberg, IEEE Photonics Technol Lett, **10**, 1247 (1998)

[9] J. M. Soto-Crespo, and Nail Akhmediev, Phys. Rev. E. **66,** 066610 (2002).

# APPENDIX A

# PULSE PEAK POWER OPTIMIZATION ASYMPTOTIC BEHAVIOR WITH LINEAR DISPERSION ONLY (GVD AND TOD)

Starting from a general transform limited input pulse $h_i(t)$, propagation of the pulse in linearly dispersive media counting linear dispersion terms up to TOD can be expressed as follows.

$$h(t) = \frac{1}{\sqrt{2\pi}} \int_{\infty}^{\infty} H_i(\omega) e^{(i(D_2\omega^2+D_3\omega^3)))} e^{(-i\omega t)} d\omega \tag{A1}$$

$H_i(\omega)$ is obtained by Fourier transform of a known initial pulse temporal profile $h_i(t)$. $D_2$ and $D_3$ are second and third order dispersion factors defined as $D_2 = GVD/2$ and $D_3 = TOD/6$. GVD and TOD are residual dispersion terms in a CPA. Equation (A1) can be integrated analytically for a Gaussian input pulse.[1] Even though the solution is in a complete analytic form, it is not very useful for further analysis since it contains an Airy function which is quite complicated. Due to the complexity of the Airy function, it is hard to figure out some important characteristics of the pulse evolution such as the pulse peak power. Furthermore, there aren't known analytic solutions for different initial pulse shapes. To circumvent the difficulty lies in the treatment of an Airy function, only a special case of a high GVD case is considered in the analysis. Equation A1 can be expressed as a convolution integral.

$$h(t) = \frac{1}{\sqrt{2\pi}} h_i(t) \bigotimes g(t) \tag{A2}$$

where

$$g(t) = \frac{1}{\sqrt{2\pi}} \int_{\infty}^{\infty} e^{(i(D_2\omega^2+D_3\omega^3)))} e^{(-i\omega t)} d\omega \tag{A3}$$

Equation A3 can be solved analytically by substituting $\omega = (3D_3)^{\frac{1}{3}}u - \frac{D_2}{3D_3}$ and using the Airy function of the first kind identity$Ai(z) = \frac{1}{2\pi}\int_{-\infty}^{\infty} e^{i(\frac{1}{3}t^3+zt)}dt$[2], the result is as follows [3].

$$g(t) = \sqrt{2\pi} b e^{i(A+Bt)} Ai(-a-bt) \tag{A4}$$

A, B, a and b are constants defined as follows.

$$A = \frac{2{D_2}^3}{27{D_3}^2}, B = \frac{D_2}{3D_3}, a = \frac{{D_2}^2}{(3D_3)^{\frac{4}{3}}}, b = \frac{1}{(3D_3)^{\frac{1}{3}}} \tag{A5}$$

Therefore, the pulse evolution due to GVD and TOD becomes as follows.

$$h(t) = b \int_{-\infty}^{\infty} h_i(t-t') e^{i(A+Bt')} Ai(-a-bt') dt' \tag{A6}$$

Note that the integral is close resemblance of a Fourier transform because of $e^{iBt}$ term in the integrand. As a matter of fact, with suitable substitution, Equation A6 can be reduced to a summation of Fourier transforms. However, since it is an infinite summation, it does not carry much advantage over the numerical Fourier transform except for some special limit cases.

### A.0.1 Gaussian input pulse

For a Gaussian input pulse, Equation A6 becomes as follows.

$$h(t) = b \int_{-\infty}^{\infty} e^{-(t-t')^2/2t_o{}^2} e^{i(A+Bt')} Ai(-a-bt')dt' \tag{A7}$$

The integral still cannot be performed analytically due to the Airy function. However, for some special limit cases, the integral can be performed approximately to predict pulse evolution. One can consider a case of a very short Gaussian input pulse ($t_o \rightarrow 0$) with very large TOD ($b \rightarrow 0$). Figure A1 shows an example of the short input Gaussian pulse with an Airy function envelope widely spread in time due to very large TOD. In this limit, the input Gaussian pulse act like a delta function and the maximum of $h(t)$ occurs around the maximum of $Ai(-a-bt)$. Maximum of $Ai(-a-bt)$ occurs at $Ai'(-s) = 0$where $s = 1.0188$. Maximum occurring time is approximately given by as follows.

$$t \approx t_m = \frac{s-a}{b} = (s - \frac{D_2{}^2}{(3D_3)^{\frac{4}{3}}})(3D_3)^{\frac{1}{3}} \tag{A8}$$

The maximum intensity is can be estimated assuming the maximum intensity occurs at $t_m$.

$$Max(|h(t)|^2) \approx |h(t_m)|^2 = |b \int_{-\infty}^{\infty} e^{-(t-t')^2/2t_o{}^2} e^{i(A+Bt')} Ai(-a-bt')dt'|^2 \tag{A9}$$

One can Taylor expand the Airy function term around $t' = t_m$. As the result, can be expressed as a summation of Fourier transforms.

$$h(t_m) = b \sum_{n=0}^{\infty} C_n \int_{-\infty}^{\infty} e^{-(\frac{s-a}{b}-t')^2/2t_o{}^2} e^{i(A+Bt')} (t' - \frac{s-a}{b})^n dt' \tag{A10}$$

Equation A10 is integrable term by term and the algebraic expression of $h(t_m)$ in terms of $t_o$, $D_2$ and $D_3$ can be obtained. Obviously, more terms included in the summation gives a better estimation. To find an analytical relationship among parameters approximately, the most simple case of $n = 0$ was considered. Integrand can be estimated as follows.

$$e^{-(\frac{s-a}{b}-t')^2/2{t_o}^2} Ai(-a-bt') \approx e^{-(\frac{s-a}{b}-t')^2/2{t_o}^2} Ai(-s) \tag{A11}$$

Substituting Equation A11 in Equation A10 becomes as follows.

$$h(t_m) \approx bAi(-s) \int_{-\infty}^{\infty} e^{-(\frac{s-a}{b}-t')^2/2{t_o}^2} e^{i(A+Bt')} dt' = \sqrt{2\pi} b t_o Ai(-s) e^{i(a+\frac{B}{b}(s-a))} e^{-\frac{B^2 {t_0}^2}{2}} \tag{A12}$$

Maximum intensity is approximately given by following equation.

$$Max(|h(t)|^2) \approx 2\pi b^2 Ai^2(-s) {t_o}^2 e^{-B^2 {t_o}^2} = \frac{2\pi b^2 Ai^2(-s) {t_o}^2 e^{-{D_2}^2 {t_o}^2/(9{D_3}^2)}}{(3D_3)^{\frac{2}{3}}} \tag{A13}$$

One can find the relationship between $D_2$ and $D_3$ to maximize easily. The final result is as follows.

$$D_3 = \frac{t_o}{\sqrt{3}} D_2 \tag{A14}$$

In terms of GVD and TOD with relationship $1.665 t_o = T_{FWHM}$ for Gaussian, Equation A14 becomes as follows.

$$\frac{|TOD/GVD|}{T_{FWHM}} = k, k = 1.040 \tag{A15}$$

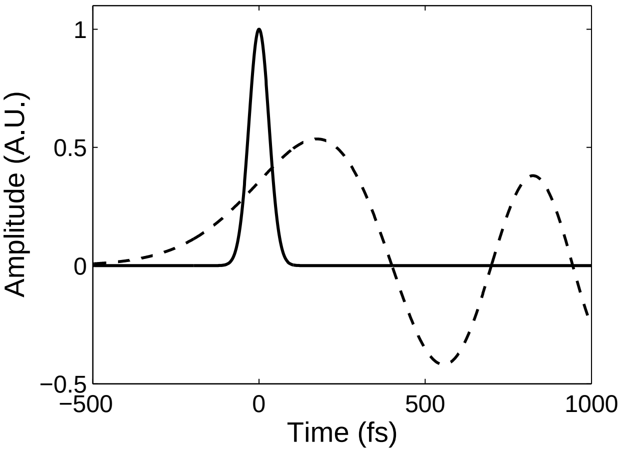

Figure A1: Input Gaussian pulse with Airy function envelop of Equation A6 $t_o = 50fs$,TOD=$1 \times 10^7 fs^3$.

Equation A15 is the relationship of $T_{FWHM}$, GVD and TOD to maximize the Gaussian pulse peak power under nonzero GVD and nonzero TOD in a limit of $TOD \rightarrow \infty$. The Equation A15 describes that when a Gaussian pulse is evolved with large TOD, adding GVD improves the peak power and the optimal ratio of TOD/GVD to maximize the peak power is roughly $T_{FWHM}$. Since GVD and TOD operators commute in the linear dispersive propagation, one can also describe the process as a highly linearly chirped pulse peak power optimization with large TOD with ratio given by Equation A15. Therefore, the limit condition $TOD \rightarrow \infty$ is equivalent to $GVD \rightarrow \infty$ when the pulse peak power is maximized. Conjunction with $t_o \rightarrow 0$ which is same as $T_{FWHM} \rightarrow 0$, the limit condition can be defined as $\frac{|GVD|}{T_{FWHM}{}^2} \rightarrow \infty$. $\frac{|GVD|}{T_{FWHM}{}^2}$ is a convenient parameter since the quantity is dimensionless and proportional to the $\frac{z}{L_D}$ assuming $\beta_2$ is constant where is a dispersion length. Figure A3 shows that $\frac{|TOD/GVD|}{T_{FWHM}}$ approaches 1.04 as $\frac{|GVD|}{T_{FWHM}{}^2}$ increases which is predicted by Equation A15

### A.0.2 Other pulse shapes

For a soliton with temporal profile $h_i(t) = Sech(\frac{t}{t_o})$, same treatment is applicable. For an ideal similariton with parabolic power spectral profile of $H_i(\omega) = \sqrt{c - d\omega^2}$ with corresponding temporal profile of $h_i(t) = \frac{1}{t}\sqrt{\frac{c\pi}{2}}J_1(\sqrt{\frac{c}{d}}t)$ where $J_1(x)$ is the Bessel function of first kind while $c$ and $d$ are constants. Again same treatment to find the relationship of Equation (A15) is applicable for an ideal similariton, too. The result is summarized in Equation 9.4 and Table 9.1 in chapter 9.

# BIBLIOGRAPHY

[1] M. Miyagi, and S. Nishida, Appl. Opt. **18,** 678 (1979).

[2] H. Hochstadt, *The function of mathematical physics,* (Dover, Mineola, NY, 1986).

[3] J. N. Elgin, T. Brabec, and S. M. J. Kelly, Opt. Commun. **114,** 321 (1995).

## APPENDIX B

# CPA OUTPUT RPP OPTIMIZATION ASYMPTOTIC BEHAVIOR (GVD, TOD AND $\Phi^{NL}$)

Starting from Equation 9.3 in chapter 9, assuming $TOD = 0$ gives the equation as follows.

$$h(t) = \frac{1}{\sqrt{2\pi}} \int_{-\infty}^{\infty} H_i(\omega) e^{(i(D_2\omega^2))} e^{(i\Phi^{NL}\bar{I}(\omega))} e^{(-i\omega t)} d\omega \tag{B1}$$

Assuming a Gaussian input of $H_i(\omega) = e^{-\omega^2 to^2/2}$ and Taylor expansion of the nonlinear phase term as $e^{i\Phi^{NL} e^{-\omega^2 to^2}} \approx e^{i\Phi^{NL}(1-\omega^2 {t_o}^2)}$ (i.e. $\Phi^{NL} \to \infty$, the DC term and the first order (second order of $\omega$) term dominates), Equation B1 is reduced as follows.

$$h(t) = \frac{1}{\sqrt{2\pi}} \int_{-\infty}^{\infty} e^{-\frac{\omega^2 {t_o}^2}{2}} e^{(i(D_2\omega^2))} e^{(i\Phi^{NL}(1-\omega^2 {t_o}^2))} e^{(-i\omega t)} d\omega \tag{B2}$$

The best pulse quality is achieved when GVD term cancels second order of nonlinear phase term. Therefore, the pulse quality is best when $D_2 = \Phi^{NL} {t_o}^2$. Substituting $D_2 = \Phi^{NL} {t_o}^2$ into Equation A17 gives an equation similar to Equation A15 but with some modifications.

$$\begin{aligned} \frac{|TOD/GVD|}{T_{FWHM}} &= k(1 - \frac{\Phi^{NL}}{2(1.665)^2} \frac{{T_{FWHM}}^2}{GVD}) \\ &= k(1 - \frac{1}{2(1.665)^2} \frac{1}{u}) = k' \end{aligned} \tag{B3}$$

$u$ can be empirically found from the slope of Figure 9.5(a) or one can use the $D_2 = \Phi^{NL} {t_o}^2$ relation as $\Phi^{SN} \to \infty$. Using relation gives $k' = 0.779$ for a Gaussian input.

It means that for a Gaussian input, $\frac{|TOD/GVD|}{T_{FWHM}}$ value asymptotically approach 0.779 as $\Phi^{SN} \rightarrow \infty$. Figure 9.6(b) clearly shows the asymptotic behavior of $\frac{|TOD/GVD|}{T_{FWHM}}$ for a Gaussian pulse. By performing same analysis for a soliton, $k' = 1.093$ is found. Again, Figure 9.6(b) clearly demonstrates the case. The result is summarized in Table 9.2.